Okinawa Institute of Science and Technology
Graduate University

Thesis submitted for the degree

Doctor of Philosophy

Contribution to Entanglement Theory, Applications in Atomic Systems and Cavity QED

by

Jérémie Gillet

Supervisor: Thierry Bastin
Co-Supervisor: Girish S. Agarwal

September, 2011

Declaration of Original and Sole Authorship

I, Jérémie Gillet, declare that this thesis entitled *Contribution to Entanglement Theory, Applications in Atomic Systems and Cavity QED* and the data presented in it are original and my own work.

I confirm that:

- This work was done solely while a candidate for the research degree at the Okinawa Institute of Science and Technology Graduate University, Japan.
- No part of this work has previously been submitted for a degree at this or any other university.
- References to the work of others have been clearly attributed. Quotations from the work of others have been clearly indicated, and attributed to them.
- In cases where others have contributed to part of this work, such contribution has been clearly acknowledged and distinguished from my own work.

Date: September, 2011
Signature:

Abstract

Contribution to Entanglement Theory, Applications in Atomic Systems and Cavity QED

We introduce in this thesis two entanglement detection criteria, the *Schrödinger-Robertson partial transpose inequality*, which can be implemented experimentally in a variety of systems and generalized *N-qubit concurrences*, which can be used to evaluate multipartite entanglement in N-qubit mixed states. Then, we investigate ways to experimentally produce entanglement by giving a theoretical model which successfully describes the *dipole blockade* effect. We study its possible applications in systems of two and three two-level atoms as well as its relations with the *EIT* effect in systems of two three-level atoms. Finally, we show the possibility of two-photon processes in a system of two two-level atoms embedded in a cavity by using perturbation theory and a full master equation approach. We unveil interesting features of blockade and transparency in such *cavity QED* systems.

Acknowledgment

First of all, I would like to thank to my advisor, Thierry Bastin, who led my efforts for four years. I learned many things on this journey and, more often than not, you were the one teaching them to me.

I want to give many thanks to Girish S. Agarwal, who co-advised me and welcomed me three times to his group in Oklahoma State University for the grand total of one year. That year was synonym of hard work and of many, many breakthroughs. I also want to thank everybody of the Quantum Optics and Quantum Information Science Group at OSU, you guys were an essential part of my adventure, I was lucky to meet you.

I vehemently thank all the members of the IPNAS in Liège, you are amazing, how do you do it? This place is like a second home to me, especially on Fridays. My second family is located elsewhere, though. Cross the street, enter the building, go up four floors. Fourth floorers and affiliated were sometimes the only thing that kept me going, may our friendship never die.

I will keep it short and not mention anybody else by name but chances are, if you are reading this thesis, you had some role to play in its development. I want you to pat yourself on the back and receive all my gratitude, that's probably the least you deserve.

Abbreviations

PPT	positive partial transpose
SRPT	Schrödinger-Robertson partial transpose
PPT	positive partial transpose
SRPT	Schrödinger-Robertson partial transpose
PPT	positive partial transpose
SRPT	Schrödinger-Robertson partial transpose
PPT	positive partial transpose
SRPT	Schrödinger-Robertson partial transpose
PPT	positive partial transpose
SRPT	Schrödinger-Robertson partial transpose
PPT	positive partial transpose
SRPT	Schrödinger-Robertson partial transpose
PPT	positive partial transpose
SRPT	Schrödinger-Robertson partial transpose
PPT	positive partial transpose
SRPT	Schrödinger-Robertson partial transpose
PPT	positive partial transpose
SRPT	Schrödinger-Robertson partial transpose
PPT	positive partial transpose
SRPT	Schrödinger-Robertson partial transpose
PPT	positive partial transpose
SRPT	Schrödinger-Robertson partial transpose
PPT	positive partial transpose
SRPT	Schrödinger-Robertson partial transpose
PPT	positive partial transpose
SRPT	Schrödinger-Robertson partial transpose
PPT	positive partial transpose
SRPT	Schrödinger-Robertson partial transpose
PPT	positive partial transpose
SRPT	Schrödinger-Robertson partial transpose
PPT	positive partial transpose
SRPT	Schrödinger-Robertson partial transpose

PPT	positive partial transpose
SRPT	Schrödinger-Robertson partial transpose
PPT	positive partial transpose
SRPT	Schrödinger-Robertson partial transpose
PPT	positive partial transpose
SRPT	Schrödinger-Robertson partial transpose
PPT	positive partial transpose
SRPT	Schrödinger-Robertson partial transpose
PPT	positive partial transpose
SRPT	Schrödinger-Robertson partial transpose
PPT	positive partial transpose
SRPT	Schrödinger-Robertson partial transpose
PPT	positive partial transpose
SRPT	Schrödinger-Robertson partial transpose
PPT	positive partial transpose
SRPT	Schrödinger-Robertson partial transpose
PPT	positive partial transpose
SRPT	Schrödinger-Robertson partial transpose
PPT	positive partial transpose
SRPT	Schrödinger-Robertson partial transpose
PPT	positive partial transpose
SRPT	Schrödinger-Robertson partial transpose
PPT	positive partial transpose
SRPT	Schrödinger-Robertson partial transpose
PPT	positive partial transpose
SRPT	Schrödinger-Robertson partial transpose
PPT	positive partial transpose
SRPT	Schrödinger-Robertson partial transpose
PPT	positive partial transpose
SRPT	Schrödinger-Robertson partial transpose
PPT	positive partial transpose
SRPT	Schrödinger-Robertson partial transpose

Glossary

Dipole Blockade	Phenomenon in which the simultaneous excitation of two atoms is inhibited by their dipolar interaction.
Cavity Induced Transparency	Phenomenon in which a cavity containing two atoms excited with light at a frequency halfway between the atomic frequencies contains the number of photons an empty cavity would contain.
Dipole Blockade	Phenomenon in which the simultaneous excitation of two atoms is inhibited by their dipolar interaction.
Cavity Induced Transparency	Phenomenon in which a cavity containing two atoms excited with light at a frequency halfway between the atomic frequencies contains the number of photons an empty cavity would contain.
Dipole Blockade	Phenomenon in which the simultaneous excitation of two atoms is inhibited by their dipolar interaction.
Cavity Induced Transparency	Phenomenon in which a cavity containing two atoms excited with light at a frequency halfway between the atomic frequencies contains the number of photons an empty cavity would contain.
Dipole Blockade	Phenomenon in which the simultaneous excitation of two atoms is inhibited by their dipolar interaction.
Cavity Induced Transparency	Phenomenon in which a cavity containing two atoms excited with light at a frequency halfway between the atomic frequencies contains the number of photons an empty cavity would contain.
Dipole Blockade	Phenomenon in which the simultaneous excitation of two atoms is inhibited by their dipolar interaction.
Cavity Induced Transparency	Phenomenon in which a cavity containing two atoms excited with light at a frequency halfway between the atomic frequencies contains the number of photons an empty cavity would contain.
Dipole Blockade	Phenomenon in which the simultaneous excitation of two atoms is inhibited by their dipolar interaction.
Cavity Induced Transparency	Phenomenon in which a cavity containing two atoms excited with light at a frequency halfway between the atomic frequencies contains the number of photons an empty cavity would contain.

Dipole Blockade	Phenomenon in which the simultaneous excitation of two atoms is inhibited by their dipolar interaction.
Cavity Induced Transparency	Phenomenon in which a cavity containing two atoms excited with light at a frequency halfway between the atomic frequencies contains the number of photons an empty cavity would contain.

Dipole Blockade	Phenomenon in which the simultaneous excitation of two atoms is inhibited by their dipolar interaction.
Cavity Induced Transparency	Phenomenon in which a cavity containing two atoms excited with light at a frequency halfway between the atomic frequencies contains the number of photons an empty cavity would contain.
Dipole Blockade	Phenomenon in which the simultaneous excitation of two atoms is inhibited by their dipolar interaction.
Cavity Induced Transparency	Phenomenon in which a cavity containing two atoms excited with light at a frequency halfway between the atomic frequencies contains the number of photons an empty cavity would contain.
Dipole Blockade	Phenomenon in which the simultaneous excitation of two atoms is inhibited by their dipolar interaction.
Cavity Induced Transparency	Phenomenon in which a cavity containing two atoms excited with light at a frequency halfway between the atomic frequencies contains the number of photons an empty cavity would contain.
Dipole Blockade	Phenomenon in which the simultaneous excitation of two atoms is inhibited by their dipolar interaction.
Cavity Induced Transparency	Phenomenon in which a cavity containing two atoms excited with light at a frequency halfway between the atomic frequencies contains the number of photons an empty cavity would contain.

Nomenclature

c Speed of light ($2.997\ 924\ 58 \times 10^{8}$ ms^{-1})
$\hbar$ Planck constant ($1.054\ 572\ 66 \times 10^{-34}$ Js)
k_B Boltzmann constant ($1.380\ 658 \times 10^{-23}$ JK^{-1})
Z_0 Impedance of free space ($376.730\ 313\ 461$ Ω)
μ_0 Permeability of free-space ($4\pi \times 10^{-7}$ Hm^{-1})
c Speed of light ($2.997\ 924\ 58 \times 10^{8}$ ms^{-1})
$\hbar$ Planck constant ($1.054\ 572\ 66 \times 10^{-34}$ Js)
k_B Boltzmann constant ($1.380\ 658 \times 10^{-23}$ JK^{-1})
Z_0 Impedance of free space ($376.730\ 313\ 461$ Ω)
μ_0 Permeability of free-space ($4\pi \times 10^{-7}$ Hm^{-1})
c Speed of light ($2.997\ 924\ 58 \times 10^{8}$ ms^{-1})
$\hbar$ Planck constant ($1.054\ 572\ 66 \times 10^{-34}$ Js)
k_B Boltzmann constant ($1.380\ 658 \times 10^{-23}$ JK^{-1})
Z_0 Impedance of free space ($376.730\ 313\ 461$ Ω)
μ_0 Permeability of free-space ($4\pi \times 10^{-7}$ Hm^{-1})
c Speed of light ($2.997\ 924\ 58 \times 10^{8}$ ms^{-1})
$\hbar$ Planck constant ($1.054\ 572\ 66 \times 10^{-34}$ Js)
k_B Boltzmann constant ($1.380\ 658 \times 10^{-23}$ JK^{-1})
Z_0 Impedance of free space ($376.730\ 313\ 461$ Ω)
μ_0 Permeability of free-space ($4\pi \times 10^{-7}$ Hm^{-1})
c Speed of light ($2.997\ 924\ 58 \times 10^{8}$ ms^{-1})
$\hbar$ Planck constant ($1.054\ 572\ 66 \times 10^{-34}$ Js)
k_B Boltzmann constant ($1.380\ 658 \times 10^{-23}$ JK^{-1})
Z_0 Impedance of free space ($376.730\ 313\ 461$ Ω)
μ_0 Permeability of free-space ($4\pi \times 10^{-7}$ Hm^{-1})
c Speed of light ($2.997\ 924\ 58 \times 10^{8}$ ms^{-1})
$\hbar$ Planck constant ($1.054\ 572\ 66 \times 10^{-34}$ Js)
k_B Boltzmann constant ($1.380\ 658 \times 10^{-23}$ JK^{-1})
Z_0 Impedance of free space ($376.730\ 313\ 461$ Ω)
μ_0 Permeability of free-space ($4\pi \times 10^{-7}$ Hm^{-1})

c Speed of light ($2.997\ 924\ 58 \times 10^8$ ms^{-1})
$\hbar$ Planck constant ($1.054\ 572\ 66 \times 10^{-34}$ Js)
k_B Boltzmann constant ($1.380\ 658 \times 10^{-23}$ JK^{-1})
Z_0 Impedance of free space ($376.730\ 313\ 461\ \Omega$)
μ_0 Permeability of free-space ($4\pi \times 10^{-7}$ Hm^{-1})
c Speed of light ($2.997\ 924\ 58 \times 10^8$ ms^{-1})
$\hbar$ Planck constant ($1.054\ 572\ 66 \times 10^{-34}$ Js)
k_B Boltzmann constant ($1.380\ 658 \times 10^{-23}$ JK^{-1})
Z_0 Impedance of free space ($376.730\ 313\ 461\ \Omega$)
μ_0 Permeability of free-space ($4\pi \times 10^{-7}$ Hm^{-1})
c Speed of light ($2.997\ 924\ 58 \times 10^8$ ms^{-1})
$\hbar$ Planck constant ($1.054\ 572\ 66 \times 10^{-34}$ Js)
k_B Boltzmann constant ($1.380\ 658 \times 10^{-23}$ JK^{-1})
Z_0 Impedance of free space ($376.730\ 313\ 461\ \Omega$)
μ_0 Permeability of free-space ($4\pi \times 10^{-7}$ Hm^{-1})
c Speed of light ($2.997\ 924\ 58 \times 10^8$ ms^{-1})
$\hbar$ Planck constant ($1.054\ 572\ 66 \times 10^{-34}$ Js)
k_B Boltzmann constant ($1.380\ 658 \times 10^{-23}$ JK^{-1})
Z_0 Impedance of free space ($376.730\ 313\ 461\ \Omega$)
μ_0 Permeability of free-space ($4\pi \times 10^{-7}$ Hm^{-1})
c Speed of light ($2.997\ 924\ 58 \times 10^8$ ms^{-1})
$\hbar$ Planck constant ($1.054\ 572\ 66 \times 10^{-34}$ Js)
k_B Boltzmann constant ($1.380\ 658 \times 10^{-23}$ JK^{-1})
Z_0 Impedance of free space ($376.730\ 313\ 461\ \Omega$)
μ_0 Permeability of free-space ($4\pi \times 10^{-7}$ Hm^{-1})
c Speed of light ($2.997\ 924\ 58 \times 10^8$ ms^{-1})
$\hbar$ Planck constant ($1.054\ 572\ 66 \times 10^{-34}$ Js)
k_B Boltzmann constant ($1.380\ 658 \times 10^{-23}$ JK^{-1})
Z_0 Impedance of free space ($376.730\ 313\ 461\ \Omega$)
μ_0 Permeability of free-space ($4\pi \times 10^{-7}$ Hm^{-1})

For Harry Wilson, the man who taught me everything.

Contents

List of Figures

List of Tables

Introduction

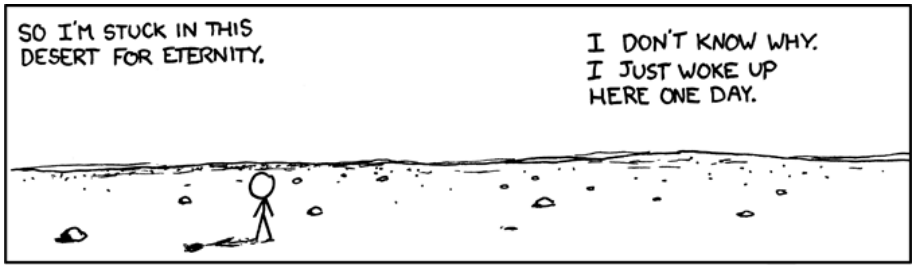

Randall Munroe, *A Bunch of Rocks* (part 1 of 9), `xkcd.com/505/`

Quantum entanglement is by far the most intriguing feature of quantum mechanics compared to any other classical theory. It plays a fundamental role in every apparent paradox or counter-intuitive consequence of quantum theory. Its mind-blowing properties have many, many application in a very large range of fields. In spite of this incredible success, characterization and classification of entanglement in a general state is still an open question of the quantum theory. That is the very issue that motivated this work. The first two chapters of this thesis introduce entanglement criteria of various domains of application that contribute to this search of entanglement characterization. For the rest of the thesis, we set aside the mathematical considerations and consider the fascinating problem of experimentally producing entanglement in physical systems and more particularly in systems of cold atoms. This entanglement production must come from ingredients available in the laboratories today: lasers, cavities, cold atoms in gazes or isolated and, most importantly, interatomic interactions. In chapters **??** to **??**, we consider dipole interactions between atoms and the phenomenon of dipole blockade as a mean to produce entanglement in systems of two or more atoms. In chapter 2, we explore the

many possibilities of cavity quantum electrodynamics. Every chapter just about stands on its own and will be duly self-introduced and placed into its context in the literature, but we present them briefly here.

Chapter 1 is devoted to *Multipartite Entanglement Criterion from Uncertainty Relations*. In this chapter, we describe a criterion which can experimentally detect the presence of entanglement in a wide variety of quantum states. That criterion is the love child of two great concepts in quantum mechanics, the Schrödinger-Robertson inequality (SRI) and the positive partial transpose (PPT) criterion. The SRI is a generalization of the even more famous Heisenberg inequality and describes how the product of the variances of two non-commuting operators can never be smaller than some particular minimal value. The PPT criterion shows that under the action of a particular mathematical operation, the partial transpose, the density matrix of a separable state must remain a physical quantity, whereas the density of an entangled state might very well not do so. By bringing those two concepts together, we were able to define the Schrödinger-Robertson partial transpose criterion. This criterion dictates that the product of the variances of two observables modified by the partial transpose operation will always be bounded by a minimal value when acting on a separable state. An entangled state, however, might violate the inequality, a certain sign of its entanglement. We show that in order to satisfy some constraints due to the SRI and the PPT criterion, the observables must obey some specific conditions and we show their general form for bipartite systems. We go on proving that our entanglement criterion is necessary and sufficient for any pure bipartite state or even any pure three-qubit state. We test its performances on a large variety of systems, harmonic oscillators, multi-photon polarization states, Schrödinger cat states and multipartite mixed states.

Chapter **??** is devoted to *Concurrences for N-qubit Systems*. In that chapter, we present another entanglement criterion inspired from the criterion of the concurrence. The concurrence is a mathematical criterion that not only detects entanglement in two-qubit states, but also quantifies the amount of entanglement for pure states or mixed states. We start the chapter by introducing the concurrence. Next, we give a series of

nine conditions that a pure three-qubit state must obey to be separable. We prove that those conditions are necessary and sufficient conditions to entanglement with a formalism that can easily be generalized to systems of more qubits. We then take advantage of those conditions to define concurrences for tripartite pure states. We show that those quantities are linked to other values used to evaluate tripartite entanglement. Using the formalism of the original concurrence, we prove that our concurrences can also be evaluated easily on mixed states. Any non-zero concurrence is a sure sign of entanglement. We finally test our criterion on different mixed states and find encouraging results. In the second part of the chapter we generalize the whole process to systems of N-qubits. We show that the number of conditions to separability grows very much with the number of qubits, but we can still compute them and we define generalized concurrences, which are necessary and sufficient conditions for entanglement in pure states. We finally prove that they may also be applied on mixed states.

Chapter **??** is devoted to *Entanglement, Antibunching, and Saturation Effects in Dipole Blockade* and leads the path of quantum information theory into the domain of quantum optics. In this chapter, we study the interaction of two identical two-level atoms immersed in a resonant laser field. The Hamiltonian model for the interaction is specifically chosen to describe the dipole blockade effect. In a blockaded system, one atom in its excited states prevents, with some degree, the other atom to get excited. The interest of such an interaction is the production of entanglement. Indeed, a system of two independent atoms can never be entangled by a laser, however a blockaded system is constrained to deal only with the ground state and a coherent superposition of "first atom excited, second not excited" and of the opposite situation and such a superposition is shown to carry maximal entanglement. After introducing our Hamiltonian, we introduce the master equation which modelizes dissipation effects in the system, allowing us, after a few considerations about the non-interactive case, to compute the time evolution of the system. We measure the concurrence as well as a quantity able to estimate the blockade on time-evolving states. We show that our model describes the dipole blockade well and

also that the strengthening of the laser power has the effect of lifting said blockade. Then, we study the equilibrium case, the steady state of the system and we give its analytical description as well as an analytical expression of its concurrence. That expression allows us to tune the laser power in order to maximize the amount of entanglement for a given interaction strength. Finally, we study another way to experimentally show the blockade effect, the photon-photon correlation.

Chapter **??** is devoted to *Dipole Blockade and Entanglement in Three-Atom Systems* and generalizes the Hamiltonian model for the dipole blockade effect on systems of three two-level atoms. We start by introducing the model, along with a particular basis which takes advantage of the possible symmetries of the system. We also define quantities which measure the blockade effect, which can now be considered for a particular pair of atoms or for the three of them altogether. We then consider several different cases of interaction: no interaction between the atoms, interaction between only two, same interaction between all atoms and aligned atoms with interaction between first neighbors only. For each case, we give an analytical value of the steady state and study their blockades. We observe blockades in the different cases with varying amplitudes except for one particular case where antiblockade is observed. After that, we study the two-atom concurrences by tracing out one atom and find that bipartite entanglement is weakened by the presence of a third interacting atom. Finally, we study tripartite entanglement using the three-qubit concurrences defined in chapter **??** and find indications of bipartite entanglement in the system as well as genuine tripartite entanglement.

Chapter **??** is devoted to *EIT, Dipole Blockade and Dipole-Dipole Interaction*. In this chapter, we introduce the electromagnetically induced transparency (EIT). The EIT is a phenomenon taking place in multi-level systems excited by two non-resonant lasers, the pump and the probe, where under some conditions the absorption of the probe laser is cancelled for a specific window of frequency. We start by quantifying this effect with the steady state of a single three-level atom and check established results. Then we investigated what would happen to the EIT if two atoms were to experience dipole blockade.

We introduce our model Hamiltonian and master equation, check the eigenstates of the system with the probe laser turned off. Armed with those weapons, we measure the dipole blockade in the system as well as the effect on EIT. In the second part of the chapter we test the effects of another type of interaction, the dipole-dipole interaction. We introduce our model, Hamiltonian and master equation, find the eigenstates of the unperturbed system and compute the values of the dipole blockade and the effect on EIT in the steady state. We find a strong modification in the behavior of the EIT.

Chapter 2 is the last chapter and is devoted to *Cavity Mediated Two-Photon Processes in Two-Qubit Circuit QED*. In free space, two non-identical two-level atoms may not be simultaneously excited by a laser through a two-photon process. We explore the possibility that this inhibition, due to interference effects, can be beaten by placing the atoms in a single mode cavity. After briefly checking what happens in free space, we give our model Hamiltonian an master equation which modelize the different atomic frequencies, the cavity mode, the interaction between them, the laser field exciting the cavity modes and the dissipation effects such as the atomic spontaneous emission and the cavity losses. We first make an assumption on the atomic frequencies which allows us to diagonalize the unperturbed Hamiltonian and find the eigenvalues and eigenstates of the bare system. Then, using a perturbative approach, we find that two-photon processes are indeed possible in such a system at some particular frequencies and we calculate the transition rates. We confirm our calculations by producing different atomic and photonic spectra in the steady state of the system. We find that the quality of the cavity has a strong effect on the structure of the spectra and induces behaviors not predicted by perturbation theory. In the last part of the chapter, we lift the constraint of the atomic frequency and confirm our results by numerically checking the same spectra for a most general configuration of the system. We also find a new feature of the system, the cavity induced transparency.

In the conclusion, we summarize all the results we were able to get and finally we give the appendices, which contain calculations not essential to the text as well as steady state

results too imposing to fit in the chapters.

Chapter 1

Multipartite Entanglement Criterion from Uncertainty Relations

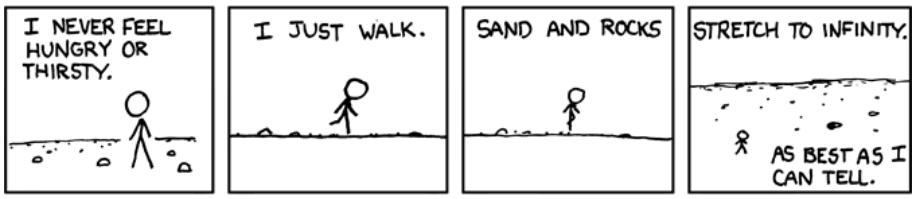

Randall Munroe, *A Bunch of Rocks* (part 2 of 9), `xkcd.com/505/`

In the past few years, many criteria detecting entanglement in bipartite and multipartite systems have been developed [1–3]. The Peres-Horodecki positive partial transpose (PPT) criterion [4] has played a crucial role in the field and provides, in some cases, necessary and sufficient conditions to entanglement. That criteria is formulated in terms of the density operator and any practical application involves state tomography. Other criteria have been proposed so they could be tested experimentally in a direct manner, as the Bell inequalities [5, 6] or the entanglement witnesses [7]. More recently, criteria based on variance measurements have been studied for continuous and discrete variable systems [8–20].

In [17] the Heisenberg relation has been used along with the partial transpose operation to obtain a criterion detecting entanglement condition in bipartite non-gaussian

states. That idea was generalized in [19, 20] with use of the Schrödinger-Robertson relation instead of the Heisenberg inequality. In this chapter, we generalize completely those concepts and prove that the Schrödinger-Robertson type inequality is able to detect entanglement in any pure state of bipartite and tripartite systems. Experimentally, it can be realized by measuring mean values and variances of different observables on a wide range of systems.

We start the chapter by introducing the Schrödinger-Robertson inequality and the PPT criterion in Sec. 1.1 and 1.2. In Sec. 1.3 we introduce our Schrödinger-Robertson partial transpose (SRPT) criterion and study its validity with a few properties of the partial transpose. We find that all observables are not suitable and we yield the general condition they must satisfy to be eligible. For 2×2 systems, we explicitly give their general form. Finally, we show that the SRPT criterion is necessary and sufficient in the case of bipartite pure states.

In Sec. 1.4, we study various different applications of the SRPT in the bipartite case, including angular momentum states of harmonic oscillators, cat states and multiphoton polarization states. In Sec. 1.5, we prove that our criterion is necessary and sufficient in the case of pure tripartite qubit states. Finally, in Sec. 1.6 we apply the criterion to mixed states and we show that the inequality detects entanglement of bipartite Werner states better than the Bell inequalities [5] and also leads to a good characterization of multipartite Werner states.

1.1 Schrödinger-Robertson Inequality

One of the great results of quantum mechanics is Heisenberg uncertainty principle, actually not a principle at all since it can be demonstrated. That principle states that one cannot measure simultaneously certain pairs of physical quantities with an arbitrarily large precision. More precisely, that uncertainty occurs when the observables corresponding to the physical quantities do not *commute*.

The Heisenberg uncertainty principle can actually be derived from a more general type of inequality, the Schrödinger-Robertson Inequality [21]. Let us consider two observables A and B and a general physical state ρ, expressed in the matrix density formalism. We define the complex quantity

$$z = \mathrm{Tr}\,(\rho AB) = \langle AB \rangle. \tag{1.1}$$

We find that

$$2i\,\mathrm{Im}(z) = \langle AB \rangle - \langle BA \rangle = \langle [A, B] \rangle, \tag{1.2}$$

$$2\,\mathrm{Re}(z) = \langle AB \rangle + \langle BA \rangle = \langle \{A, B\} \rangle, \tag{1.3}$$

where $[A, B] \equiv AB - BA$ and $\{A, B\} \equiv AB + BA$ are respectively the commutator and anticommutator of A and B. We therefore have

$$|\langle [A, B] \rangle|^2 + |\langle \{A, B\} \rangle|^2 = 4|\langle AB \rangle|^2. \tag{1.4}$$

Here, we apply Cauchy-Schwarz inequality and get

$$|\langle AB \rangle|^2 \leq \langle A^2 \rangle \langle B^2 \rangle, \tag{1.5}$$

which combined with Eq. (1.4) gives

$$|\langle [A, B] \rangle|^2 + |\langle \{A, B\} \rangle|^2 \leq 4\langle A^2 \rangle \langle B^2 \rangle. \tag{1.6}$$

Let us define some new observables $C = A - \langle A \rangle$ and $D = B - \langle B \rangle$. Clearly, we have

$$\langle [C, D] \rangle = \langle [A, B] \rangle, \tag{1.7}$$

$$\langle \{C, D\} \rangle = \langle \{A, B\} \rangle - 2\langle A \rangle \langle B \rangle. \tag{1.8}$$

Since we can write Eq. (1.6) for the observables C and D with the *variance*

$$(\Delta A)^2 = \langle (A - \langle A \rangle)^2 \rangle = \langle C^2 \rangle, \tag{1.9}$$

we can finally write the Schrödinger-Robertson Inequality:

$$(\Delta A)^2 (\Delta B)^2 \geq \frac{1}{4} |\langle [A, B] \rangle|^2 + \frac{1}{4} |\langle \{A, B\} \rangle - 2\langle A \rangle \langle B \rangle|^2. \tag{1.10}$$

This result is a remarkable and very general feature of quantum mechanics, which is completely inherent to the physical state being investigated and not at all related to the ability of a researcher to measure the quantities.

The Heisenberg inequality is simply obtained by ignoring the second term on the right-hand side of (1.10), which only accentuates the inequality.

1.2 Positive Partial Transpose Criterion

In 1996, Asher Peres [4] published a criterion able to characterize the entanglement in bipartite systems, either pure or mixed. Let us consider a separable system acting in $\mathcal{H}$ composed of two subsystems described by the individual density matrices ρ_i^1 et ρ_i^2. The state of the system is in general

$$\rho = \sum_i p_i \, \rho_i^1 \otimes \rho_i^2, \tag{1.11}$$

with $p_i \geq 0, \forall i$ et $\sum_i p_i = 1$. The individual matrix elements will be described as

$$\rho_{m\mu,n\nu} = \langle m\mu | \rho | n\nu \rangle = \sum_i p_i \, \left(\rho_i^1\right)_{mn} \left(\rho_i^2\right)_{\mu\nu}, \tag{1.12}$$

where the states described by latin indices are the basis states of the first subsystem and the ones described by the greek indices are those of the second subsystem, which may

have a different dimension. Let us form a new density matrix σ defined by

$$\sigma_{m\mu,n\nu} \equiv \rho_{n\mu,m\nu}. \tag{1.13}$$

The matrix σ is defined from ρ where the latin indices have been switched, but not the greek ones. This definition of σ is equivalent to

$$\sigma = \rho^{\mathrm{pt}} \equiv \sum_i p_i \left(\rho_i^1\right)^{\mathrm{T}} \otimes \rho_i^2, \tag{1.14}$$

where "pt" stands for *partial transpose* and represents the operator that transposes the density matrix of the first subsystem. The partial transpose of a density matrix as defined by Eq. (1.13) is a very general concept which holds for any state, entangled or not. It is also applicable to any bipartite hermitian operator A and we define similarly

$$\left(A^{\mathrm{pt}}\right)_{m\mu,n\nu} \equiv A_{n\mu,m\nu}. \tag{1.15}$$

The transposed density matrices $\left(\rho_i^1\right)^{\mathrm{T}}$ of our separable state are still hermitian, positive operators and therefore are legitimate density matrices describing a physical state, which implies that so does σ. In other words, any separable state must have a positive partial transpose. From the physical sense of σ, the Peres criterion is stated.

Criterion 1. Peres Criterion (PPT Criterion) — *If a bipartite state described by the density matrix ρ is separable, then its partial transpose ρ^{pt} is positive.*

Equivalently, if one eigenvalues of ρ^{pt} is found to be negative, then the state ρ is entangled.

This first statement of the criterion is only a necessary condition and was unfortunately proven to remain only necessary for the general case. However, its was proven by the Horodecki [22] that this criterion was indeed necessary and sufficient in the case of systems of dimension 2×2 or 2×3.

Criterion 2. Peres-Horodecki Criterion — *A bipartite state described by the density matrix ρ of dimension 2×2 or 2×3 is separable if and only if its partial transpose ρ^{pt} is positive.*

Although this criterion is very powerful, it cannot be implemented experimentally right away since the operation of partial transposition is a mathematical operator and not a physical one. That is why we found a way to make use of the PPT criterion in an experimental context, namely the measurement of Scrödinger-Robertson inequalities.

1.3 Schrödinger-Robertson Partial Transpose Criterion

For any observables A, B and any density operator ρ, the Schrödinger-Robertson inequality is observed. In this section, we use that property together with the PPT criterion to build a new entanglement criterion.

The partial transpose ρ^{pt} of a bipartite separable density operator must be positive, which implies it does describe some physical state and must therefore obey the Schrödinger-Robertson uncertainty relation for any observables A and B, i.e. Eq. (1.10) also holds with ρ^{pt} if ρ is separable. In the density matrix formalism, this inequality is written

$$\begin{aligned}&\left(\text{Tr}\left(\rho^{\text{pt}}A\right)^2 - \text{Tr}\left(\rho^{\text{pt}}A^2\right)\right)\left(\text{Tr}\left(\rho^{\text{pt}}B\right)^2 - \text{Tr}\left(\rho^{\text{pt}}B^2\right)\right)\\ &\qquad \geq \tfrac{1}{4}\left|\text{Tr}\left(\rho^{\text{pt}}[A,B]\right)\right|^2 + \tfrac{1}{4}\left|\text{Tr}\left(\rho^{\text{pt}}\{A,B\}\right) - 2\text{Tr}\left(\rho^{\text{pt}}A\right)\text{Tr}\left(\rho^{\text{pt}}B\right)\right|^2.\end{aligned} \tag{1.16}$$

This inequality always holds when applied on separable state, but might not do so when ρ^{pt} represents a non-physical state, i. e. when ρ is entangled. Since we cannot produce a ρ^{pt} states with the experimental tools available, we could think of "switching" the partial transpose sign from $\text{Tr}\left(\rho^{\text{pt}}A\right)$ to $\text{Tr}\left(\rho A^{\text{pt}}\right)$ and from $\text{Tr}\left(\rho^{\text{pt}}A^2\right)$ to $\text{Tr}\left(\rho(A^{\text{pt}})^2\right)$, which would yield the Scrödinger-Robertson partial transpose (SRPT) inequality

$$(\Delta A^{\text{pt}})^2(\Delta B^{\text{pt}})^2 \geq \frac{1}{4}|\langle[A,B]^{\text{pt}}\rangle|^2 + \frac{1}{4}|\langle\{A,B\}^{\text{pt}}\rangle - 2\langle A^{\text{pt}}\rangle\langle B^{\text{pt}}\rangle|^2, \tag{1.17}$$

which would never be violated for separable states and violated by entangled states only. The key result of this chapter is that unlike the PPT criterion in itself, Eq. (1.17) has the property of being experimentally implementable since it deals with observable quantities. However, "switching" the partial transpose sign is not a trivial operation, we need to make sure the operation is valid.

First of all the partial transpose A^{pt} of an observable A must remain an observable; if that is the case then the mean value $\text{Tr}\,(\rho A^{\text{pt}})$ of a partially transposed observable must be equal to the mean value $\text{Tr}\,(\rho^{\text{pt}} A)$ of the observable measured on the partially transposed density matrix and finally the value of the variance $(\Delta A^{\text{pt}})^2$ must also follow that rule. In the next subsection, we investigate those conditions and prove a few properties, which will lead us to believe that not all observables can be considered in order to get a valid SRPT relation.

1.3.1 Properties of the Partial Transposition

In this subsection, we talk about a pair observables A or B that are considered to act on a system composed of two subsystems of size n and n', finite or not. We consider the matrix elements $A^{\dagger}_{i\mu,j\nu}$ with the latin indices i, j referring to the first subsystem taking the values $1, 2, \cdots, n$ and the greek indices μ, ν referring to the second subsystem taking the values $1, 2, \cdots, n'$.

Property 1.1. *The partial transposition of an observable A is an observable.*

Proof: The only requirement for an operator A to be an observable is to be hermitian, i. e. to verify $A^{\dagger} = A$. We have

$$\begin{aligned}\left((A^{\mathrm{pt}})^{\dagger}\right)_{i\mu,j\nu} &= (A^{\mathrm{pt}})^{*}_{j\nu,i\mu}, && (1.18)\\ &= A^{*}_{i\nu,j\mu}, && (1.19)\\ &= A_{j\mu,i\nu}, && (1.20)\\ &= (A^{\mathrm{pt}})_{i\mu,j\nu}, && (1.21)\end{aligned}$$

which concludes the proof.

The next proposition deals with the mean values of observables.

Property 1.2. *For any operators A, B, we have*

$$\mathrm{Tr}\left(A^{\mathrm{pt}}B\right) = \mathrm{Tr}\left(AB^{\mathrm{pt}}\right). \tag{1.22}$$

Proof: in order to simplify the developments, we use the convention of a repeated index implying a summation over all values of said index. We have

$$\begin{aligned}\mathrm{Tr}\left(A^{\mathrm{pt}}B\right) &= (A^{\mathrm{pt}}B)_{i\mu,i\mu} = (A^{\mathrm{pt}})_{i\mu,l\lambda}\, B_{l\lambda,i\mu}, && (1.23)\\ &= A_{l\mu,i\lambda}B_{l\lambda,i\mu} = A_{l\mu,i\lambda}\left(B^{\mathrm{pt}}\right)_{i\lambda,l\mu}, && (1.24)\\ &= (AB^{\mathrm{pt}})_{l\mu,l\mu} = \mathrm{Tr}\left(AB^{\mathrm{pt}}\right), && (1.25)\end{aligned}$$

which concludes.

Hence, if B represents a density matrix, this result means that the mean value of a partially transposed observable is equal to the mean value of the observable measured on the partially transposed density matrix. The next proposition deals with the variance.

Property 1.3. *For any observable A, we have*

$$\mathrm{Tr}\left(\rho^{\mathrm{pt}}A^{2}\right) = \mathrm{Tr}\left(\rho\left(A^{\mathrm{pt}}\right)^{2}\right), \tag{1.26}$$

for any density matrix ρ if and only if

$$(A^{\mathrm{pt}})^2 = \left(A^2\right)^{\mathrm{pt}}. \tag{1.27}$$

Proof: if $(A^{\mathrm{pt}})^2 = (A^2)^{\mathrm{pt}}$, then the result is a direct consequence of Prop. 1.2. On the other hand, if the traces are identical

$$\mathrm{Tr}\left(\rho^{\mathrm{pt}} A^2\right) - \mathrm{Tr}\left(\rho\,(A^{\mathrm{pt}})^2\right) = \mathrm{Tr}\left(\rho\left[\left(A^2\right)^{\mathrm{pt}} - (A^{\mathrm{pt}})^2\right]\right) = 0, \tag{1.28}$$

and in particular, we must have

$$\langle\psi|\left(A^2\right)^{\mathrm{pt}} - (A^{\mathrm{pt}})^2\,|\psi\rangle = 0, \tag{1.29}$$

for *any* state vector $|\psi\rangle$ including all the eigenstates of the observable, which is only possible if $(A^{\mathrm{pt}})^2 = (A^2)^{\mathrm{pt}}$. This result shows that the variance $(\Delta A^{\mathrm{pt}})^2 = \mathrm{Tr}\,(\rho(A^{\mathrm{pt}})^2) - \mathrm{Tr}\,(\rho A^{\mathrm{pt}})^2$ is not always equal to the variance $(\Delta A)^2$ applied on the partially transposed state ρ^{pt}.

This result is the major constraint about using SRPT inequalities. In general, observables do not satisfy Eq. (1.27), which can result in a violation of an SRPT inequality applied on a separable state with unsuitable observables.

To illustrate this, we consider the inequality corresponding to the computational basis vector $|00\rangle$ of a two-qubit system using the observables

$$A = \sigma_x \otimes \sigma_x, \tag{1.30}$$

$$B = \sigma_x \otimes \sigma_y + \sigma_y \otimes \sigma_x, \tag{1.31}$$

with σ_x and σ_y the Pauli operators. Even though the state $|00\rangle$ is separable, we find $\Delta B^{\mathrm{pt}} = 0$ and $|\langle[A,B]^{\mathrm{pt}}\rangle| = 2$ which means the SRPT inequality is violated. That violation could happen since $(B^{\mathrm{pt}})^2 \neq (B^2)^{\mathrm{pt}}$. This example illustrates the importance of

using suitable observables in the SRPT inequality. Now that we defined the conditions for the SRPT inequality to be used, we can formulate our new criterion.

Criterion 3. Schrödinger-Robertson Partial Transpose Criterion — *If there are two observables A, B satisfying*

$$(A^{\mathrm{pt}})^2 = \left(A^2\right)^{\mathrm{pt}}, \ (B^{\mathrm{pt}})^2 = \left(B^2\right)^{\mathrm{pt}}, \tag{1.32}$$

such that the Schrödinger-Robertson inequality

$$(\Delta A^{\mathrm{pt}})^2(\Delta B^{\mathrm{pt}})^2 \geq \frac{1}{4}|\langle [A,B]^{\mathrm{pt}}\rangle|^2 + \frac{1}{4}|\langle \{A,B\}^{\mathrm{pt}}\rangle - 2\langle A^{\mathrm{pt}}\rangle\langle B^{\mathrm{pt}}\rangle|^2, \tag{1.33}$$

measured on a state ρ is violated, then the ρ is entangled.

1.3.2 Form of the Suitable Observables

The first step into actually being able to use our criterion is getting more information about the specific observables that can be used. If there is no observable A satisfying Eq. (1.27), then the criterion is useless. In the following, we show that such observables do exist and that the criterion is actually necessary and sufficient for bipartite pure states.

Let us now characterize the form of the observables A of dimension $N = n \times n'$ that satisfy $(A^{\mathrm{pt}})^2 = (A^2)^{\mathrm{pt}}$. In order to do so, wee need to define a matrix orthogonal basis that will span all hermitian matrices.

Suitable candidates for that basis are the infinitesimal generators of the special unitary group SU(N), as they are all hermitian. The number of independent generators of SU(N) is $N^2 - 1$ and we need to add the identity matrix to the set to obtain the matrix basis we are looking for.

By definition, the $N^2 - 1$ generators S_i are $N \times N$, traceless and hermitian matrices such that

$$S_a S_b = \frac{1}{2N}\delta_{ab} I_N + \frac{1}{2}\sum_{c=1}^{N^2-1}(if_{abc} + d_{abc})S_c, \tag{1.34}$$

with $a, b = 1, 2, \cdots, N^2 - 1$ and where I_N is the $N \times N$ identity matrix ,δ_{ab} the Kronecker symbol, the f_{abc} and d_{abc} are structure constants and are respectively antisymmetric and symmetric in all indices. As it follows,

$$\{S_a, S_b\} = \frac{1}{N}\delta_{ab} I_N + \sum_{c=1}^{N^2-1} d_{abc} S_c, \tag{1.35}$$

$$[S_a, S_b] = i \sum_{c=1}^{N^2-1} f_{abc} S_c. \tag{1.36}$$

That basis is orthogonal in the sense of the inner product

$$2 \text{ Tr}\,(S_a S_b) = \delta_{ab}. \tag{1.37}$$

The Pauli matrices

$$\sigma_x = \begin{pmatrix} 0 & 1 \\ 1 & 0 \end{pmatrix}, \quad \sigma_y = \begin{pmatrix} 0 & -i \\ i & 0 \end{pmatrix}, \quad \sigma_z = \begin{pmatrix} 1 & 0 \\ 0 & -1 \end{pmatrix}, \tag{1.38}$$

are (when divided by 2) such examples of generators for $N = 2$, in which case the d constants are all zero and the f constants take the values of the Levi-Civita symbol ϵ_{ijk}. The Gell-Mann matrices

$$\lambda_1 = \begin{pmatrix} 0 & 1 & 0 \\ 1 & 0 & 0 \\ 0 & 0 & 0 \end{pmatrix}, \quad \lambda_2 = \begin{pmatrix} 0 & -i & 0 \\ i & 0 & 0 \\ 0 & 0 & 0 \end{pmatrix}, \quad \lambda_3 = \begin{pmatrix} 1 & 0 & 0 \\ 0 & -1 & 0 \\ 0 & 0 & 0 \end{pmatrix},$$

$$\lambda_4 = \begin{pmatrix} 0 & 0 & 1 \\ 0 & 0 & 0 \\ 1 & 0 & 0 \end{pmatrix}, \quad \lambda_5 = \begin{pmatrix} 0 & 0 & -i \\ 0 & 0 & 0 \\ i & 0 & 0 \end{pmatrix}, \quad \lambda_6 = \begin{pmatrix} 0 & 0 & 0 \\ 0 & 0 & 1 \\ 0 & 1 & 0 \end{pmatrix}, \tag{1.39}$$

$$\lambda_7 = \begin{pmatrix} 0 & 0 & 0 \\ 0 & 0 & -i \\ 0 & i & 0 \end{pmatrix}, \quad \lambda_8 = \frac{1}{\sqrt{3}} \begin{pmatrix} 1 & 0 & 0 \\ 0 & 1 & 0 \\ 0 & 0 & -2 \end{pmatrix},$$

are also matrices of that form for $N = 3$ when divided by 2 for normalization.

Generalizing from the Pauli and Gell-Mann matrices, we can find a general set of SU(N) infinitesimal generators. Written in an operator-like fashion on the basis $\{|1\rangle, |2\rangle, \cdots, |N\rangle\}$ we find the first set of $(N^2 - N)/2$ matrices

$$S_{i,j}^{(1)} = \frac{1}{2}(|i\rangle\langle j| + |j\rangle\langle i|), \tag{1.40}$$

for $i = 1, 2, \cdots, N-1$ and $j = i+1, i+2, \cdots, N$. With the same conditions on i, j we give the second set of $(N^2 - N)/2$ matrices

$$S_{i,j}^{(2)} = \frac{-i}{2}(|i\rangle\langle j| - |j\rangle\langle i|). \tag{1.41}$$

The last set of $N - 1$ matrices is given by

$$S_i^{(3)} = \frac{1}{\sqrt{2(i^2+i)}}\left(\sum_{k=1}^{i}|k\rangle\langle k| - i|i+1\rangle\langle i+1|\right), \tag{1.42}$$

for $i = 1, 2, \cdots, N-1$. All the matrices are properly normalized, and by relabeling them, one finds a set of $N^2 - 1$ matrices with the coefficients f_{abc}, d_{abc} easily found from the commutation and anticommutation relations.

Let us now consider a general system composed of two subsystems of respective dimensions n and n', with $N = n \times n'$, which are spanned by the base matrices S_i and S'_i with structure constants f, d and f', d'. We add to the basis identity matrices by defining $S_0 \equiv I_n/\sqrt{2n}$ and $S'_0 \equiv I_{n'}/\sqrt{2n'}$ and use once again the convention that any repeated index implies a sum over all of its possible values. We can therefore write a general hermitian matrix A as

$$A = a_{ij} S_i \otimes S'_j, \tag{1.43}$$

with the real coefficients a_{ij} defined as $a_{ij} \equiv 4\mathrm{Tr}\left(A S_i \otimes S'_j\right)$ and i and j running from 0

to n^2-1 and n'^2-1. Hence, we have

$$(A^{\mathrm{pt}})^2 = a_{ij}a_{kl}(S_kS_i)^{\mathrm{T}} \otimes S'_jS'_l, \tag{1.44}$$

$$\left(A^2\right)^{\mathrm{pt}} = a_{kj}a_{il}(S_kS_i)^{\mathrm{T}} \otimes S'_jS'_l. \tag{1.45}$$

We can see that if S_k and S_i commute, one only needs to switch their order in Eq. (1.45) and rename i as k and vice versa for the matrices to be equal. However, given the commutation property (1.36), it is clear that in general they do not do so and the only matrix that is assured to commute with all others is the identity matrix S_0. The same can be said of S'_j and S'_l and therefore, we see that every term with a 0 index in (1.44) will be found exactly the same in (1.45), which means there are no restrictions on the values of the a_{ij} coefficients when i or j is zero. For the rest of the $(n-1)\times(n'-1)$ coefficients, we need to investigate further. Letting go of all the terms including a zero index, we find that the quantities (1.44) and (1.45) are equal if and only if

$$0 = (a_{ij}a_{kl}-a_{kj}a_{il})(S_kS_i)^{\mathrm{T}} \otimes S'_jS'_l, \tag{1.46}$$

$$= \frac{1}{4}(a_{ij}a_{kl}-a_{kj}a_{il})\left(\delta_{ki}\frac{I_n}{n}+(if_{kip}+d_{kip})S_p^{\mathrm{T}}\right)\otimes\left(\delta_{jl}\frac{I_{n'}}{n'}+(if'_{jlq}+d'_{jlq})S'_q\right), \tag{1.47}$$

$$= \frac{1}{4}(a_{ij}a_{kl}-a_{kj}a_{il})\left((if_{kip}+d_{kip})S_p^{\mathrm{T}}\right)\otimes\left((if'_{jlq}+d'_{jlq})S'_q\right), \tag{1.48}$$

$$= -\frac{1}{4}f_{kip}f'_{jlq}(a_{ij}a_{kl}-a_{kj}a_{il})S_p^{\mathrm{T}}\otimes S'_q, \tag{1.49}$$

$$= -\frac{1}{2}f_{kip}f'_{jlq}a_{ij}a_{kl}S_p^{\mathrm{T}}\otimes S'_q, \tag{1.50}$$

$$\tag{1.51}$$

where in the third and fourth step we used the fact that an antisymmetric quantity such as $(a_{ij}a_{kl}-a_{kj}a_{il})$ summed with a symmetric factor δ_{ki} or d_{kip} will amount to zero and in the last step we noted that $f_{kip}f'_{jlq}a_{kj}a_{il} = -f_{kip}f'_{jlq}a_{ij}a_{jl}$. We end up with an null operator expressed in the $S_p^{\mathrm{T}}\otimes S'_q$ basis which is completely legitimate and we find the

following result : the matrix A will satisfy $(A^{\mathrm{pt}})^2 = (A^2)^{\mathrm{pt}}$ if and only if

$$f_{kip} f'_{jlq} a_{ij} a_{kl} = 0, \tag{1.52}$$

for all p, q and all indices above 0.

In the case of two-qubit systems, that condition has a simple interpretation. Indeed, for 2×2 systems, the Pauli matrices form the matrix basis and the condition is expressed as

$$\epsilon_{kip} \epsilon_{jlq} a_{ij} a_{kl} = 0, \tag{1.53}$$

for all p, q above 0, which expresses that every 2×2 minor of the 3×3 matrix a_{ij} must be zero. Therefore all the lines (or columns) of that matrix must be linearly dependent and we can write $a_{ij} = a_i b_j$. The general form of the matrices is then

$$A = (\mathbf{a} \cdot \boldsymbol{\sigma}) \otimes (\mathbf{b} \cdot \boldsymbol{\sigma}) + I_2 \otimes (\mathbf{c} \cdot \boldsymbol{\sigma}) + (\mathbf{d} \cdot \boldsymbol{\sigma}) \otimes I_2 + \eta \, I_4, \tag{1.54}$$

where $\boldsymbol{\sigma}$ is the vector composed of the 3 Pauli operators, $\mathbf{a}, \mathbf{b}, \mathbf{c}$ and $\mathbf{d}$ are four real vectors and η is a real number.

As a particular case of this general result, we note that if A can be written as $A_1 \otimes A_2$ with A_1 and A_2 two observables from the two subsystems, then A satisfies Eq. (1.27) immediately.

1.3.3 Necessary and sufficient criterion for pure states

In this subsection we state a necessary and sufficient version of our criterion.

Criterion 4. SRPT Criterion with Pure States — *A bipartite pure state* $|\psi\rangle \in \mathcal{H}_1 \otimes \mathcal{H}_2$*, with* $\mathcal{H}_1$ *and* $\mathcal{H}_2$ *two Hilbert spaces of any dimension is entangled if and only if there are observables* A*,* B *acting on* $\mathcal{H}_1 \otimes \mathcal{H}_2$ *satisfying*

$$(A^{\mathrm{pt}})^2 = \left(A^2\right)^{\mathrm{pt}}, \ (B^{\mathrm{pt}})^2 = \left(B^2\right)^{\mathrm{pt}}, \tag{1.55}$$

such that the SRPT inequality

$$(\Delta A^{\mathrm{pt}})^2 (\Delta B^{\mathrm{pt}})^2 \geq \frac{1}{4}|\langle [A,B]^{\mathrm{pt}}\rangle|^2 + \frac{1}{4}|\langle \{A,B\}^{\mathrm{pt}}\rangle - 2\langle A^{\mathrm{pt}}\rangle\langle B^{\mathrm{pt}}\rangle|^2, \tag{1.56}$$

is violated.

Proof: Let us consider an entangled state $|\psi\rangle$ and express it in the following decomposition:

$$|\psi\rangle = \sum_i c_i |i\rangle_1 \otimes |i\rangle_2, \tag{1.57}$$

where the $|i\rangle_j$ are a basis of $\mathcal{H}_j$ and the c_i complex numbers. Such a decomposition is always possible, the Schmidt decomposition being a particular one with real c_i coefficients [1]. We will work in the $|ij\rangle \equiv |i\rangle_1 \otimes |j\rangle_2$ basis, expressing operators through that basis.

If there is only one non-zero coefficient c_0, the state is written $|\psi\rangle = |00\rangle$ and is obviously separable. Therefore, since $|\psi\rangle$ is entangled, there are at least two non-zero coefficients; let us assume without loss of generality $c_0 \neq 0 \neq c_1$. We define two observables

$$A = |01\rangle\langle 01|, \tag{1.58}$$

$$B = \sigma_x \otimes \sigma_x, , \tag{1.59}$$

with the Pauli operator $\sigma_x \equiv |0\rangle\langle 1| + |1\rangle\langle 0|$. First, we have $A^{\mathrm{pt}} = A$, $B^{\mathrm{pt}} = B$ and we find

that

$$(A^{\mathrm{pt}})^2 = (|01\rangle\langle 01|)^{\mathrm{pt}}(|01\rangle\langle 01|)^{\mathrm{pt}} = |01\rangle\langle 01|, \tag{1.60}$$

$$\left(A^2\right)^{\mathrm{pt}} = (|01\rangle\langle 01| \cdot |01\rangle\langle 01|)^{\mathrm{pt}} = |01\rangle\langle 01|, \tag{1.61}$$

$$(B^{\mathrm{pt}})^2 = B^2 = \sigma_x\sigma_x \otimes \sigma_x\sigma_x = I_4, \tag{1.62}$$

$$\left(B^2\right)^{\mathrm{pt}} = I_4^{\mathrm{pt}} = I_4, \tag{1.63}$$

therefore A and B do satisfy Eq. (1.55). We further find

$$A \cdot B = |01\rangle\langle 10| \tag{1.64}$$

$$[A,B]^{\mathrm{pt}} = (|01\rangle\langle 10| - |10\rangle\langle 01|)^{\mathrm{pt}} = |11\rangle\langle 00| - |00\rangle\langle 11|, \tag{1.65}$$

$$\{A,B\}^{\mathrm{pt}} = (|01\rangle\langle 10| + |10\rangle\langle 01|)^{\mathrm{pt}} = |11\rangle\langle 00| + |00\rangle\langle 11|. \tag{1.66}$$

For the mean values,

$$\langle A^{\mathrm{pt}}\rangle = \langle\psi|01\rangle\langle 01|\psi\rangle = 0, \tag{1.67}$$

$$(\Delta A^{\mathrm{pt}})^2 = \langle (A^{\mathrm{pt}})^2\rangle = \langle\psi|01\rangle\langle 01|\psi\rangle = 0, \tag{1.68}$$

hence we do not need to calculate $\langle B^{\mathrm{pt}}\rangle$ or $(\Delta B^{\mathrm{pt}})^2$ since they will not appear in the final SRPT inequality. We also have

$$\frac{1}{4}|\langle [A,B]^{\mathrm{pt}}\rangle|^2 = \frac{1}{4}|c_0^*c_1 - c_0c_1^*|^2 = \mathrm{Im}(c_0^*c_1)^2 \tag{1.69}$$

$$\frac{1}{4}|\langle \{A,B\}^{\mathrm{pt}}\rangle - 2\langle A^{\mathrm{pt}}\rangle\langle B^{\mathrm{pt}}\rangle|^2 = \frac{1}{4}|c_0^*c_1 + c_0c_1^*|^2 = \mathrm{Re}(c_0^*c_1)^2. \tag{1.70}$$

The SRPT inequality is then written

$$0 \geq \mathrm{Re}(c_0^*c_1)^2 + \mathrm{Im}(c_0^*c_1)^2 = |c_0|^2|c_1|^2, \tag{1.71}$$

and is always violated for non-zero c_0 and c_1. We therefore have an experimentally

implementable necessary and sufficient criterion for bipartite entanglement on pure states.

The case of mixed states is a more complicated one. To this date, there is still no general method allowing to show the entanglement of two subsystems of any dimensions. Our original criterion remains: if one can find a couple of observables satisfying Eq. (1.55) and violating a SRPT inequality, then the mixed state is entangled, however there is no general method to find such observables given a particular entangled state or to even prove their existence.

1.4 Applications to Bipartite Systems

We will now discuss some applications of the SRPT inequality starting by the bipartite case.

2D Harmonic Oscillator.

We consider entanglement in states of an isotropic two dimensional oscillator with definite energy and angular momentum (see e.g. Ref. [23] describing the experimental production of entangled angular momentum states of photons). Those states are the common eigenvectors $|\psi_{k,M}\rangle$ (k, M integers) of the hamiltonian

$$H = \hbar\omega(aa^\dagger + bb^\dagger + 1), \tag{1.72}$$

with a and b the oscillator annihilation operators and of the angular momentum

$$L_z = i\hbar(ab^\dagger - a^\dagger b), \tag{1.73}$$

with eigenvalues $\hbar\omega(n+1)$ (with $n = 2k + |M|$) and $\hbar M$, respectively . The states $|\psi_{k,M}\rangle$ is expressed in the number state basis $|n_1, n_2\rangle$ as

$$|\psi_{k,M}\rangle = \sum_{j=0}^{n} c_j |n-j, j\rangle, \tag{1.74}$$

with

$$c_j = (-\text{sign}(M)i)^j \sqrt{\frac{\binom{n}{k}}{2^n \binom{n}{j}}} \sum_{l=0}^{j} (-1)^l \binom{k+|M|}{l} \binom{k}{j-l}. \tag{1.75}$$

The proof of that result is shown in Appendix A. The decomposition (1.74) is already in a Schmidt-like basis (with the c_j complex) hence if there are two non zero coefficients, the state is entangled and it is a simple application of the proof for pure states to find the observables that will detect the entanglement. It is easy to find

$$c_0 = \sqrt{\frac{\binom{n}{k}}{2^n}}, \tag{1.76}$$

and in Appendix A we also show the additional property $|c_j| = |c_{n-j}|$. Therefore, except for the ground state for which $c_0 = 1$, all angular momentum eigenstates are entangled in terms of the number states and the entanglement is well detected by the pair of observables

$$A = |ii\rangle\langle ii|, \tag{1.77}$$

$$B = \sigma_x^{(i,j)} \otimes \sigma_x^{(i,j)}, \tag{1.78}$$

with $\sigma_x^{(i,j)} \equiv |i\rangle\langle j| + |j\rangle\langle i|$ and $i + j = n$ which yields for those states the SRPT inequality

$$|c_i||c_j| = |c_i|^2 \leq 0, \tag{1.79}$$

evidently violated for $i = 0$, but in general for several other values as well.

Multiphoton Polarization State.

For some particular experiments, the SRPT inequality can be particularly efficient. Here, we show that on some multiphoton polarization states, the detection of entanglement only involves the measurement of two projectors. Let us consider the entangled two-photon state

$$|\psi\rangle = \alpha|0,2\rangle + \beta|1,1\rangle + \gamma|2,0\rangle, \tag{1.80}$$

where α, β, γ are arbitrary coefficients such that $\mathrm{Re}(\alpha^*\gamma) \neq 0$ and $|m,n\rangle$ denotes m photons in a given polarization state and n photons orthogonally polarized to the m firsts. The production and properties of those states have been studied in [24]. Of course, this state is also entangled since it is already in a Schmidt-like basis. Using the observables

$$A = |00\rangle\langle 00|, \tag{1.81}$$

$$B = \sigma_x^{(0,2)} \otimes \sigma_x^{(0,2)}, \tag{1.82}$$

and dropping the commutator term in (1.17), we get the inequality $0 \geq |\mathrm{Re}(\alpha^*\gamma)|$. Since $|\psi\rangle$ is never the vacuum, we have $\langle A^{\mathrm{pt}}\rangle = \Delta A^{\mathrm{pt}} = 0$ and B^{pt} does not need to be measured. All that is needed to detect entanglement is the measurement of

$$\{A,B\}^{\mathrm{pt}} = |02\rangle\langle 20| + |20\rangle\langle 02| = |\psi^+\rangle\langle\psi^+| - |\psi^-\rangle\langle\psi^-|, \tag{1.83}$$

with $|\psi^\pm\rangle \equiv (|02\rangle \pm |20\rangle)/\sqrt{2}$. More generally, the entanglement of an N-photon state of the form $\sum_{i=0}^{N} c_i|i, N-i\rangle$ will always be easily detectable with similar observables.

Cat States.

In quantum electrodynamics (QED), a coherent state α is defined to be an eigenstate of the annihilation operator a, with the eigenvalue α, i. e. $a|\alpha\rangle = \alpha|\alpha\rangle$ and can be written

as

$$|\alpha\rangle = e^{-\frac{|\alpha|^2}{2}} \sum_{n=0}^{\infty} \frac{\alpha^n}{\sqrt{n!}} |n\rangle, \tag{1.84}$$

with $|n\rangle$ the Fock state basis of the considered mode.

We consider the normalized Schrödinger cat state

$$|\psi\rangle = \frac{1}{\mathcal{N}}(|\alpha, \beta\rangle + |-\alpha, -\beta\rangle), \tag{1.85}$$

where $|\alpha\rangle, |\beta\rangle$ are coherent states and $\mathcal{N} = \sqrt{2 + 2e^{-2|\alpha|^2 - 2|\beta|^2}}$. The state $|\psi\rangle$ is a bipartite even state whose production and properties are discussed in [25]. We want to find operators that will show its entanglement with an SRPT inequality.

Our first step to simplify the problem is to find a basis in which α can be considered real. Let us consider that the cast state $|\alpha\rangle$ is expressed in the electromagnetic field mode a. The quadrature operators are defined as

$$x = \frac{1}{\sqrt{2}}(a^\dagger + a), \tag{1.86}$$

$$p = \frac{i}{\sqrt{2}}(a^\dagger - a), \tag{1.87}$$

$$\tag{1.88}$$

and by remembering that the cat states are eigenvalues of the annihilation operator, we easily find for the mean values

$$\langle\alpha|x|\alpha\rangle = \frac{1}{\sqrt{2}}(\alpha^* + \alpha) = \sqrt{2}\mathrm{Re}(\alpha), \tag{1.89}$$

$$\langle\alpha|p|\alpha\rangle = \frac{i}{\sqrt{2}}(\alpha^* - \alpha) = \sqrt{2}\mathrm{Im}(\alpha). \tag{1.90}$$

$$\tag{1.91}$$

We can always find a rotated basis such that we do not need to deal with imaginary

parts, let us define

$$\begin{aligned} x' &= \cos\theta\, x + \sin\theta\, p = \frac{1}{\sqrt{2}}\left(a^\dagger(\cos\theta + i\sin\theta) + a(\cos\theta - i\sin\theta)\right), \\ &= \frac{1}{\sqrt{2}}\left(b^\dagger + b\right), \qquad (1.92) \\ p' &= -\sin\theta\, x + \cos\theta\, p = \frac{i}{\sqrt{2}}\left(a^\dagger(\cos\theta + i\sin\theta) - a(\cos\theta - i\sin\theta)\right), \\ &= \frac{i}{\sqrt{2}}\left(b^\dagger - b\right), \qquad (1.93) \\ & \qquad (1.94) \end{aligned}$$

with $b \equiv e^{-i\theta}a$. By setting $e^{i\theta} = \alpha/|\alpha|$, we find,

$$\begin{aligned} \langle\alpha|x'|\alpha\rangle &= \frac{1}{\sqrt{2}|\alpha|}(\alpha^*\alpha + \alpha\alpha^*) = \sqrt{2}|\alpha|, \qquad (1.95) \\ \langle\alpha|p'|\alpha\rangle &= \frac{i}{\sqrt{2}|\alpha|}(\alpha^*\alpha - \alpha\alpha^*) = 0, \qquad (1.96) \\ & \qquad (1.97) \end{aligned}$$

which is the result we were looking for, since expressed in the mode b, the parameter α can be considered real. Even for a state such as the $|\psi\rangle$ state given in (1.85), the same method can be applied since the two cat states $|\pm\alpha\rangle$ have the same imaginary part, up to the sign. We therefore assume that we are working in the electromagnetic modes a and b which treats α and β as real numbers, when measuring quadrature operators, which are precisely the operators we use to find a violation of the SRPT inequality.

Experimentally, it is possible to show the entanglement of $|\psi\rangle$ with

$$\begin{aligned} A &= a_1(a^\dagger + a) + b_1(b^\dagger + b), \qquad (1.98) \\ B &= ia_2(a^\dagger - a) + ib_2(b^\dagger - b), \qquad (1.99) \end{aligned}$$

where a_i and b_i are real parameters and a and b are the annihilation operators of the fields

of $|\alpha\rangle$ and $|\beta\rangle$ chosen such that they treat α and β as real numbers. We get

$$(\Delta A^{\mathrm{pt}})^2 = a_1^2 + b_1^2 + 4\frac{(a_1\alpha + b_1\beta)^2}{1 + e^{-2(\alpha^2+\beta^2)}}, \tag{1.100}$$

$$(\Delta B^{\mathrm{pt}})^2 = a_2^2 + b_2^2 - 4\frac{(a_2\alpha - b_2\beta)^2}{1 + e^{2(\alpha^2+\beta^2)}}, \tag{1.101}$$

$$\frac{1}{4}|\langle [A,B]^{\mathrm{pt}}\rangle|^2 = (a_1a_2 + b_1b_2)^2, \tag{1.102}$$

$$\frac{1}{4}|\langle \{A,B\}^{\mathrm{pt}}\rangle - 2\langle A^{\mathrm{pt}}\rangle\langle B^{\mathrm{pt}}\rangle|^2 = 0. \tag{1.103}$$

Setting $a_1 = -a_2 = -\beta$ and $b_1 = -b_2 = \alpha$ insures a violation of the SRPT inequality for non-zero α and β, since we get

$$\left(\alpha^2+\beta^2\right)\left(\alpha^2+\beta^2 - \frac{16\alpha^2\beta^2}{1+e^{2\alpha^2+2\beta^2}}\right) \geq \left(\alpha^2+\beta^2\right)^2, \tag{1.104}$$

equivalent to

$$-\frac{\alpha^2\beta^2}{1+e^{2\alpha^2+2\beta^2}} \geq 0, \tag{1.105}$$

which is obviously always violated for non-zero parameters. Numerically speaking, the violation of the inequality is the strongest for values of α and β around 0.74.

In order to compare the results, one may try to apply the entanglement criterion introduced by Duan *et al.* [8] on $|\psi\rangle$. That criterion is a sufficient condition for entanglement and is also necessary when applied on gaussian states. Clearly, the state $|\psi\rangle$ is not gaussian, but the criterion may still be applied. The calculation is very close to the previous on, however it can be shown that the cat state $|\psi\rangle$ never violates Duan *et al.*'s inequality.

1.5 Necessary and Sufficient Criterion for Pure three-qubit States

The SRPT inequality is also a strong criterion in the tripartite case. A tripartite pure state $|\psi\rangle$ is fully separable if it can be written as a combination of three separable subsystems

as in $|\psi\rangle = |\psi_1\rangle \otimes |\psi_2\rangle \otimes |\psi_3\rangle$, biseparable if it can be written as a combination of one subsystem separated from the other (entangled) subsystems as in $|\psi\rangle = |\psi_1\rangle \otimes |\psi_{23}\rangle$ in the case of the first system being separable and fully entangled otherwise. In that last case, for three qubit, there are two separate classes of entanglement represented by the states $|\mathrm{GHZ}\rangle = (|000\rangle + |111\rangle)/\sqrt{2}$ and $|\mathrm{W}\rangle = (|001\rangle + |010+\rangle|100\rangle)/\sqrt{3}$ [26].

In the multipartite case, the partial transposition may be defined to act on any number of subsystems. In this chapter, when talking about multipartite states, we will always consider the partial transposition to act on the first subsystem of the state (or of the operator) only.

It has been shown that any three-qubit state can always be written under the form [27]:

$$|\psi\rangle = \lambda_0|000\rangle + \lambda_1|100\rangle + \lambda_2|101\rangle + \lambda_3|110\rangle + \lambda_4|111\rangle, \tag{1.106}$$

where one λ_i is complex and the other ones are real. We get to our next result:

Criterion 5. SRPT Criterion for Three-Qubit case — *A three-qubit pure state is entangled if and only if there are observables satisfying Eq. (1.27) such that a Schrödinger-Robertson partial transpose inequality is violated.*

Proof. We first consider a three-qubit state and express it as in Eq. (1.106). The three sets of observables

$$A = |001\rangle\langle 001| \qquad B = \sigma_x \otimes I_2 \otimes \sigma_x, \tag{1.107}$$

$$A = |010\rangle\langle 010| \qquad B = \sigma_x \otimes \sigma_x \otimes I_2, \tag{1.108}$$

$$A = |011\rangle\langle 011| \qquad B = \sigma_x \otimes \sigma_x \otimes \sigma_x, \tag{1.109}$$

lead to the SRPT inequalities

$$|\lambda_0||\lambda_2| \leq 0, \tag{1.110}$$

$$|\lambda_0||\lambda_3| \leq 0, \tag{1.111}$$

$$|\lambda_0||\lambda_4| \leq 0. \tag{1.112}$$

If $\lambda_0 = 0$ the inequalities are not violated, but in that case

$$|\psi\rangle = |1\rangle \otimes (\lambda_1|00\rangle + \lambda_2|01\rangle + \lambda_3|10\rangle + \lambda_4|11\rangle), \tag{1.113}$$

is biseparable. We already know that every entangled two-qubit state can be detected with the mean of an SRPT inequality. If $\lambda_2 = \lambda_3 = \lambda_4 = 0$, there is no violation of the inequalities either, but in that case

$$|\psi\rangle = (\lambda_0|0\rangle + \lambda_1|1\rangle) \otimes |00\rangle, \tag{1.114}$$

is fully separable. Therefore, there is always an SRPT inequality able to detect the entanglement of $|\psi\rangle$.

An interesting result is the fact that a pair of bipartite operators can never detect a GHZ-type state. Indeed, the expectation value of an observable A on a GHZ-type state expressed as in Eq. (1.106) will be a combination of the terms $\langle 000|A|000\rangle$, $\langle 000|A|111\rangle$, $\langle 111|A|000\rangle$ and $\langle 111|A|111\rangle$. If A is a bipartite observable acting, e.g., on the first two subsystems, we have $\langle 000|A|111\rangle = \langle 00|A_{12}|11\rangle\langle 0|I_2|1\rangle = 0$. Thus, the mean value of the observable A acting on a GHZ-type state is the same as if A were acting on a separable state of the form $\rho = \lambda_0^2|000\rangle\langle 000| + \lambda_4^2|111\rangle\langle 111|$. Therefore there cannot be any violation of an SRPT inequality.

1.6 Application to Mixed States

Let us now investigate the performances of the SRPT criterion on mixed states.

Bipartite Werner States.

The generalization of the SRPT criterion to mixed states is a difficult task. We may try, as an illustrative example, to detect the Werner mixed state [28]

$$\rho_x = x|\psi\rangle\langle\psi| + (1-x)\frac{I_4}{4} \tag{1.115}$$

with the normalized state $|\psi\rangle = a|00\rangle + b|11\rangle$.

The PPT criterion, which is necessary and sufficient for the 2×2 mixed state case may be used to describe the entanglement of the state. We find that the partially transposed state $\rho_x^{\rm pt}$ has the eigenvalues

$$\frac{1-x}{4} + x|a|^2, \tag{1.116}$$

$$\frac{1-x}{4} + x|b|^2, \tag{1.117}$$

$$\frac{1-x}{4} + x|a||b|, \tag{1.118}$$

$$\frac{1-x}{4} - x|a||b|. \tag{1.119}$$

The three first ones can never be negative, but we find that the last one is negative, i. e. the state is entangled, if and only if $x > 1/(1+4|a||b|)$.

Using the pair of observables:

$$A = \sigma_z \otimes \sigma_z, \tag{1.120}$$

$$B = \sigma_x \otimes (\cos\varphi\,\sigma_x + \sin\varphi\,\sigma_y), \tag{1.121}$$

our SRPT inequality detects the entanglement of ρ_W when $x > 2/(1+\sqrt{1+32\,\mathrm{Re}(e^{i\varphi}a^*b)})$.

In the particular case when $|\psi\rangle$ is the Bell state $|\phi^\pm\rangle$, i. e. when $a = \pm b = 1/\sqrt{2}$, and $\varphi = 0$, ρ_x is entangled if and only if $x > 1/3$ whereas it is detected via the SRPT inequality when $x > 1/2$. This result improves the limits of detection given by the Bell inequalities ($x > 1/\sqrt{2}$, see [4]) or by the uncertainty relations of Gühne [16] ($x > 1/\sqrt{3}$).

Multipartite Werner States.

The SRPT inequality can be applied on mixed states of multipartite systems. Let us look at its results on the N-dimensional Werner mixed state

$$\rho(x) = x|\mathrm{GHZ}_N\rangle\langle\mathrm{GHZ}_N| + (1-x)\frac{I_{2^N}}{2^N}, \tag{1.122}$$

with $|\mathrm{GHZ}_N\rangle \equiv (|0\cdots0\rangle + |1\cdots1\rangle)/\sqrt{2}$. Using the observables

$$A = |01\cdots1\rangle\langle01\cdots1| + |10\cdots0\rangle\langle10\cdots0|, \tag{1.123}$$

$$B = |0\cdots0\rangle\langle1\cdots1| + |1\cdots1\rangle\langle0\cdots0| + |01\cdots1\rangle\langle10\cdots0| + |10\cdots0\rangle\langle01\cdots1|, \tag{1.124}$$

we find an SRPT inequality violated if $x > 1/(1+2^{N-2})$. The PPT criterion gives the sufficient limit of entanglement $x > 1/(1+2^{N-1})$ and we can find in [29] a witness giving the detection limit of $x > (2-2^{2-N})/(3-2^{2-N})$, which is strictly smaller than our result for $N \geq 3$ (also, that limit approaches $2/3$ as N grows, where ours approaches 0). For $N = 3$, the PPT criterion gives $x > 1/5$, we find the limit $x > 1/3$ while in [29] the limit is $x > 3/5$ and another witness in [16] gives the limit $x > 3/7$.

Finally it should be kept in mind that any criterion based on inequalities would be restrictive as these are based on two chosen observables unlike the density operators which contain all the information. One could of course increase the number of observables and work a stronger criterion based on the positivity condition $\langle(\sum_i c_i A_i)^\dagger (\sum_i c_i A_i)\rangle \geq 0$ [30], for any observable A_i. Further possibilities consist of using generalized uncertainty relations which are especially suitable for mixed states [31].

Most of the results from this chapter were published in Phys. Rev. A **78**, 052317 (2008).

Chapter 2

Cavity Mediated Two-Photon Processes in Two Qubits Circuit QED

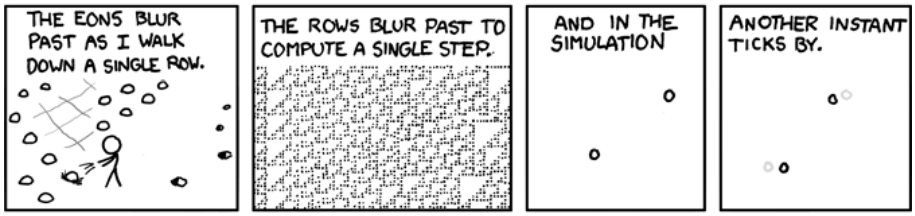

Randall Munroe, *A Bunch of Rocks* (part 7 of 9), `xkcd.com/505/`

In free space, two non-interacting and non-identical atoms immersed in a laser field will never be excited simultaneously. This results from a destructive interference phenomenon in the two-photon absorption process of the two atoms in the laser. The two quantum paths underlying the double excitation (one atom excited first, then the second, and vice-versa) interfere destructively precisely when the laser frequency matches the resonance condition for the excitation of the two atoms [32]. This interference effect can be interestingly annulled if the two atoms are within a distance much smaller than the wavelength of the transition [33–35]. In this case dipole-dipole interaction comes into play and breaks the destructive character of the interference, resulting in a possible simultaneous excitation of the two atoms.

In Ref. [32], the indirect interaction between two atoms placed in a lossless single mode cavity is exploited to obtain a similar cancellation of the destructive interference effect. Here, we wish to extend significantly that initial proposal by considering the huge potentialities offered by circuit-QED systems. Our model is intended to provide realistic experimental predictions by considering dissipation and steady-state regimes using a driving field. A perturbative approach is first proposed to grasp the essentials of the underlying physics in an idealized case.

The organization of the chapter is as follows. In Section 2.1, we introduce the free space case for future comparison with the cavity case and show why simultaneous excitation is not possible in free space. In Sec. 2.2 we give our Hamiltonian for the atoms imbedded in the cavity which includes the modelization of two internal states and transitional frequency for each atom, the electromagnetic field mode of the cavity, the coupling between the atoms and the field and finally the driving laser field. We also introduce the master equation which modelizes spontaneous emission or dissipation effects in the atoms as well as the photon loss of the cavity.

In Sec. 2.3, we introduce a constraint that allows the diagonalization of the undriven Hamiltonian. Thanks to the diagonalization we are able to understand the structure of the dressed states and we can use perturbation theory to predict two-photon transition rates in the system. Then, after discussing some numerical issues, we study one and two-photon spectra as well as the population of the excited atoms in the steady states of the system numerically found with the master equation. We study some effects of the cavity decay rate that could not be including in the perturbation theory analysis.

In Sec. 2.4, we drop the constraint previously used, which lifts degeneracies, and although we lose the analytical description of the system (except for the particular case of identical atoms) we still use the master equation to calculate atomic, one and two-photon spectra of the system. We compare the general system with the constrained one and confirm several observations. We also observe a new effect in the system, the cavity induced transparency.

In Sec. 2.5, we give a summary of all the theoretical predictions we could make and we discuss the possibility of experimental observation of said predictions.

2.1 Atoms in Free Space

Before considering two atoms immersed in a cavity and two-photon processes, we first consider the problem of two atoms in free space excited by a laser and show that in that kind of system, two-photon processes are prohibited.

Let us consider two non-interacting atoms with internal levels $|e_i\rangle$ and $|g_i\rangle$ $(i = 1, 2)$ of transition frequency ω_1 and ω_2 and single atom spontaneous emission rate $2\gamma_i$. They are excited by a non-resonant laser field of wave vector $\mathbf{k}_L$, Rabi frequency 2ϵ and driving frequency ω. The Hamiltonian H_f of the system, where f stands for *free*, is

$$H_f = \sum_{i=1}^{2} \left(\hbar(\omega_i - \omega)\sigma_i^z + \hbar\epsilon \left(e^{i\mathbf{k}_L\cdot\mathbf{x}_i}\sigma_i^+ + e^{-i\mathbf{k}_L\cdot\mathbf{x}_i}\sigma_i^- \right) \right), \tag{2.1}$$

where $\sigma_i^+ = (\sigma_i^-)^\dagger$ is the atom raising operator $|e_i\rangle\langle g_i|$ and σ_i^z the atomic inversion operator $(|e_i\rangle\langle e_i| - |g_i\rangle\langle g_i|)/2$. We assume that the atoms are placed such that $\mathbf{k}_L \cdot \mathbf{x}_1 = \mathbf{k}_L \cdot \mathbf{x}_2 = 0$.

When considering dissipation in the Markov and Born approximation, the time evolution of the system is governed by the master equation

$$\dot{\rho} = -\frac{i}{\hbar}[H, \rho] - \sum_{i=1}^{2} \gamma_i(\sigma_i^+\sigma_i^-\rho + \rho\sigma_i^+\sigma_i^- - 2\sigma_i^-\rho\sigma_i^+), \tag{2.2}$$

We now treat the laser as a perturbation by considering a small ϵ. According to Fermi's Golden Rule of the standard second-order perturbation theory [36], the $|gg\rangle \to |ee\rangle$ transition rate through a strict two-photon process reads

$$R_{gg\to ee} = \frac{2\pi}{\hbar^4}|W^{(2)}_{(gg,ee)}|^2\delta(\omega_1 + \omega_2 - 2\omega), \tag{2.3}$$

with

$$W^{(2)}_{(gg,ee)} = \sum_{j=eg,ge} \frac{\langle ee|H|j\rangle\langle j|H|gg\rangle}{\omega_j - \omega}, \tag{2.4}$$

where here the sum is restricted to the one-excitation $|eg\rangle$ and $|ge\rangle$ states, since they are the only ones to be simultaneously coupled by the perturbation to the $|gg\rangle$ and $|ee\rangle$ states.

Calculating $W^{(2)}_{(gg,ee)}$ is straightforward, we find

$$\begin{aligned} W^{(2)}_{(gg,ee)} &= \frac{\langle ee|H|eg\rangle\langle eg|H|gg\rangle}{\omega_1 - \omega} + \frac{\langle ee|H|ge\rangle\langle ge|H|gg\rangle}{\omega_2 - \omega}, & (2.5)\\ &= \frac{\hbar^2\epsilon^2}{\omega_1 - \omega} + \frac{\hbar^2\epsilon^2}{\omega_2 - \omega}, & (2.6)\\ &= \hbar^2\epsilon^2 \frac{2\omega - \omega_1 - \omega_2}{(\omega_1 - \omega)(\omega_2 - \omega)}, & (2.7) \end{aligned}$$

which is equal to zero when $2\omega = \omega_1 + \omega_2$. We can see that, due to the destructive interference between the two possible excitation paths $|gg\rangle \to |eg\rangle \to |ee\rangle$ and $|gg\rangle \to |ge\rangle \to |ee\rangle$, the simultaneous excitation of both atoms is prohibited.

The system in its steady state can be can be found posing that the master equation (2.2) is zero. The system can actually be decomposed in two subsystems whose master equation can be solved individually. The steady state solution of two atoms excited in free space is

$$\rho^S_f = \rho^S_1 \otimes \rho^S_2, \tag{2.8}$$

with

$$\rho^S_i = \frac{1}{2\epsilon^2 + \gamma_i^2 + (\omega_i - \omega)^2} \left(|\phi_i\rangle\langle\phi_i| + \epsilon^2 |g_i\rangle\langle g_i|\right), \tag{2.9}$$

with the unnormalized

$$|\phi_i\rangle = \epsilon|e_i\rangle - (\omega_i - \omega + i\gamma)|g_i\rangle. \tag{2.10}$$

The populations of each excited atoms are

$$P_{e_i} = \frac{\epsilon^2}{2\epsilon^2 + \gamma_i^2 + (\omega_i - \omega)^2}, \tag{2.11}$$

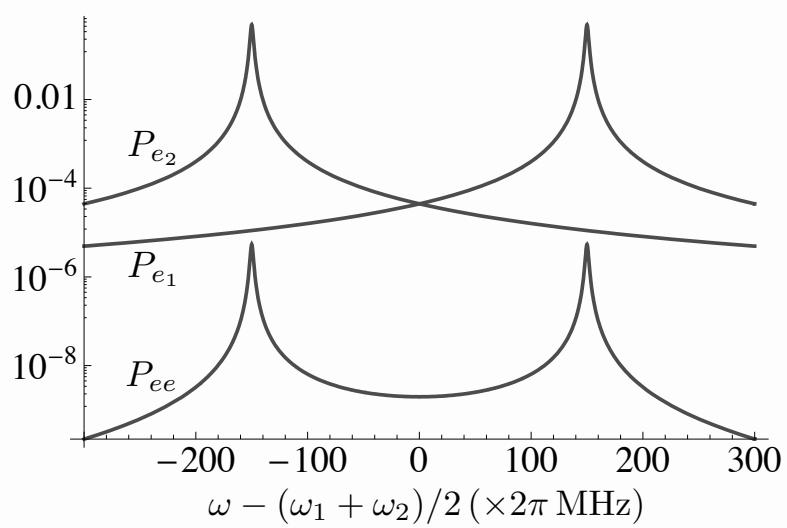

Figure 2.1: Populations of $|e_1\rangle, |e_2\rangle$ and $|ee\rangle$ in the steady state with $(\omega_1 - \omega_2)/2 = 150 \times 2\pi\,\mathrm{MHz}, \epsilon = 2\pi\,\mathrm{MHz}, \gamma = 0.2 \times 2\pi\,\mathrm{MHz}$. There are two peaks located at the frequencies of the individual atoms and none at the frequency $2\omega = \omega_1 + \omega_2$.

and the population in the $|ee\rangle$ state is $P_{ee} = P_{e_1} P_{e_2}$ since the atoms are independent.

We represented in Fig. 2.1 those populations. We see that there is no particular peak at the two-photon transition frequency 2ω, which was expected since due to the interference, there can be no two-photon process there. The numerical values and units do not actually apply to real atomic frequencies, but rather to superconducting qubits frequencies existing in circuit QED experiments, as in [37]. Such qubits are modelized exactly the same way as two-level atoms and are easily manipulated when embedded in a microwave resonator, which is the setup we investigate in the rest of the chapter.

It has been shown that some kind of interaction may counteract the interference and allow two-photon processes to happen[33]. In the next sections, we investigate the possibility of allowing two-photon processes by immersing the atoms in a cavity and letting them interact through the cavity coupling.

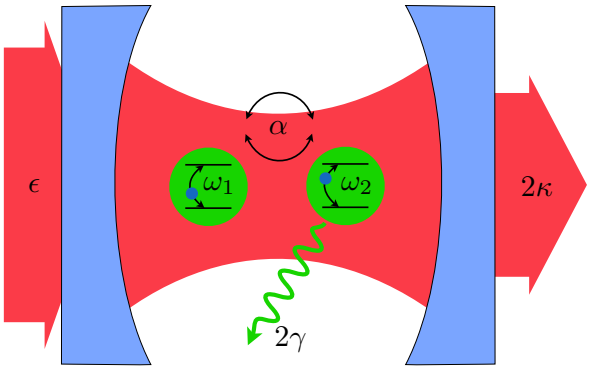

Figure 2.2: Schematic of the two-atom system immersed in a single-mode cavity. Two two-level atoms of transition frequencies ω_1 and ω_2 are identically coupled to the cavity mode of frequency ω_c with a coupling constant α. The cavity has a photon decay rate 2κ, while the atoms have a spontaneous emission rate 2γ. The cavity mode is being driven by a laser of strength ϵ and frequency ω.

2.2 Atoms Embedded in a Cavity

We now consider two atoms 1 and 2 with internal levels $|e_i\rangle$ and $|g_i\rangle$ $(i = 1, 2)$ of transition frequency ω_i and spontaneous emission rate 2γ (identical for both atoms). The two atoms are embedded in a single mode cavity of resonance frequency ω_c and decay rate 2κ. The two atoms are supposed to be identically coupled to the cavity with a coupling constant α. The cavity is driven by a non-resonant laser field of amplitude ϵ and driving frequency ω (see Fig. 2.2). The two atoms are considered sufficiently far apart so that there is no direct interaction of any kind between them but through the cavity coupling. That situation is encountered in most circuit-QED systems, like, e.g., in the experimental setup reported in Ref. [37] where the qubits are several hundred micrometers apart.

In the rotating-wave approximation, the coherent evolution of the system is described by the interaction Hamiltonian

$$H = \hbar(\omega_c - \omega)a^\dagger a + \sum_{i=1}^{2} \hbar(\omega_i - \omega)\sigma_i^z + \sum_{i=1}^{2} \hbar\alpha(a\sigma_i^+ + a^\dagger\sigma_i^-) + i\hbar\epsilon(a^\dagger - a), \qquad (2.12)$$

where a $[a^\dagger]$ is the photon annihilation [creation] operator for the cavity field mode,

$\sigma_i^+ = (\sigma_i^-)^\dagger$ $(i = 1, 2)$ is the atom raising operator $|e_i\rangle\langle g_i|$, and σ_i^z is the atomic inversion operator $(|e_i\rangle\langle e_i| - |g_i\rangle\langle g_i|)/2$.

When considering dissipation in the Markov and Born approximation, the time evolution of the density operator ρ of the system is governed by the master equation [38]

$$\dot{\rho} = \frac{1}{i\hbar}[H, \rho] - \kappa(a^\dagger a\rho - 2a\rho a^\dagger + \rho a^\dagger a) - \sum_{i=1}^{2} \gamma(\sigma_i^+\sigma_i^-\rho - 2\sigma_i^-\rho\sigma_i^+ + \rho\sigma_i^+\sigma_i^-). \qquad (2.13)$$

This time evolution leads invariably to a steady-state ρ^S of the system that is determined by equating the left-hand side term of Eq. (2.13) to zero. We denote hereafter by $|N, xy\rangle \equiv |N\rangle \otimes |x_1\rangle \otimes |y_2\rangle$ the bare basis elements of the atom-cavity system, with N the photon number and $x, y \in \{e, g\}$.

First, we may want to study the Hamiltonian of the system using a perturbative approach to grasp the essentials of the physics of the system. The driving laser field defines the perturbation and the unperturbed Hamiltonian is given by Eq. (2.12) with ϵ and ω set to 0. Let us show that H commutes with the global excitation number operator $\hat{n} \equiv a^\dagger a + \sum_i \sigma_i^z + 1$, which counts the number of photons in the system plus the number of excited atoms. Obviously, $\hat{n}$ commutes with the first two terms of the Hamiltonian, we are left with

$$\begin{aligned}
[\hat{n}, H] &= [a^\dagger a + \sum_i \sigma_i^z, \hbar\alpha \sum_i (a\sigma_i^+ + a^\dagger\sigma_i^-)], && (2.14)\\
&= \hbar\alpha \sum_i [a^\dagger a, a\sigma_i^+ + a^\dagger\sigma_i^-] + \hbar\alpha \sum_i [\sigma_i^z, a\sigma_i^+ + a^\dagger\sigma_i^-], && (2.15)\\
&= \hbar\alpha \sum_i \left(-a\sigma_i^+ + a^\dagger\sigma_i^-\right) + \hbar\alpha \sum_i \left(a\sigma_i^+ - a^\dagger\sigma_i^-\right), && (2.16)\\
&= 0, && (2.17)
\end{aligned}$$

where we used the properties $[a^\dagger a, a] = [a^\dagger, a]a = -a$, $[a^\dagger a, a^\dagger] = a^\dagger[a, a^\dagger] = a^\dagger$ and $[\sigma_i^z, \sigma_j^\pm] = \pm\delta_{ij}\sigma_i^\pm$. It follows that in the $|N, xy\rangle$ bare basis of the atom-cavity system, the unperturbed Hamiltonian has a block-diagonal form, with blocks associated with the

global excitation number $n = N + m(x, y)$, where $m(x, y)$ is the number of excited atoms in the $|x, y\rangle$ state ($m = 0$, 1, or 2).

For $n = 0$, the dimension of the diagonal block is 1×1, in association with the only bare basis element $|0\rangle \equiv |0, gg\rangle$. For $n = 1$, the diagonal block is of 3×3 dimension with the 3 basis elements $|1, gg\rangle$, $|0, eg\rangle$, and $|0, ge\rangle$. From $n \geq 2$, the diagonal blocks are of 4×4 dimension in association with the 4 basis elements $|n, gg\rangle$, $|n-1, eg\rangle$, $|n-1, ge\rangle$, and $|n-2, ee\rangle$. The eigenstates and eigenvalues of the unperturbed Hamiltonian yield, respectively, the dressed states of the two-atom-cavity system and their energy. They follow immediately from the block diagonalization.

2.3 Even Atomic Frequency Spread

The diagonalization of the unperturbed Hamiltonian is possible to realize analytically if we make the assumption that

$$\omega_1 + \omega_2 = 2\omega_c, \tag{2.18}$$

in which case we define the frequency difference $\Delta \equiv (\omega_1 - \omega_2)/2$. This means that the frequencies of the atoms are evenly spread around the cavity mode frequency, at the frequencies $\omega_c \pm \Delta$.

2.3.1 Eigenstates and Eigenvalues

Let us now show the results of the block diagonalizations. For $n = 0$, $|0\rangle$ is the only eigenstate with an eigenvalue 0. For $n \geq 1$, the eigenvalues read with respect to the ground state energy

$$\hbar\lambda^{(n,0)} = n\hbar\omega_c, \quad \hbar\lambda^{(n,\pm)} = n\hbar\omega_c \pm \hbar\lambda_n, \tag{2.19}$$

with $\hbar\lambda^{(n,0)}$ twice degenerated for $n \geq 2$ and where

$$\lambda_n = \sqrt{2(2n-1)\alpha^2 + \Delta^2}. \tag{2.20}$$

For $n = 1$, the three associated eigenvectors are, respectively,

$$|1,0\rangle = \frac{1}{\lambda_1}\left(\Delta|1,gg\rangle - \sqrt{2}\alpha|\psi_1^-\rangle\right), \tag{2.21}$$

$$|1,\pm\rangle = \frac{1}{\sqrt{2}\lambda_1}\left(\sqrt{2}\alpha|1,gg\rangle + \Delta|\psi_1^-\rangle \pm \lambda_1|\psi_1^+\rangle\right), \tag{2.22}$$

and, for $n \geq 2$, respectively,

$$|n,0_a\rangle = \sqrt{\frac{n-1}{2n-1}}|n,gg\rangle - \sqrt{\frac{n}{2n-1}}|n-2,ee\rangle, \tag{2.23}$$

$$|n,0_b\rangle = \frac{1}{\lambda_n}\left(\Delta|\phi_n\rangle - \sqrt{2(2n-1)}\alpha|\psi_n^-\rangle\right), \tag{2.24}$$

$$|n,\pm\rangle = \frac{1}{\sqrt{2}\lambda_n}\left(\sqrt{2(2n-1)}\alpha|\phi_n\rangle + \Delta|\psi_n^-\rangle \pm \lambda_n|\psi_n^+\rangle\right), \tag{2.25}$$

with, for $n \geq 1$,

$$|\psi_n^\pm\rangle = \frac{1}{\sqrt{2}}\left(|n-1,eg\rangle \pm |n-1,ge\rangle\right), \tag{2.26}$$

and, for $n \geq 2$,

$$|\phi_n\rangle = \sqrt{\frac{n}{2n-1}}|n,gg\rangle + \sqrt{\frac{n-1}{2n-1}}|n-2,ee\rangle. \tag{2.27}$$

The energy structure is shown on Fig. 2.3. If we turn on the laser perturbation term W of the Hamiltonian defined as

$$W = i\hbar\epsilon(a^\dagger - a), \tag{2.28}$$

the structure of H ceases to be diagonal in the eigenstate basis. The off-diagonal, perturbation terms coming from the laser are expressed, in the unperturbed Hamiltonian

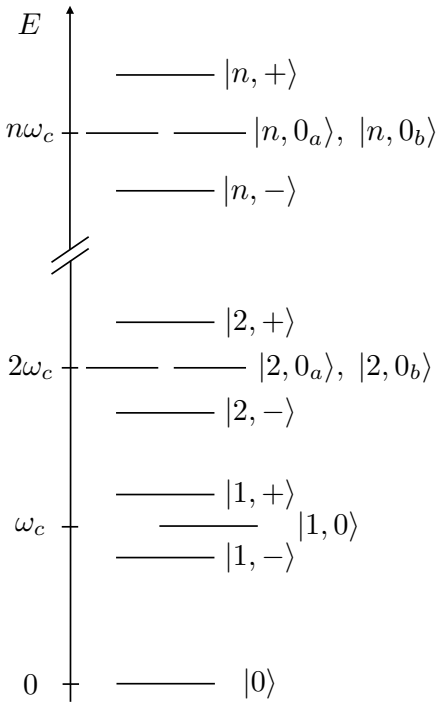

Figure 2.3: Energy diagram for the dressed states of the two-atom-cavity system when $\omega_1 + \omega_2 = 2\omega_c$.

eigenstates base, as, for the $n = 0 \rightarrow n = 1$ transitions

$$\langle 0|W|1,0\rangle = -i\,\frac{\Delta}{\lambda_1}\,\epsilon, \tag{2.29}$$

$$\langle 0|W|1,\pm\rangle = -i\,\frac{\alpha}{\lambda_1}\,\epsilon. \tag{2.30}$$

The $n = 1 \to n = 2$ transitions are written

$$\langle 1,0|W|2,0_a\rangle = -i\sqrt{\frac{2}{3}}\,\frac{\Delta}{\lambda_1}\,\epsilon, \tag{2.31}$$

$$\langle 1,0|W|2,0_b\rangle = -\frac{2i}{\sqrt{3}}\,\frac{3\alpha^2+\Delta^2}{\lambda_1\lambda_2}\,\epsilon, \tag{2.32}$$

$$\langle 1,0|W|2,\pm\rangle = -i\,\frac{\alpha\Delta}{\lambda_1\lambda_2}\,\epsilon, \tag{2.33}$$

$$\langle 1,\pm|W|2,0_a\rangle = -i\sqrt{\frac{2}{3}}\,\frac{\alpha}{\lambda_1}\,\epsilon, \tag{2.34}$$

$$\langle 1,\pm|W|2,0_b\rangle = \frac{i}{\sqrt{3}}\,\frac{\alpha\Delta}{\lambda_1\lambda_2}\,\epsilon, \tag{2.35}$$

$$\langle 1,\pm|W|2,\pm\rangle = -\frac{i}{4}\,\frac{(\lambda_1+\lambda_2)^2}{\lambda_1\lambda_2}\,\epsilon, \tag{2.36}$$

$$\langle 1,\pm|W|2,\mp\rangle = -\frac{i}{4}\,\frac{(\lambda_1-\lambda_2)^2}{\lambda_1\lambda_2}\,\epsilon. \tag{2.37}$$

Finally, the $n \to n+1$ transitions with $n \geq 2$ are written

$$\langle n,0_a|W|n+1,0_a\rangle = -2i\sqrt{\frac{n(n^2-1)}{4n^2-1}}\,\epsilon, \tag{2.38}$$

$$\langle n,0_a|W|n+1,0_b\rangle = -i\sqrt{\frac{n-1}{4n^2-1}}\,\frac{\Delta}{\lambda_{n+1}}\,\epsilon, \tag{2.39}$$

$$\langle n,0_a|W|n+1,\pm\rangle = -i\sqrt{\frac{n-1}{2n-1}}\,\frac{\alpha}{\lambda_{n+1}}\,\epsilon, \tag{2.40}$$

$$\langle n,0_b|W|n+1,0_a\rangle = -i\sqrt{\frac{n+1}{4n^2-1}}\,\frac{\Delta}{\lambda_n}\,\epsilon, \tag{2.41}$$

$$\langle n,0_b|W|n+1,0_b\rangle = -i\sqrt{\frac{n}{4n^2-1}}\,\frac{(n+1)\lambda_n^2+(n-1)\lambda_{n+1}^2}{\lambda_n\lambda_{n+1}}\,\epsilon, \tag{2.42}$$

$$\langle n,0_b|W|n+1,\pm\rangle = -i\,\frac{\alpha\Delta}{\lambda_n\lambda_{n+1}}\,\epsilon, \tag{2.43}$$

$$\langle n,\pm|W|n+1,0_a\rangle = -i\sqrt{\frac{n+1}{2n+1}}\,\frac{\alpha}{\lambda_n}\,\epsilon, \tag{2.44}$$

$$\langle n,\pm|W|n+1,0_b\rangle = i\sqrt{\frac{n}{2n+1}}\,\frac{\alpha\Delta}{\lambda_n\lambda_{n+1}}\,\epsilon, \tag{2.45}$$

$$\langle n,\pm|W|n+1,\pm\rangle = -i\frac{\sqrt{n}}{4}\,\frac{(\lambda_n+\lambda_{n+1})^2}{\lambda_n\lambda_{n+1}}\,\epsilon, \tag{2.46}$$

$$\langle n,\pm|W|n+1,\mp\rangle = -i\frac{\sqrt{n}}{4}\,\frac{(\lambda_n-\lambda_{n+1})^2}{\lambda_n\lambda_{n+1}}\,\epsilon. \tag{2.47}$$

$$\tag{2.48}$$

From the matrix elements, we identify three one-photon transitions from the ground state at frequencies ω_c and $\omega_c \pm \lambda_1$ and two two-photon transitions $|0\rangle \rightarrow |2,\pm\rangle$ at frequencies $\omega_c \pm \lambda_2/2$. Unlike the free space case, the transition at $2\omega = \omega_1 + \omega_2 = 2\omega_c$ which corresponds to $|0\rangle \rightarrow |2, 0_{a,b}\rangle$ does not identify as two-photon processes but rather to stepwise one-photon transitions through the intermediate state $|1,0\rangle$ with photons at frequency ω_c.

In general, n-photon transitions to the states $|n,\pm\rangle$ at the frequencies $\omega_c \pm \lambda_n/n$ are conceivable, although the transition rates are proportional to ϵ^{2n} in the perturbation regime.

2.3.2 Perturbative Approach

We now consider the action of the driving field at frequency ω and investigate the possibility of getting both atoms excited through strict two-photon processes, a result that is not achievable when the two atoms are solely in free space. Here, the two-photon transitions $|0\rangle \rightarrow |2,\pm\rangle$ make this possible because of the $|0, ee\rangle$ component of the upper states $|2,\pm\rangle$.

According to Fermi's Golden Rule of the standard second-order perturbation theory [36], the $|0\rangle \rightarrow |0, ee\rangle$ transition rate through a strict two-photon process reads

$$R_{gg\rightarrow ee} = \frac{2\pi}{\hbar^4} |\langle 0, ee|2,\pm\rangle|^2 |W^{(2)}_{0,(2,\pm)}|^2 \delta(\lambda^{(2,\pm)} - 2\omega), \tag{2.49}$$

with

$$W^{(2)}_{0,(2,\pm)} = \sum_{j=0,\pm} \frac{\langle 2,\pm|W|1,j\rangle\langle 1,j|W|0\rangle}{\lambda^{(1,j)} - \omega}, \tag{2.50}$$

where here the sum is only restricted to the one-excitation $|1,j\rangle$ states, since they are the only ones to be simultaneously coupled by the perturbation W to the $|0\rangle$ and $|2,\pm\rangle$ states.

In Eq. (2.49), the δ-function yields the two-photon resonance condition $\omega = \omega_c \pm \lambda_2/2$

that must be fulfilled to get the sought double-excitation process. Let us first calculate

$$\langle 2,\pm|W|1,0\rangle\langle 1,0|W|0\rangle = -\frac{\alpha\Delta^2}{\lambda_1^2\lambda_2}\,\epsilon^2, \tag{2.51}$$

$$\langle 2,\pm|W|1,\pm\rangle\langle 1,\pm|W|0\rangle = -\frac{1}{4}\,\frac{\alpha(\lambda_1+\lambda_2)^2}{\lambda_1^2\lambda_2}\,\epsilon^2, \tag{2.52}$$

$$\langle 2,\pm|W|1,\mp\rangle\langle 1,\mp|W|0\rangle = -\frac{1}{4}\,\frac{\alpha(\lambda_1-\lambda_2)^2}{\lambda_1^2\lambda_2}\,\epsilon^2. \tag{2.53}$$

We then have

$$W^{(2)}_{0,(2,\pm)} = -\frac{\alpha\epsilon^2}{\lambda_1^2\lambda_2}\left(\frac{\Delta^2}{\omega_c-\omega}+\frac{(\lambda_1\pm\lambda_2)^2}{4(\omega_c-\omega+\lambda_1)}+\frac{(\lambda_1\mp\lambda_2)^2}{4(\omega_c-\omega-\lambda_1)}\right), \tag{2.54}$$

$$= -\frac{\alpha\epsilon^2}{\lambda_2}\,\frac{\Delta^2+(\omega_c-\omega)\left(\lambda_2\mp 2(\omega_c-\omega)\right)}{(\omega_c-\omega)(\omega_c-\omega+\lambda_1)(\omega_c-\omega-\lambda_1)}, \tag{2.55}$$

which gives, at the resonance condition $\omega=\omega_c\pm\lambda_2/2$ and after a few simplifications

$$R_{gg\to ee} = 2\pi f(r)\frac{\epsilon^4}{\Delta^2}\delta(\lambda^{(2,\pm)}-2\omega), \tag{2.56}$$

where $r=\alpha/\Delta$ and

$$f(r) = \frac{2304r^8}{(1+6r^2)^3(3+2r^2)^2}. \tag{2.57}$$

As expected, this rate is strongly dependent on the coupling constant α and on the spread 2Δ in atomic frequencies, but there will be two-photon transitions as long as the atoms are coupled with the cavity. For $r\ll 1$, the rate behaves as r^8, while it behaves as r^{-2} for $r\gg 1$. The optimal rate is obtained for $r\sim 1.51$ that yields $2\pi f(r)\sim 2.16$.

When the atoms are identical, i. e. when $\Delta=0$, the $|0\rangle\to|2,\pm\rangle$ transitions still take place, at the transition rate

$$R_{gg\to ee}(\Delta=0) = 2\pi\frac{8\epsilon^4}{3\alpha^2}\delta(\lambda^{(2,\pm)}-2\omega). \tag{2.58}$$

Let us examine the possible transitions at $\omega=\omega_c$ when the atoms are identical. We note that when this is the case, the system becomes symmetric with the exchange of the

two atoms. It is easy to see that the states $|1,0\rangle$ and $|n,0_b\rangle$ are now antisymmetric with the exchange of the atoms while the other states are symmetric. It is apparent from the perturbation terms in the Hamiltonian that the antisymmetric states only couple to each other and are completely decoupled from the symmetric states, including the ground state, and should therefore never be populated. In other words, since $\langle 0|W|1,0\rangle = 0$, the only one-photon transition from the ground state at $\omega = \omega_c$ is impossible. The two-photon process $|0\rangle \to |2,0_b\rangle$ is also impossible since $W^{(2)}_{0,(2,0_b)}$ is always zero, as we have $\langle 2,0_b|W|1,\pm\rangle = 0$.

There might still remain the possibility of a transition at $\omega = \omega_c$ if the $|2,0_a\rangle$ state is populated from the ground state by a two-photon process. The rate of this process is proportional to $|W^{(2)}_{0,(2,0_a)}|^2$, with

$$
\begin{aligned}
W^{(2)}_{0,(2,0_b)} &= \sum_{j=\pm} \frac{\langle 2,0_b|W|1,j\rangle\langle 1,j|W|0\rangle}{\lambda^{(1,j)} - \omega}, && (2.59)\\
&= \frac{\langle 2,0_a|W|1,+\rangle\langle 1,+|W|0\rangle}{\omega_c - \omega + \lambda_1} + \frac{\langle 2,0_a|W|1,-\rangle\langle 1,-|W|0\rangle}{\omega_c - \omega + \lambda_1}, && (2.60)\\
&= -\sqrt{\frac{2}{3}}\frac{\alpha^2\epsilon^2}{\lambda_1^2\lambda_2}\left(\frac{1}{\omega_c - \omega + \lambda_1} + \frac{1}{\omega_c - \omega + \lambda_1}\right), && (2.61)\\
&= -\sqrt{\frac{2}{3}}\frac{\alpha^2\epsilon^2}{\lambda_1^2\lambda_2}\frac{2(\omega_c - \omega)}{(\omega_c - \omega + \lambda_1)(\omega_c - \omega - \lambda_1)}, && (2.62)\\
& && (2.63)
\end{aligned}
$$

which is always zero on the resonance condition $\omega = \omega_c$. Therefore no transition takes place at the atomic frequencies when they are identical.

Here, we investigated the transition rates for both atoms to simultaneously go from their ground state to their excited state. We may also be interested in the possibility of the number of photons in the cavity going from $N = 0$ to $N = 2$ instantly. The golden rule (2.49) may be modified to calculate such a two-photon process. Since the ground state is the same for atoms or photons, one just needs to replace the $|\langle 0, ee|2,\pm\rangle|^2$ term which calculates the proportion of $|ee\rangle$ state in $|2,\pm\rangle$ by $\langle 2,\pm|(a^\dagger)^2a^2|2,\pm\rangle$ which calculates the number of pairs of photons in $|2,\pm\rangle$. The $W^{(2)}_{0,(2,\pm)}$ needs no modification, therefore all

Table 2.1: Numerical values of the model.

Parameter	Value ($\times 2\pi$ MHz)
Δ	0, 150
α	85
ϵ	6
κ	6.8
γ	0.2

Numerical values used in the numerical processes, unless stated otherwise.

qualitative result on $|gg\rangle \rightarrow |ee\rangle$ also applies to the photon sates $|N = 0\rangle \rightarrow |N = 2\rangle$.

2.3.3 Master Equation Approach

In this section, we refine our analysis by using a more general, although numerical, method to investigate the behavior of the system. A master equation approach is used, into which dissipations such as atomic spontaneous emission and cavity loss are considered. We numerically solve the master equation for the steady state of the system and measure different observables. The results obtained will be interpreted in light of the perturbative approach of the previous section and we will show that two-photon processes are indeed allowed in the present system.

Numerical Considerations

Here, we discuss the numerical methods used to calculate the following results. In order to obtain results as realistic as possible, we chose to give to our parameters values close to what has been used in recent circuit QED experiments, as in [37]. The typical values we used are listed in Tab. 2.1, unless stated otherwise.

Our goal in this chapter is to highlight the two-photon processes, which are proportional to ϵ^4, compared to the one-photon processes, proportional to ϵ^2 in the perturbation regime. With that in mind, it makes sense to choose a high laser power in order to increase the visibility of the two-photon transitions. However, as the strength of the laser

Table 2.2: Other numerical values of the model.

Parameter	Value ($\times 2\pi$ MHz)
Δ	0, 150
α	85
ϵ	6
κ	6.8
γ	0.2

Numerical values used in the numerical processes, unless stated otherwise. Totally different from the previous table

probing the system is increased, more and more excitation modes are being populated and for numerical purposes we cannot use an infinite vector basis for the photon number $|N\rangle$. Therefore, we need to make approximations in order to solve the master equation by cutting off the excitation number to a maximum $n_{\max}$. Unfortunately, with a truncated basis for high laser power the populations come numerically to a saturation and harmonization of all the different populations in the density matrix. We need a way to evaluate this effect in order to chose a laser power as high as possible which still minimizes numerical errors.

It would possible to estimate the saturation effect in the numerical process by comparing the number of photons calculated for an empty cavity to the number it should really have, which can be calculated analytically for an infinite basis. Indeed, the master equation relating to an empty cavity is written

$$\dot{\rho} = \frac{1}{i\hbar}[H_0, \rho] - \kappa(a^\dagger a\rho - 2a\rho a^\dagger + \rho a^\dagger a), \tag{2.64}$$

with the excited empty cavity Hamiltonian

$$H_0 = \hbar(\omega_c - \omega)a^\dagger a + i\hbar\epsilon(a^\dagger - a). \tag{2.65}$$

The time variation of any operator A is calculated using Eq. (2.64) as

$$\begin{aligned}
\frac{d}{dt}\langle A\rangle &= \mathrm{Tr}\left(A\dot{\rho}\right), && (2.66)\\
&= -i(\omega_c-\omega)\mathrm{Tr}\left(Aa^\dagger a\rho - A\rho a^\dagger a\right) + \epsilon\mathrm{Tr}\left(Aa^\dagger\rho - A\rho a^\dagger - Aa\rho + A\rho a\right)\\
&\quad -\kappa\mathrm{Tr}\left(Aa^\dagger a\rho\right) + 2\kappa\mathrm{Tr}\left(Aa\rho a^\dagger\right) - \kappa\mathrm{Tr}\left(A\rho a^\dagger a\right), && (2.67)\\
&= -i(\omega_c-\omega)\langle[A,a^\dagger a]\rangle + \epsilon\left(\langle[A,a^\dagger]\rangle - \langle[A,a]\rangle\right)\\
&\quad -\kappa\left(\langle Aa^\dagger a - 2a^\dagger Aa + a^\dagger aA\rangle\right), && (2.68)
\end{aligned}$$

where we used the invariance of the trace under cyclic permutations of the operators it act on. If we want to calculate the time variation of the mean number of photons, we have $A = a^\dagger a$ and we calculate

$$[A,a^\dagger a] = 0,\quad [A,a^\dagger] = a^\dagger[a,a^\dagger] = a^\dagger,\quad [A,a] = -[a,a^\dagger]a = a, \tag{2.69}$$

$$Aa^\dagger a - 2a^\dagger Aa + a^\dagger aA = 2(a^\dagger aa^\dagger a - a^\dagger a^\dagger aa) = 2a^\dagger[a,a^\dagger]a = 2a^\dagger a, \tag{2.70}$$

where we used the commutation relation $[a,a^\dagger] = 1$. We finally find

$$\frac{d}{dt}\langle a^\dagger a\rangle = \epsilon(\langle a^\dagger\rangle + \langle a\rangle) - 2\kappa\langle a^\dagger a\rangle. \tag{2.71}$$

Let us also calculate the time variation of the annihilation operator $A = a$. We have

$$[A,a^\dagger a] = [a,a^\dagger]a = -a,\quad [A,a^\dagger] = 1,\quad [A,a] = 0, \tag{2.72}$$

$$Aa^\dagger a - 2a^\dagger Aa + a^\dagger aA = aa^\dagger a - a^\dagger aa = a[a,a^\dagger] = a, \tag{2.73}$$

and we find

$$\frac{d}{dt}\langle a\rangle = -i(\omega_c-\omega)\langle a\rangle + \epsilon - \kappa\langle a\rangle, \tag{2.74}$$

and $\frac{d}{dt}\langle a^\dagger\rangle$ is the complex conjugate of $\frac{d}{dt}\langle a\rangle$. At the system equilibrium, the time varia-

tions are null and as we solve the system we find for the steady state

$$\langle a^\dagger a\rangle = \frac{\epsilon^2}{\kappa^2 + (\omega_c - \omega)^2}. \tag{2.75}$$

Now we can compare the value we numerically obtain from the steady state using a truncated basis to (2.75) to get an idea of the saturation effect. In this work, we always consider excitation numbers going up to $n_{\max} = 5$. When the cavity is empty and on resonance, which is obtained by setting $\alpha = 0$ and $\omega_c = \omega$, we find, using the parameter values shown in Table 2.1, a difference with Eq. (2.75) of $\sim 0.5\%$. We did not use a higher power laser, to prevent going beyond that margin of error.

One and two-photon Spectroscopy

The transmission T of an optical cavity of decay rate κ is the quantity of photons that filter out of one of the mirrors of the cavity and is given by $T = \kappa\langle a^\dagger a\rangle$. The second order transmission $T^{(2)}$ consider the events involving more than one photon detected at the same time by a photodetector and is given by $T^{(2)} = \kappa^2\langle (a^\dagger)^2 a^2\rangle$. In the following section, we study the values of the populations $\langle a^\dagger a\rangle$ and $\langle (a^\dagger)^2 a^2\rangle$ inside the cavity for the steady state ρ^S in function of the laser frequency ω_c, the transmissions being directly proportional.

First we study the resonant case. When the atoms have the same internal frequency than the cavity, i. e. when $\Delta = 0$, we found that the state $|1, 0\rangle$ does not get populated, since $\langle 1, 0|W|0, gg\rangle$ vanishes and neither do the states $|2, 0_{a,b}\rangle$. Hence, we should not expect to see a one photon transition peak at the frequency $\omega = \omega_c$. We plotted the photon spectrum in Fig. 2.4, and we see that, indeed, on the top curve the photon population at $\omega = \omega_c$ is highly inhibited, the main peaks of the spectrum are those due to the $|n, \pm\rangle$ transitions, for $n = 1, 2$ and slightly $n = 3$.

We see the peaks due to the one-photon processes $|0\rangle \to |1, \pm\rangle$ in the $\langle (a^\dagger)^2 a^2\rangle$ spectrum, but the laser power is strong enough for the amplitude of the two-photon

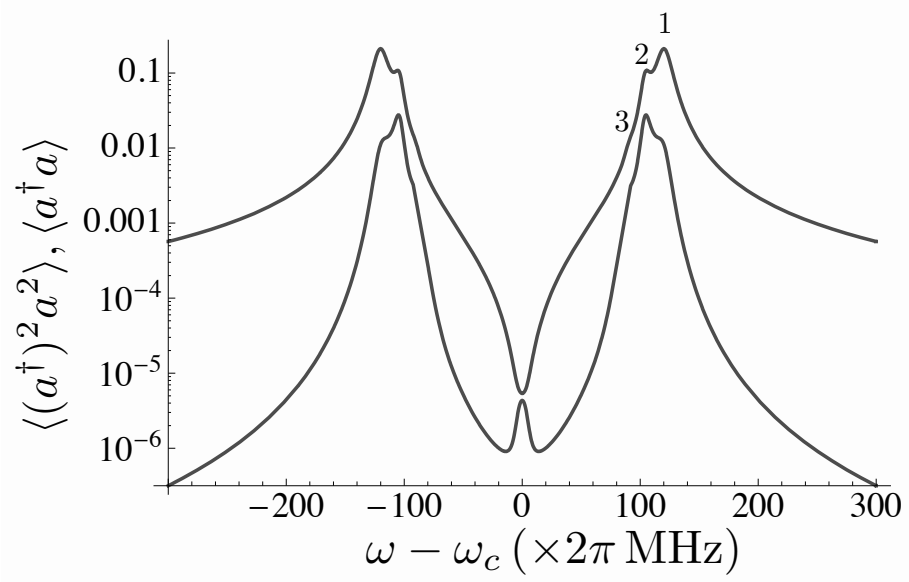

Figure 2.4: Spectra of $\langle a^\dagger a \rangle$ (top) and $\langle (a^\dagger)^2 a^2 \rangle$ (bottom) in function of $\omega - \omega_c$ for the values in Tab. 2.1 and $\Delta = 0$. Note the absence of peak at $\omega = \omega_c$. The other peaks are numbered as the order of the n-photon transition $|0\rangle \to |n, +\rangle$ at $\omega - \omega_c = \lambda_n/n$: one-photon, two-photon and an embryo of the three-photon transition can be made out. The symmetrical peaks on the left side correspond to the n-photon transition $|0\rangle \to |n, -\rangle$.

$|0\rangle \to |2, \pm\rangle$ transition peak to dominate it and to bring a non-negligible contribution in the spectrum of $\langle a^\dagger a \rangle$. That dominance grows as the laser power increases, since the n photons transitions rates scale as $\sim \epsilon^{2n}$. We note a small peak at $\omega = \omega_c$ for $\langle (a^\dagger)^2 a^2 \rangle$. That peak might be explained by higher order transitions ($n \geq 3$) which are not inhibited, but also not strong enough to show on $\langle a^\dagger a \rangle$.

Then we study the non-resonant case by setting $\Delta = 150 \times 2\pi$ MHz in Fig. 2.5. In that situation, the matrix element $\langle 1, 0|W|0\rangle$ is no longer zero and the transitions at $\omega = \omega_c$ are allowed again, hence the observed peak at the cavity resonance frequency which largely dominates the other transition peaks. The transition at $\omega = \omega_c$ is the condition for the consecutive one-photon transitions $|0\rangle \to |1, 0\rangle \to \cdots \to |n, 0_{a,b}\rangle$, which is why the peak is also very important on $\langle (a^\dagger)^2 a^2 \rangle$, unlike the peak corresponding to the $|0\rangle \to |1, \pm\rangle$, which does not correspond to a two-photon process and is henceforth comparatively much weaker on the $\langle (a^\dagger)^2 a^2 \rangle$ spectrum. Once again, we note that in the two-photon spectrum the two-photon transmission to $|2, \pm\rangle$ is of the same order of magnitude than the transmission to

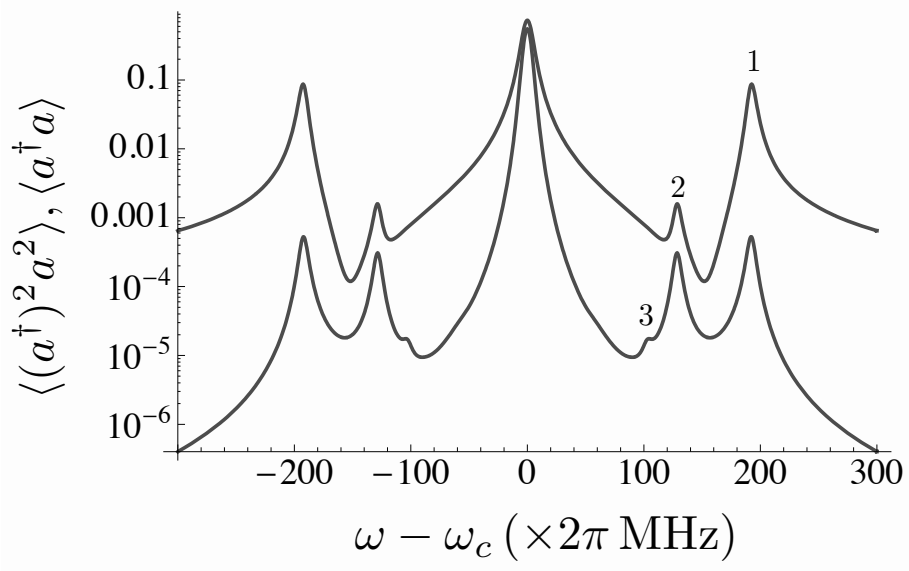

Figure 2.5: Spectra of $\langle a^\dagger a \rangle$ (top) and $\langle (a^\dagger)^2 a^2 \rangle$ (bottom) in function of $\omega - \omega_c$ for the values in Tab. 2.1 and $\Delta = 150 \times 2\pi\,\mathrm{MHz}$. The transition at $\omega = \omega_c$ is not inhibited anymore, on the contrary it yields the most important peak. The other peaks are numbered as the order of the n-photon transition $|0\rangle \to |n, +\rangle$ at $\omega - \omega_c = \lambda_n/n$: one-photon, two-photon and three-photon (not visible on the $\langle a^\dagger a \rangle$ spectrum). The symmetrical peaks on the left side correspond to the n-photon transitions $|0\rangle \to |n, -\rangle$.

$|1, \pm\rangle$, due to the strength of the laser power. Also, we note the emergence of two new peaks, only visible on $\langle (a^\dagger)^2 a^2 \rangle$, which are due to three-photon transitions.

Cavity quality

In this section, we study the influence of the quality of the cavity on various possible spectra by superposing plots or the same quantity for different values of the decay rate κ. A theoretical, perfect cavity is characterized by $\kappa = 0$ (in which case the transmission actually vanishes) while an imperfect cavity will have κ greater than zero. The greater κ is, the closer the cavity will mimic free space.

First we study the transmission spectra, shown in Fig 2.6, for different values of κ and $\Delta = 150 \times 2\pi\,\mathrm{MHz}$. When the cavity decay rate is great, the $\langle a^\dagger a \rangle$ spectrum obtained is a typical one-photon absorption spectrum, with dips located at the two atomic frequencies, $\omega_c \pm \Delta$, which is similar to the case of two atoms in a vacuum. There is no other visible

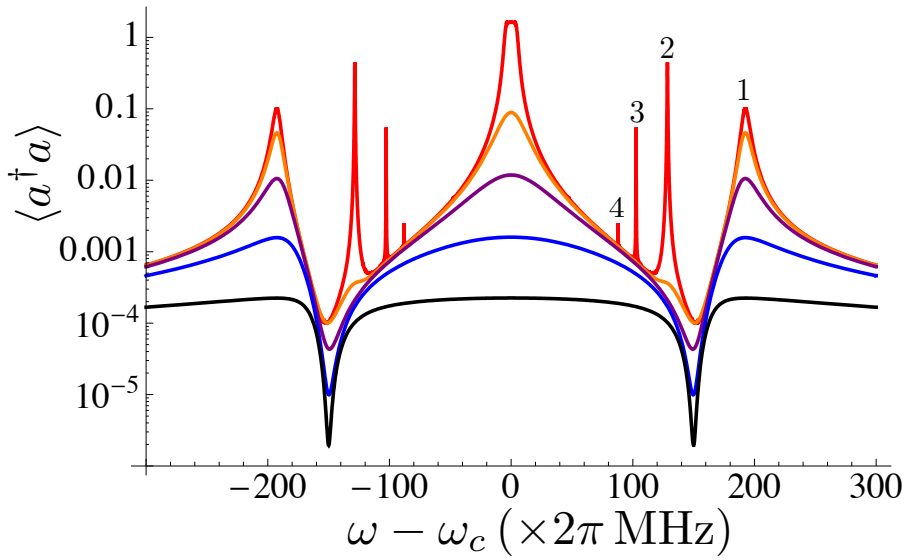

Figure 2.6: Spectra of $\langle a^\dagger a \rangle$ in function of $\omega - \omega_c$ for the values in Tab. 2.1, $\Delta = 150 \times 2\pi$ MHz and different values of κ (in 2π MHz): 0 (Red); 20 (Orange); 55 (Purple); 150 (Blue); 400 (Black). The peaks are numbered in function of the order of the transitions at $\omega - \omega_c = \lambda_n/n$.

structure for cavities of such low quality.

When the cavity quality increases, peaks progressively start to appear at the frequencies of all the allowed transitions. In a perfect cavity, the amplitude of the peaks becomes very important and we observe several peaks numbered on the plot, corresponding to the n-photon processes $|0\rangle \to |n, \pm\rangle$ at $\omega - \omega_c = \lambda_n/n$ for $n = 1, 2, 3, 4$. We also note the amplitude of the central peak at $\omega = \omega_c$, which corresponds to all the consecutive one-photon transitions $|0\rangle \to |1, 0\rangle \to \cdots \to |n, 0_{a,b}\rangle$.

Let us now study another aspect of the system and measure the populations of the excited states $|e_1\rangle$ and $|ee\rangle$ in the steady state ρ^S in function of the laser frequency ω. The quantities $\langle e_1|\rho^S|e_1\rangle$ and $\langle ee|\rho^S|ee\rangle$ will be considered, where the traces over the subsystems of no direct interest, namely the photon field and the second atom, is implied. Those atomic populations can be measured in circuit-QED [39].

In Fig. 2.7 we plotted the spectrum of $\langle ee|\rho^S|ee\rangle$. For a lossless cavity (in red) we observe transition peaks corresponding to the n-photon processes $|0\rangle \to |n, \pm\rangle$ at $\omega - \omega_c = \lambda_n/n$ for n up to 5, all numbered on the figure. Between the peak number five and the

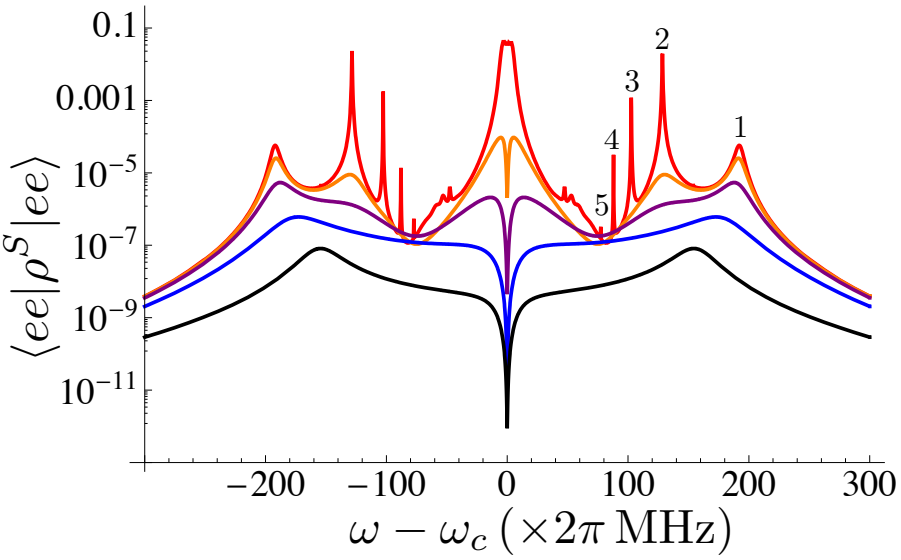

Figure 2.7: Spectra of $\langle ee|\rho^S|ee\rangle$ in function of $\omega - \omega_c$ for the values in Tab. 2.1, $\Delta = 150 \times 2\pi\,\mathrm{MHz}$ and different values of κ (in 2π MHz): 0 (Red); 20 (Orange); 55 (Purple); 150 (Blue); 400 (Black). The peaks are numbered in function of the order of the transitions at $\omega - \omega_c = \lambda_n/n$.

central peak we can distinguish a few small peaks. It can be shown that those peaks correspond to the transitions $|1,\pm\rangle \to |n,\pm\rangle$ with $n \geq 2$, which happen at the frequencies $\omega = \omega_c \pm (\lambda_n - \lambda_1)/(n-1)$. That second series of excitations is made possible thanks to the strength of the laser which populates the $|1,\pm\rangle$ states even away from resonance.

For cavities of lesser quality, the peaks quickly start to fade away. For the worst cavity we considered (in black), we see the apparition of two peaks, who are actually centered on the atomic frequencies $\omega - \omega_c = \pm 150 \times 2\pi\,\mathrm{MHz}$, a behavior we would expect from the ionization spectrum of two atoms in free space, as in Fig. 2.1. We also note the apparition of a dip at the frequency $\omega = \omega_c$. We saw in Sec. 2.1 that in free space the transition are $2\omega = \omega_1 + \omega_2$ was prohibited by Fermi's golden rule, although that prohibition in the perturbation theory did not translate in the steady state behavior by an interference or a dip, but rather simply by an absence of peak. In our case, for a low quality cavity, the $\omega = \omega_c$ transition to the $|ee\rangle$ state is strictly prohibited unlike the photonic transitions shown in Fig. 2.5, even though they are both predicted to happen by perturbation theory. At this stage, we can only assume that this behavior is induced by the cavity decay

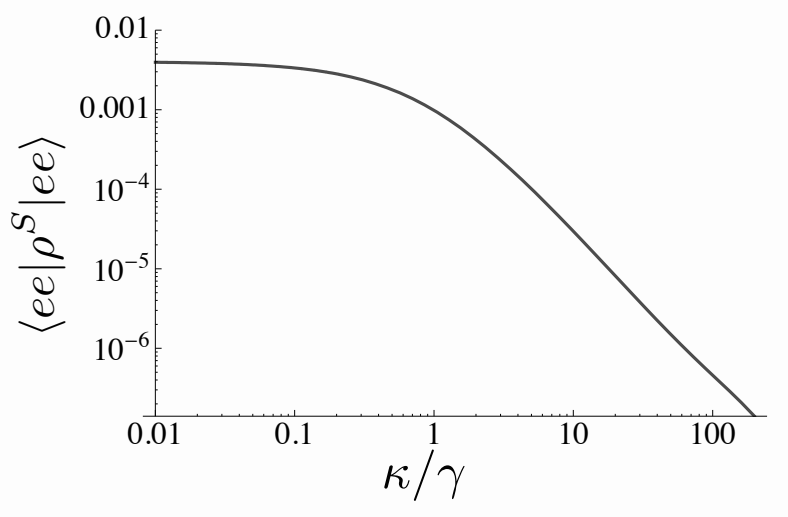

Figure 2.8: Spectrum of $\langle ee|\rho^S|ee\rangle$ in function of κ for the values in Tab. 2.1, $\Delta = 150 \times 2\pi$ MHz at the resonance $\omega = \omega_c + \lambda_2/2$. For $\kappa \ll \gamma$ the population is saturated by the spontaneous emission, it then decreases following a power law as κ grows beyond γ.

mechanisms which are not considered in Fermi's golden rule and more calculations should be made in order to understand this phenomenon completely.

In Fig. 2.8, we study the diminution of the peak amplitude of $\langle ee|\rho^S|ee\rangle$ at the frequency $\omega = \omega_c + \lambda_2/2$ in function of κ/γ. Clearly, when $\kappa \ll \gamma$ the amplitude saturates, i. e. the population of the doubly excited atoms is limited by the spontaneous emission, but another regime is reached when $\kappa \gg \gamma$ where the amplitude is decreased following a power law. We therefore see that the best amplitudes are reached for the cavity decay rate smaller or of the order of the atomic decay rate.

In Fig. 2.9, we study the probability to observe only one of the atoms excited $\langle e_1|\rho^S|e_1\rangle$ in function of $\omega - \omega_c$. For a perfect cavity (in red), we observe once again transition peaks for the transitions $|0\rangle \to |n, \pm\rangle$ at $\omega - \omega_c = \lambda_n/n$ for n up to 3, although the two higher order peaks are very thin and disappear completely for $\kappa = 20 \times 2\pi$ MHz which is easily understood since those are multi-photon processes measured on a single excitation spectrum, just as the two-photon peaks on $\langle a^\dagger a\rangle$ in Fig. 2.5 was several orders of magnitude smaller than the one-photon peaks on $\langle a^\dagger a\rangle$.

For greater values of cavity decay rate, all the peaks begin to fade away until only

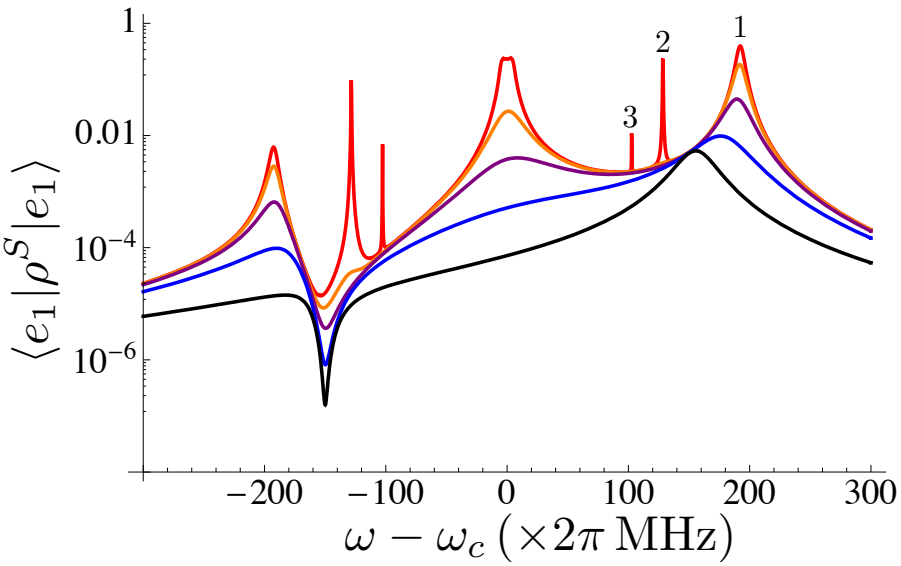

Figure 2.9: Spectra of $\langle e_1|\rho^S|e_1\rangle$ in function of $\omega - \omega_c$ for the values in Tab. 2.1, $\Delta = 150 \times 2\pi\,\mathrm{MHz}$ and different values of κ (in 2π MHz): 0 (Red); 20 (Orange); 55 (Purple); 150 (Blue); 400 (Black). The peaks are numbered in function of the order of the transitions at $\omega - \omega_c = \lambda_n/n$.

one peak is left around the first internal atomic frequency at $\omega - \omega_c = 150 \times 2\pi\,\mathrm{MHz}$, as we would expect from a spectrum of an atom in free space. What we would not expect from such a spectrum however is the dip that forms around the second atomic internal frequency $\omega - \omega_c = -150 \times 2\pi\,\mathrm{MHz}$. That new behavior is once again due to the cavity decay process in the system. Note that even though the presence of the $|ee\rangle$ state is strongly inhibited for finite κ at the frequency $2\omega = \omega_1 + \omega_2$, the presence of only one excited atom is not affected at all, which induces a strong blockade in the system, even if the two atoms do not interact directly with each other.

One interesting feature we also observe on the graph is that at the amplitude of the population of the $\langle e_1|\rho^S|e_1\rangle$ at the first atomic internal frequency $\omega - \omega_c = 150 \times 2\pi\,\mathrm{MHz}$ seems to be completely independent from the value of κ. For a perfect cavity, there is no discernible peak at that location, but as the decay rate grows, the population stays the same while for all the other frequencies it weakens, which eventually yields a peak at the atomic frequency.

2.4 General Atomic Frequency Spread

In this section, we investigate the behavior of the system not being restrained by the constraint $\omega_1 + \omega_2 = 2\omega_c$. For this general setup of the atomic frequencies, we are no longer able to diagonalize the unperturbed Hamiltonian or perturbation theory. We will rely purely on numerical considerations and analogies with the previous case.

We define the atomic frequencies to be

$$\omega_1 = \omega_c + \Delta + \phi, \tag{2.76}$$

$$\omega_2 = \omega_c - \Delta + \phi, \tag{2.77}$$

which yield every possible value of ω_1 and ω_2 when Δ and ϕ are allowed to vary. The particular case $\omega_1 + \omega_2 = 2\omega_c$ is found when $\phi = 0$.

2.4.1 Eigenstates and Eigenvalues

We showed in Sec. 2.2 that the Hamiltonian H always commutes with the global excitation number operator $\hat{n}$ without making any assumptions on the atomic frequencies. This means that H keeps its block diagonal form described earlier, however we were unable to diagonalize the different blocks with general atomic internal frequencies. Although the analytical form of the eigenvalues and eigenstates are not generally known, except for the ground state $|0\rangle$, we may still numerically identify them. We keep the notation previously used and call the $n = 1$ excited states $|1, 0\rangle, |1, \pm\rangle$ and the n excited states $|n, 0_{a,b}\rangle, |n, \pm\rangle$ with the respective eigenvalues 0, $\hbar\omega_c + \hbar\lambda^{(1,0)}$, $\hbar\omega_c + \hbar\lambda^{(1,\pm)}$, $n\hbar\omega_c + \hbar\lambda^{(n,0_{a,b})}$ and $n\hbar\omega_c + \hbar\lambda^{(n,\pm)}$. Although we do not now the analytical form of these eigenvalues, we can identify them from the values they have for $\phi = 0$.

In Fig. 2.10, we show the numerical values of $\lambda^{(1,0)}$, $\lambda^{(1,\pm)}$, $\lambda^{(2,0_{a,b})}/2$ and $\lambda^{(2,\pm)}/2$ as well as ω_1, ω_2 and $(\omega_1 + \omega_2)/2$ in function of ϕ for $\Delta = 150 \times 2\pi$ MHz. We identify which eigenvalue is which from the initial values at $\phi = 0$, with some uncertainty about $\lambda^{(2,0_a)}$

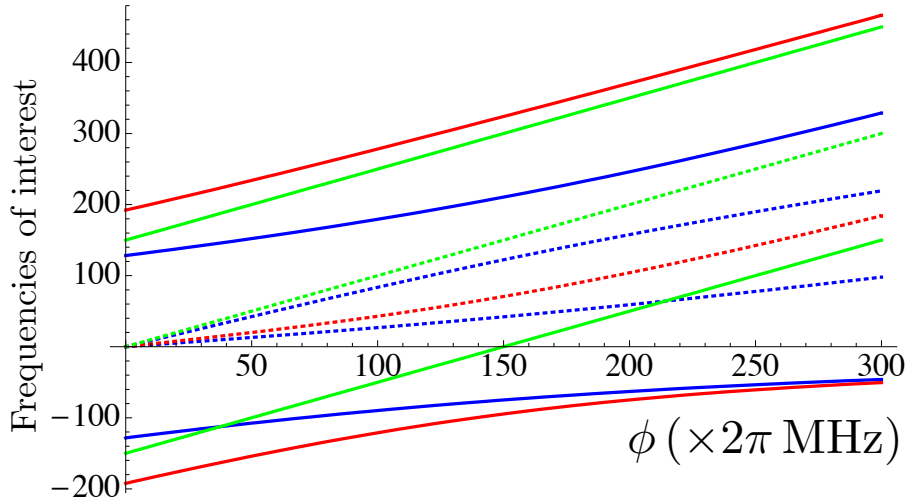

Figure 2.10: Numerical values of $\lambda^{(1,0)}$ (red, dotted), $\lambda^{(1,\pm)}$ (red), $\lambda^{(2,0_{a,b})}/2$ (blue, dotted) and $\lambda^{(2,\pm)}/2$ (red) as well as ω_1, ω_2 (green) and $(\omega_1+\omega_2)/2$ (green, dotted) in function of ϕ for $\alpha = 85\times 2\pi\,\mathrm{MHz}, \Delta = 150\times 2\pi\,\mathrm{MHz}$. The red and blue lines represent the values of $\omega-\omega_c$ a which one and two-photon transitions are expected and the green lines the values we might expect dips for different quantities. The dotted lines are transition values that are degenerate when $\Delta = 0$.

and $\lambda^{(2,0_b)}$ which are degenerate for $\phi = 0$. We will shortly solve this problem.

We chose for the next numerical calculations to settle on the numerical parameter $\phi = 130\times 2\pi\,\mathrm{MHz}$ which spreads as evenly as possible all the numerical values plotted in an attempt to separate the possible peaks and dips as well as possible. We used in the previous calculations a high laser strength $\epsilon = 6\times 2\pi\,\mathrm{MHz}$ in order to maximize the visibility of the two-photon processes in the spectra. Unfortunately, using a high laser power also broadens the peaks and as we now investigate a more general case with a more complex structure, we will use the smaller value $\epsilon = 2\pi\,\mathrm{MHz}$ to separate the peaks more effectively.

In the particular case of two identical atoms, i. e. when $\Delta = 0$, we can partially diagonalize the blocks of the unperturbed Hamiltonian and find a few eigenstates. These

eigenvectors are

$$|1,0\rangle = \frac{1}{\sqrt{2}}\left(|0,eg\rangle - |0,ge\rangle\right), \tag{2.78}$$

$$|1,\pm\rangle = \frac{1}{\sqrt{2\alpha^2 + (\lambda^{(1,\pm)})^2}}\left(\alpha|0,eg\rangle + \alpha|0,ge\rangle - \lambda^{(1,\pm)}|1,gg\rangle\right), \tag{2.79}$$

$$|2,0_b\rangle = \frac{1}{\sqrt{2}}\left(|1,eg\rangle - |1,ge\rangle\right), \tag{2.80}$$

and the other ones were not found. We chose to call the last state $|2,0_b\rangle$ rather than $|2,0_a\rangle$ since it is actually the same as the case $\phi = 0$. Note that $|1,0\rangle$ and $|2,0_b\rangle$ are again antisymmetrical under the permutation of the two atoms and are again decoupled from the other states. We can also calculate the respective eigenvalues to the eigenstates and we find that $\lambda^{(1,0)} = \Delta$, $\lambda^{(1,\pm)} = (\Delta \pm \sqrt{8\alpha^2 + \Delta^2})/2$ and $\lambda^{(2,0_b)} = \Delta$. Numerically, starting from that situation, we checked that value of $\lambda^{(2,0_b)}$ is always smaller than $\lambda^{(2,0_a)}$ for other values of Δ and ϕ and the uncertainty about their respective denomination is lifted.

We can calculate the few off-diagonal terms coming from the perturbation W linking those eigenstates, which are expressed, in the unperturbed Hamiltonian eigenstates basis, as

$$\langle 0|W|1,0\rangle = 0, \tag{2.81}$$

$$\langle 0|W|1,\pm\rangle = -i\,\frac{\lambda^{(1,\pm)}}{\sqrt{2\alpha^2 + (\lambda^{(1,\pm)})^2}}\,\epsilon, \tag{2.82}$$

$$\langle 1,0|W|2,0_b\rangle = -i\epsilon, \tag{2.83}$$

$$\langle 1,\pm|W|2,0_b\rangle = 0, \tag{2.84}$$

which indicates that, because of their antisymmetry, the $|1,0\rangle$ and $|2,0_b\rangle$ states do not get populated by the perturbation by either one or two-photon processes.

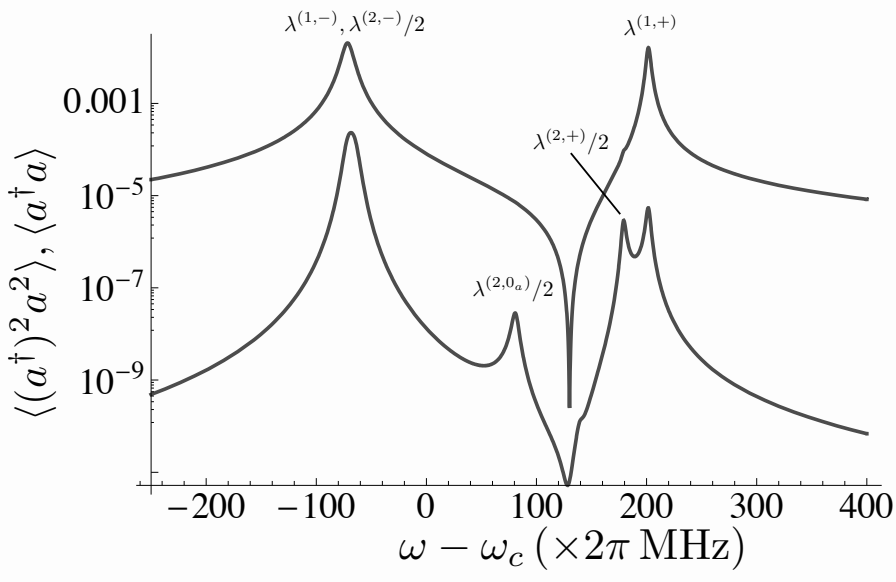

Figure 2.11: Spectra of $\langle a^\dagger a \rangle$ (top) and $\langle (a^\dagger)^2 a^2 \rangle$ (bottom) in function of $\omega - \omega_c$ for the values in Tab. 2.1, $\epsilon = 2\pi\,\mathrm{MHz}$, $\Delta = 0$ and $\phi = 130 \times 2\pi\,\mathrm{MHz}$. We find two peaks at $\omega - \omega_c = \lambda^{(1,\pm)}$ corresponding to one-photon transitions and three peaks at $\omega - \omega_c = \lambda^{(2,\pm)}/2$ and $\lambda^{(2,0_a)}/2$ corresponding to the two-photon transitions. No trace of transitions involving the states $|1,0\rangle$ or $|n,0_b\rangle$. We also find a dip at the atomic frequencies $\omega_1 = \omega_2 = \omega_c + \Delta$.

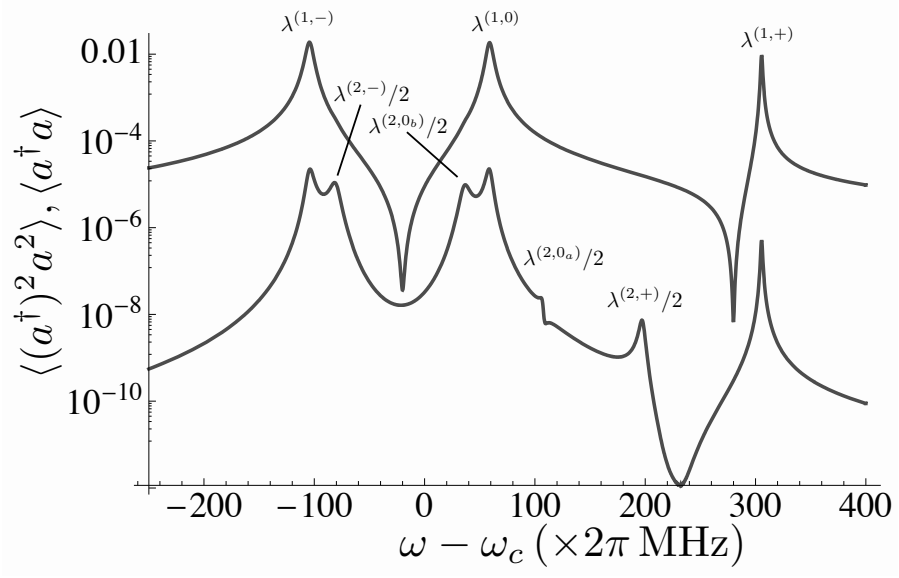

Figure 2.12: Spectra of $\langle a^\dagger a\rangle$ (top) and $\langle (a^\dagger)^2 a^2\rangle$ (bottom) in function of $\omega - \omega_c$ for the values in Tab. 2.1, $\epsilon = 2\pi$ MHz, $\Delta = 150 \times 2\pi$ MHz and $\phi = 130 \times 2\pi$ MHz. We find three peaks at $\omega - \omega_c = \lambda^{(1,\pm)}$ and $\lambda^{(1,0)}$ corresponding to one-photon transitions and four peaks at $\omega - \omega_c = \lambda^{(2,\pm)}/2$ and $\lambda^{(2,0_{a,b})}/2$ corresponding to two-photon transitions. We also find two dips at the atomic frequencies $\omega - \omega_c = 280 \times 2\pi$ MHz and $\omega - \omega_c = -20 \times 2\pi$ MHz.

Atomic, one and two-photon Spectroscopy

Let us now study the different spectra of the general steady state case. We show in Fig. 2.11 the $\langle a^\dagger a\rangle$ and $\langle (a^\dagger)^2 a^2\rangle$ spectra of the particular case $\Delta = 0$. As we expected, there is no peak at $\omega = \omega_c$, on the contrary we find there a strong dip in the populations at the atomic frequencies $\omega_1 = \omega_2 = \omega_c$, due once again to the cavity decay process. We find two-photon peaks in the $\langle (a^\dagger)^2 a^2\rangle$ spectrum (and a beginning of a three-photon peak around $\omega - \omega_c \simeq 140 \times 2\pi$ MHz), although the peak at $\lambda^{(2,-)}/2$ happens to be very close to the one-photon peak at $\lambda^{(1,-)}$ and those two are not resolved but yield a peak of consequently greater amplitude than the peak at $\lambda^{(2,+)}/2$.

Let us now investigate the more general case $\Delta = 150 \times 2\pi$ MHz and $\phi = 130 \times 2\pi$ MHz, of which we plotted the $\langle a^\dagger a\rangle$ and $\langle (a^\dagger)^2 a^2\rangle$ spectra in Fig. 2.12. We count three one-photon peaks, all associated with one $n = 1$ eigenvalue and four two-photon peaks, again associated with the four $n = 2$ eigenvalues. We find two important dips in $\langle a^\dagger a\rangle$ located

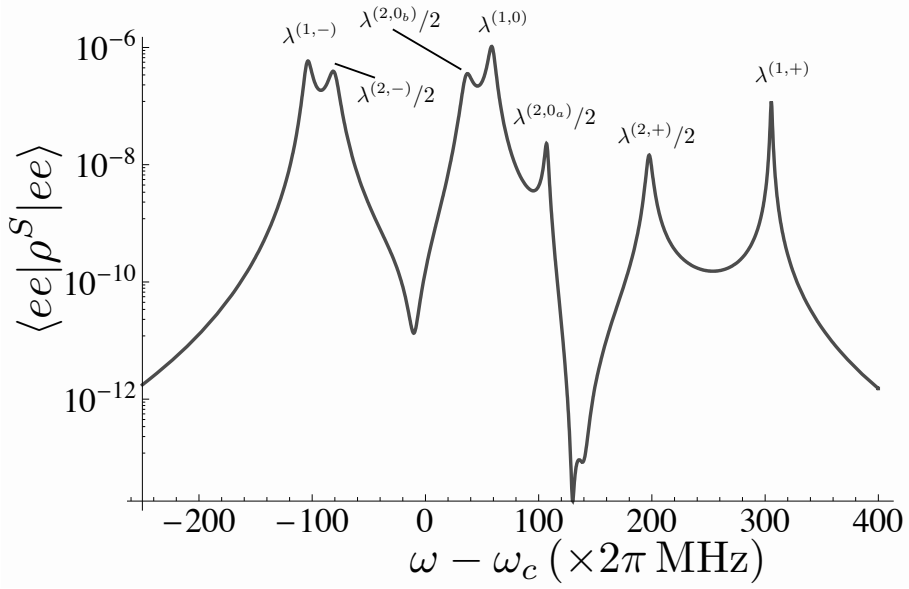

Figure 2.13: Spectrum of $\langle ee|\rho^S|ee\rangle$ in function of $\omega - \omega_c$ for the values in Tab. 2.1, $\epsilon = 2\pi\,\mathrm{MHz}$, $\Delta = 150 \times 2\pi\,\mathrm{MHz}$ and $\phi = 130 \times 2\pi\,\mathrm{MHz}$. We find three peaks at $\omega - \omega_c = \lambda^{(1,\pm)}$ and $\lambda^{(1,0)}$ corresponding to all possible one-photon transitions and four peaks at $\omega - \omega_c = \lambda^{(2,\pm)}/2$ and $\lambda^{(2,0_{a,b})}/2$ corresponding to all possible two-photon transitions. We also count three dips, two small ones at the atomic frequencies and an important one at the mean frequency $\omega - \omega_c = 130 \times 2\pi\,\mathrm{MHz}$.

at the two atomic frequencies $\omega - \omega_c = 280 \times 2\pi\,\mathrm{MHz}$ and $\omega - \omega_c = -20 \times 2\pi\,\mathrm{MHz}$ which is a cavity decay related process. In the $\langle (a^\dagger)^2 a^2 \rangle$ spectrum, the same dips are not visible, but we see the apparition of a new one around $\omega - \omega_c \simeq 225 \times 2\pi\,\mathrm{MHz}$ that does not seem to correspond to any particular value we used up until now.

In Fig. 2.13 we plotted the spectrum of $\langle ee|\rho^S|ee\rangle$ in function of $\omega - \omega_c$ also for $\Delta = 150 \times 2\pi\,\mathrm{MHz}$ and $\phi = 130 \times 2\pi\,\mathrm{MHz}$. We count seven peaks, three associated one-photon processes and four associated two-photon processes. This is the most general case where there is no interference between the different excitation paths that lead to an inhibition of a peak. We also count three different dips, two of them of weak amplitude located at the atomic frequencies $\omega - \omega_c = 280 \times 2\pi\,\mathrm{MHz}$ and $\omega - \omega_c = -20 \times 2\pi\,\mathrm{MHz}$, and a very strong one located at the half-sum of the frequencies $\omega - \omega_c = 130 \times 2\pi\,\mathrm{MHz}$, once again linked with the cavity decay process.

2.4.2 Cavity Induced Transparency

Let us investigate another property of two atoms in a cavity. We showed in Eq. (2.75) the spectrum of the mean number of photon $\langle a^\dagger a\rangle$ in an empty cavity. Using the same formalism we will derive the analytical expression of $\langle a^\dagger a\rangle$ in an empty cavity and show that

$$\langle (a^\dagger)^2 a^2\rangle = (\langle a^\dagger a\rangle)^2. \tag{2.85}$$

For that, we use Eq. (2.68) with $A = (a^\dagger)^2 a^2$ and we calculate

$$[A, a^\dagger a] = 0, \;\; [A, a^\dagger] = 2a^\dagger a^\dagger a, \;\; [A, a] = -2a^\dagger a a, \tag{2.86}$$

$$Aa^\dagger a - 2a^\dagger A a + a^\dagger a A = 2a^\dagger a^\dagger a a, \tag{2.87}$$

where we used the basic commutation relations $[a, a^\dagger] = 1$ to find the final results. We find

$$\frac{d}{dt}\langle (a^\dagger)^2 a^2\rangle = 2\epsilon(\langle a^\dagger a^\dagger a\rangle + \langle a^\dagger a a\rangle) - 4\kappa\langle (a^\dagger)^2 a^2\rangle, \tag{2.88}$$

and we have to calculate the time variation of $\langle a^\dagger a^\dagger a\rangle$. Let us pose $B = a^\dagger a^\dagger a$ and we have

$$[B, a^\dagger a] = -a^\dagger a^\dagger a, \;\; [B, a^\dagger] = a^\dagger a^\dagger, \;\; [B, a] = -2a^\dagger a, \tag{2.89}$$

$$Ba^\dagger a - 2a^\dagger B a + a^\dagger a B = 3a^\dagger a^\dagger a. \tag{2.90}$$

We have

$$\frac{d}{dt}\langle a^\dagger a^\dagger a\rangle = \left(i(\omega_c - \omega) - 3\kappa\right)\langle a^\dagger a^\dagger a\rangle + \epsilon(\langle a^\dagger a^\dagger\rangle + 2\langle a^\dagger a\rangle), \tag{2.91}$$

and with $\frac{d}{dt}\langle a^\dagger a a\rangle$ its complex conjugate. There is one more the time variation to calculate.

With $C = a^2$ we have

$$[C, a^\dagger a] = 2aa, \quad [C, a^\dagger] = 2a, \quad [C, a] = 0, \tag{2.92}$$

$$Ca^\dagger a - 2a^\dagger Ca + a^\dagger aC = 2aa, \tag{2.93}$$

and we have

$$\frac{d}{dt}\langle a^2\rangle = 2\left(-i(\omega_c - \omega) - \kappa\right)\langle a^2\rangle + 2\epsilon\langle a\rangle. \tag{2.94}$$

and with $\frac{d}{dt}\langle (a^\dagger)^2\rangle$ its complex conjugate.

Globally, in the steady state, we have

$$\langle a\rangle = \frac{\epsilon}{\kappa + i(\omega_c - \omega)}, \tag{2.95}$$

$$\langle a^\dagger a\rangle = \frac{\epsilon^2}{\kappa^2 + (\omega_c - \omega)^2} = \langle a^\dagger\rangle\langle a\rangle, \tag{2.96}$$

$$\langle a^2\rangle = \frac{\epsilon\langle a\rangle}{\kappa + i(\omega_c - \omega)} = \langle a\rangle^2, \tag{2.97}$$

$$\langle a^\dagger a^\dagger a\rangle = \frac{\epsilon(\langle a^\dagger a^\dagger\rangle + 2\langle a^\dagger a\rangle)}{3\kappa - i(\omega_c - \omega)} = \epsilon\langle a^\dagger\rangle\frac{\langle a^\dagger\rangle + 2\langle a\rangle}{3\kappa - i(\omega_c - \omega)} = \langle a^\dagger\rangle\langle a^\dagger a\rangle, \tag{2.98}$$

$$\langle (a^\dagger)^2 a^2\rangle = \frac{\epsilon}{2\kappa}(\langle a^\dagger a^\dagger a\rangle + \langle a^\dagger aa\rangle) = \frac{\epsilon}{2\kappa}\langle a^\dagger a\rangle(\langle a^\dagger\rangle + \langle a\rangle) = \langle a^\dagger a\rangle^2, \tag{2.99}$$

and we have the desired result.

We showed in Fig. 2.14 (a) the same plot as in Fig. 2.12 (blue) along with the spectrum obtained by setting the atom-field coupling constant α to zero (red, dotted). We noted that at the frequency $\omega = (\omega_1 + \omega_2)/2 = \omega_c + \phi$ both red lines crossed the blue lines. In other words, at that particular frequency, the number of photons in the cavity is exactly the number of photons that would be expected in an empty cavity, furthermore the same result holds for the mean number of pairs of photons. It is easy to check numerically that the relation

$$\langle (a^\dagger)^2 a^2\rangle = (\langle a^\dagger a\rangle)^2, \tag{2.100}$$

also holds for our two-atom system at the frequency $2\omega = \omega_1 + \omega_2$.

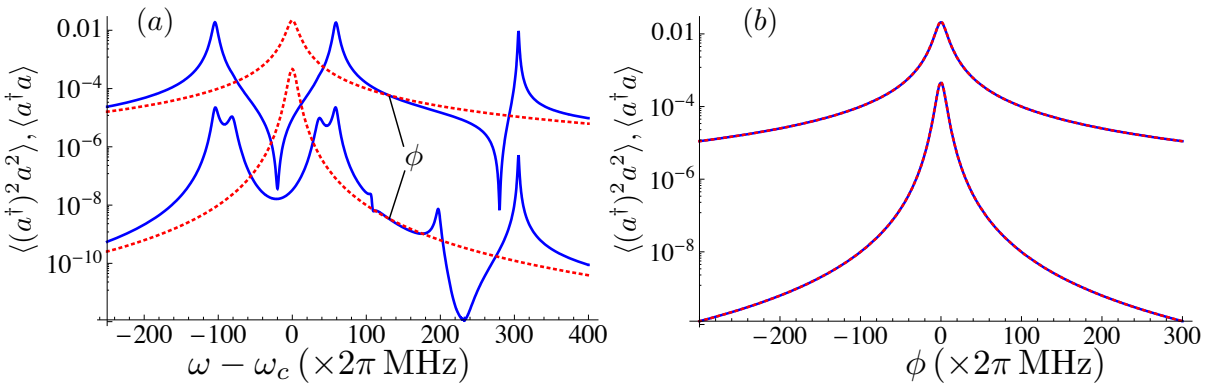

Figure 2.14: On (a), spectra of $\langle a^\dagger a \rangle$ (top) and $\langle (a^\dagger)^2 a^2 \rangle$ (bottom) in function of $\omega - \omega_c$ for the values in Tab. 2.1, $\epsilon = 2\pi$ MHz, $\Delta = 150 \times 2\pi$ MHz and $\phi = 130 \times 2\pi$ MHz (blue) along with the same spectra of an empty cavity (red, dotted) with the same settings and $\alpha = 0$. On (b), the same spectra of the system with the laser frequency set on $\omega = \omega_c + \phi = (\omega_1 + \omega_2)/2$ in function of ϕ (blue), along with the spectra of the empty cavity (red, dotted). At the frequency $2\omega = \omega_1 + \omega_2$, the system behaves as if the atoms were not in the cavity.

In Fig. 2.14 (b) we plotted $\langle a^\dagger a \rangle$ and $\langle (a^\dagger)^2 a^2 \rangle$ in function of ϕ for a laser frequency $\omega = \omega_c + \phi = (\omega_1 + \omega_2)/2$ (blue) along with the same quantities obtained for an empty cavity (red, dotted) for comparison. The two plots are identical, signature of some kind of cavity induced transparency (CIT) of the system.

Those figures were plotted with the atomic frequency difference $\Delta = 150 \times 2\pi$ MHz, however we may recall that the all the photon spectra we presented showed dips at the atomic frequencies ω_1 and ω_2 (although not very obvious on Fig. 2.5 due to the large value of ϵ), we would therefore suspect that the transparency effect would not be observed when the atoms have identical frequencies, i. e. when $\Delta = 0$. Indeed, the mean number of photons in a cavity with a laser on resonance with two identical atoms does not go beyond $\langle a^\dagger a \rangle \simeq 3\ 10^{-10}$, a value of about 6 orders of magnitude smaller than the one obtained for $\Delta = 150 \times 2\pi$ MHz.

In Fig. 2.15 we plotted the same plot as in Fig. 2.14 (b), but with a smaller gap in atomic frequencies $\Delta = 50 \times 2\pi$ MHz. We can see that on most of the spectrum the CIT effect is observed, although around $\phi = 0$ the number of photons in the cavity is slightly

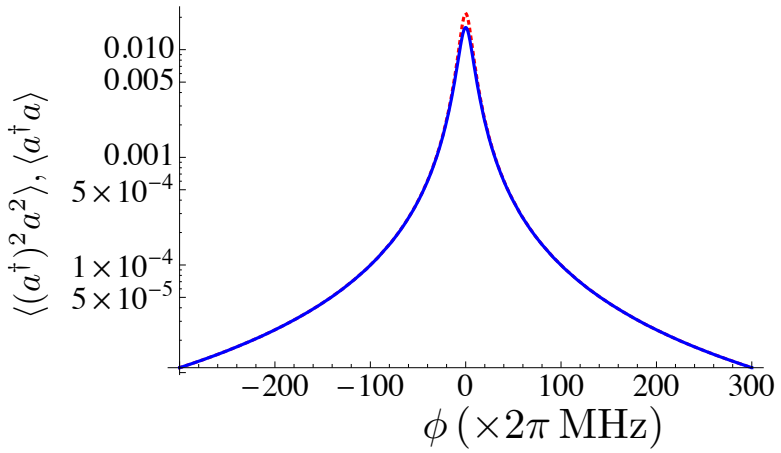

Figure 2.15: Spectra of $\langle a^\dagger a\rangle$ (top) and $\langle (a^\dagger)^2 a^2\rangle$ (bottom) of the system with the laser frequency set on $\omega = \omega_c + \phi = (\omega_1 + \omega_2)/2$ in function of ϕ (blue) along with the spectra of the empty cavity (red, dotted). The CIT effect is not perfectly observed around $\phi = 0$ since the atom frequencies are not spread out enough.

smaller than what it would be in an empty cavity. We conclude that the CIT effect is stronger when the gap in the atomic frequencies is larger and not in competition with the cavity decay induced photon inhibition at the atomic frequencies.

We see on Fig. 2.10 that the $(\omega_1 + \omega_2)/2$ values for non-zero ϕ never coincide with another transition value, therefore we should not expect a strong competition between the CIT and other transition resonances.

2.5 Summary and Discussion

In this chapter, we have studied the behavior of two unidentical two-level atoms in a single mode cavity driven by a laser under realistic conditions of spontaneous emission and cavity losses. In free space, two-photon processes for independent atoms do not happen, as we checked by using perturbation theory and further with a master equation calculation. Our next objective was to show that two-level processes are possible in a cavity ad to study their occurrences in realistic experimental conditions.

In order to study the system using perturbation theory, we made the simplification of considering two atoms with frequencies evenly spread around the cavity mode frequency.

We were then able to express analytically the eigenstates and eigenvalues of the unperturbed Hamiltonian, which allowed us to show that two-photon processes were possible for different dressed states of the system. In the free space case, the two-photon processes would have to happen at the mean of the atomic frequencies, but we found that in a cavity the transitions at that particular frequency were merely one-photon processes which could however be suppressed if the two atoms were identical with internal frequencies equal to the cavity's.

We confirmed that analysis with the steady states of the master equation and we observed peaks due to multi-photon processes, up to five-photon processes in a perfect cavity[1]. The mean number of photons in the cavity, the mean number of pairs of photons, the population of a single excited atom as well as the population of two excited atoms in the system were studied.

Some effect that were not expected from the perturbation theory were observed for important cavity decay rates. Dips in the mean number of photons spectra were found whenever the laser hit the atomic frequencies. The population of two excited atoms was strongly weakened when the laser frequency was in the middle of the atomic frequencies but peaked on the atomic frequencies themselves for very poor quality cavities. Also for those cavities, the population of a single excited atom peaked when the laser resonated with its frequency but dipped for the other atom's frequency. The shifting of the peaks is understood easily as when the cavity loses more and more photons, it becomes similar with free space. However some kind of coupling still remains and causes dips that are not observed in free space.

The purely numerical study of steady states of the system without the simplification on the atomic frequencies was also conducted. The degeneracies on some dressed states were lifted and the number of one and two-photon peaks augmented as could have been expected. The results coming from the cavity decay processes were also observed and

[1]Five-photon processes are obviously the highest multi-photon processes one could obtain with a truncated basis with $n_{\max} = 5$. However, attempts were made with $n_{\max} = 7$ and no higher order process was noticed for the same value of ϵ.

confirmed to exist in the general case.

A last effect, the cavity induced transparency, was observed. We showed that when the laser frequency was in the middle of the atomic frequencies, not only the population of the doubly excited state dropped but also the number of photons and of pairs of photons were found to be identical to the number that would have been found in an empty cavity, therefore yielding no particular multi-photon process, exactly as what we found in free space. The CIT effect was not found to be as strong when the atomic frequencies were very close from each other, as in this case the cavity decay induced drop in the mean photon number takes precedence.

Actual experimental realizations of atoms in resonant cavities have been realized in circuit cavity QED. In that type of experiments, like in [37, 40, 41] a lot of parameters, such at the atomic frequencies, are independently controllable. Monitoring the transmission at low enough power exhibits the usual vacuum Rabi splitting, specific to two atoms as the Rabi splitting depends on the number of atoms [42–47]. With an increase of the input power, the transmission could show the cavity two-photon resonance and exhibit all the effects we spoke of. A particular immediate realization of that two-photon effect could be realized in circuit cavity QED considering the setup used in [37] with two superconducting qubits instead of three. In that experiment, the frequency of each qubit is separately tunable, and we deliberately chose in this paper parameters close to what has been achieved.

Clearly, the existence of cavity induced two-photon transition implies the existence of cavity induced inter-qubits interaction. This would suggest that all inter-atomic forces can be manipulated by using cavities, as we have control over parameters like frequencies or coupling strengths. Cavities offer many possibilities, as whole ladders of dressed states and one or more external fields can be used to manipulate interactions inside the cavity [48, 49].

Conclusion

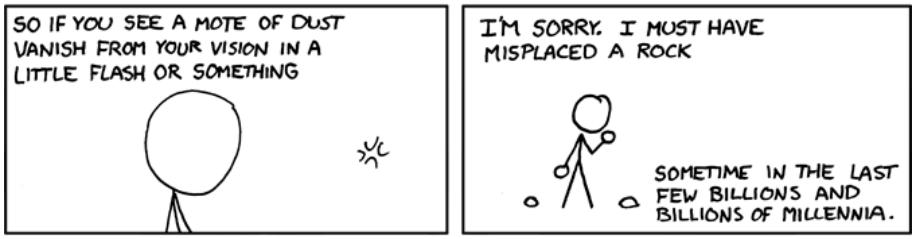

Randall Munroe, *A Bunch of Rocks* (part 8 of 9), `xkcd.com/505/`

In chapter 1, we made a contribution to quantum entanglement theory by introducing a new entanglement criterion, the Schrodinger-Robertson partial transpose inequality. We took advantage of the physicality of a partially transposed separable state to constrain the product of the variances of two operators to a minimal value. The violation of that constraint when measured on some state is the indisputable sign of entanglement in the state. We showed that not just any operator could be used in that inequality, and we gave a precise description of acceptable operators. We proved that there is always a pair of suitable operators that are able to detect the entanglement of any pure bipartite state of any dimension, giving a necessary and sufficient criterion for the detection of entanglement. We also proved that the criterion was necessary and sufficient in the case of pure three-qubit state. The Schrodinger-Robertson partial transpose inequality has a very wide range of application and we tested it on a few systems, multipartite mixed states, harmonic oscillators, multiphoton polarization states, continuous variable states or Schrodinger cat states with very encouraging results.

In chapter **??**, we introduced an N-qubit generalization of the concurrence, originally

defined for two qubits. We started off with three qubits and we gave a series of conditions that we proved to be necessary and sufficient for the entanglement of pure states. We used these conditions to construct nine matrices that lead to the definition of the three-qubit concurrences for pure states. We showed that those concurrences were not unrelated to other established measures of entanglement, such as the three-tangle or another type of multipartite concurrence defined in the literature. Following in the footsteps of the original concurrence, we generalized the application of our concurrences to mixed sates and we showed that any linear combination of the nine original matrices could be used to define a concurrence applicable on mixed states. Any observed non-zero concurrence in a state immediately indicates the presence of entanglement in the system. We showed that in the case of symmetric states, the number of concurrences could be reduced to three, with which a non-zero value directly indicates the presence of genuine tripartite entanglement. We pushed the generalization to N-qubit states by determining all the necessary and sufficient conditions to entanglement of a pure state. Those conditions allowed us to define the concurrences for pure and mixed states of N-qubits. We concluded with an example application on a family of mixed states into which any N-qubit state can be depolarized and saw that the entanglement of those state could always be detected with our concurrences.

In chapter **??**, we started to get interested in ways to produce entanglement in physical systems such as cold atoms. We investigated the dipole blockade effect observed in such systems and modelized it with an interaction term in the Hamiltonian and master equation of the system. We showed that if the doubly excited state was shifted out of resonance far enough, the system would evolve from the ground state into a mixture of ground state and maximally entangled state. We measured the intensity of the blockade as well as the concurrence in different situations and we concluded that indeed the amplitude of the blockade in the system was a good marker for the amount of entanglement shared in the atoms. We also saw that the blockade could be lifted by considering a strong enough laser excitation. This observation lead us to investigate the steady state of the system

towards which all systems tend to. We were able to find the analytical expression of the steady state, which allowed us to give the expression for the amplitude of the blockade. Furthermore, we were able to give an analytical expression of the concurrence in the state. This expression can be used to calculate the laser strength that will maximize the amount of entanglement in the system for a given interaction strength. We concluded the chapter by giving another way to probe the blockade effect in the system, the photon-photon correlation. We showed a connection between values of the photon-photon correlation and the blockade, which provides a new way to measure the effect in an atomic system in the case where the spontaneous emission dominates over other dissipation effects.

In chapter **??**, we extended our model to three-atom systems. We showed that it was enough to consider the sum of the pairwise atomic interactions to find the global interactive terms in the Hamiltonian. We studied the system in a mixed symmetry basis that helped us along the way to interpret several results. After a few considerations on general configurations of the system, we studied different cases: no interaction between the atoms, interaction between only two, same interaction between all atoms and aligned atoms with interaction between first neighbors only. For each case we were able to give a complete analytical expression of the steady state. We studied the different blockades in the system and saw that the maximally excited state tended to be very far away from resonance in genuine tripartite interactions. The blockades observed in pairs of atoms with the third atom traced out showed no great difference with the bipartite case except when we considered the atoms from the extremities of the chain of atoms. In that case, the population of these two atoms in their excited states was actually enhanced even though the atoms share no direct interaction. Then, we studied the two-atom concurrences in the different subsystems by tracing out one atom. We noted a general decrease of the amount of bipartite entanglement as a third atom was set to interact with the original pair. Anecdotally, no entanglement was associated with the enhancing observed earlier. Finally, we studied tripartite entanglement using our concurrences defined the second chapter. We saw clear signs of genuine tripartite entanglement, especially of the W-

type in the symmetric configuration, and thus we confirmed the interest of defining our concurrences.

In chapter **??**, we investigated the EIT, which was shown to be able to detect Rydberg states. We wondered if, conversely, the long range interactions observed in Rydberg states could influence the EIT. We first gave an overview of the phenomenon and used our master equation formalism to give an analytical expression of the steady state for the a three-level atom in the ladder scheme excited by two lasers. By considering the steady state term responsible for EIT in the lowest order of the probe laser strength, we found the usual expression of the EIT. We then gave our model of dipole blockade interaction for two of such atoms in our Hamiltonian and steady state. After finding the eigenstates of the unperturbed basis, we investigated the possible two-photon processes and found that one possible excitation was forbidden for a non-zero interaction but that two others were always non-zero since they relied on only one possible excitation path. We then computed numerical simulations of the steady state and measured the blockade and its effect on EIT. We found that the blockade and antiblockade effects were important and in accordance with our perturbation theory considerations, although the EIT was only slightly affected. This can be explained by the fact that EIT is not a saturation effect, i. e. the population in the top level state is of less importance as the simple possibility for a transition. At that point, we considered another kind of possible interaction for the system, the dipole-dipole interaction, and presented our theoretical model. The effects of the interaction on the eigenstates of the unperturbed Hamiltonian were found to be deeper than those of the previously considered interaction since it increased the number of possible transitions. The two-photon transitions were also studied and we found that one of them was still forbidden while the other two were not. We found that the effect on the EIT in the steady state were considerably more important as we noted the apparition of three windows of transparency instead of one, which can be explained by the apparition of the new transition frequencies, in particular in the antisymmetric states of the system.

In chapter 2, we studied two-photon processes in cavity QED. After checking why such

processes were forbidden for two unidentical atoms in free space, we gave our Hamiltonian modelizing the atoms, the cavity mode, the coupling between them and the laser excitation. We also gave the master equation which includes dissipations effects like atomic spontaneous emission and cavity losses in the model. We considered a constraint on the atomic frequencies that allowed us to analytically express the eigenstates and eigenvalues of the unperturbed Hamiltonian, which lead us to calculate, with perturbation theory, the possibility of two-photon processes within the cavity. We found that those processes were indeed possible when considering transitions to two of the dressed states of the system and we noted that the transitions to the other possible states could not be identified as two-photon processes but rather as two consecutive one-photon transitions. After a few numerical considerations, we studied the steady state of the system by computing different photonic and atomic spectra that confirmed the existence of two-photon processes. By studying the influence of lowering the cavity quality on the different spectra, we found that some behaviors could be interpreted with a free space model, but others, such as the strong inhibition of the doubly excited state population at the mean atomic frequency, could not. We then numerically considered a more general setup by lifting the constraint on the atomic frequencies which lifted degeneracies and allowed us to confirm previous observations. One more effect was noted, the cavity induced transparency. For the same laser frequency that inhibits doubly excited states, the number of photons in the cavity is found to be the same as it should be in an empty cavity. This effect was found to be stronger when the atomic frequencies were far apart and annulled for identical frequencies.

Appendix A

Expression of Angular Eigenstates of Harmonic Oscillators

In this appendix, we derive some results on harmonic oscillators which are useful to show the abilities of entanglement detection of the SRPT criterion.

A.1 Two Dimensional Harmonic Oscillator

In two dimensions, the Hamiltonian describing a particle of mass m subject to an isotropic harmonic potential is

$$H = \frac{p_x^2}{2m} + \frac{p_y^2}{2m} + \frac{1}{2}m\omega^2\left(x^2 + y^2\right), \tag{A.1}$$

with x_i, p_i the position and momentum of the particle in the directions $i = x, y$ and ω a constant. Since H is the sum of two oscillators Hamiltonians along the directions x and y, it is clear that the eigenvalues of the hamiltonian will be written as

$$|n_x, n_y\rangle \equiv |n_x\rangle \otimes |n_y\rangle, \tag{A.2}$$

when the $|n_i\rangle$ are the eigenstates of the two one dimensional Hamiltonians. We may define the annihilation operators:

$$a_x = \frac{1}{\sqrt{2}}\left(\sqrt{\frac{m\omega}{\hbar}}x + \frac{i}{\sqrt{m\hbar\omega}}p_x\right), \tag{A.3}$$

$$a_y = \frac{1}{\sqrt{2}}\left(\sqrt{\frac{m\omega}{\hbar}}y + \frac{i}{\sqrt{m\hbar\omega}}p_y\right). \tag{A.4}$$

The creation operators $a_i^\dagger$ are the hermitian conjugates of the above operators. We have

$$[a_x, a_x^\dagger] = [a_y, a_y^\dagger] = 1, \tag{A.5}$$

while all other commutators between the four operators are zero. Let us finally define the number operators

$$N_x = a_x^\dagger a_x, \tag{A.6}$$

$$N_y = a_y^\dagger a_y, \tag{A.7}$$

which allow us to write H as

$$H = (N_x + N_y + 1)\hbar\omega. \tag{A.8}$$

The eigenstates have the properties

$$a_i|n_i\rangle = \sqrt{n_i}|n_i - 1\rangle, \tag{A.9}$$

$$a_i^\dagger|n_i\rangle = \sqrt{n_i + 1}|n_i + 1\rangle, \tag{A.10}$$

$$N_i|n_i\rangle = n_i|n_i\rangle, \tag{A.11}$$

and therefore, we have

$$|n_x, n_y\rangle = \frac{1}{\sqrt{n_x! n_y!}}\left(a_x^\dagger\right)^{n_x}\left(a_y^\dagger\right)^{n_y}|0,0\rangle, \tag{A.12}$$

with $|0,0\rangle$ the ground state of the oscillator.

We can also prove that

$$H|n_x, n_y\rangle = (n_x + n_y + 1)\hbar\omega|n_x, n_y\rangle. \tag{A.13}$$

If we define the total quantum number

$$n = n_x + n_y, \tag{A.14}$$

we note that one particular value of n corresponds to the $n+1$ orthogonal eigenstates

$$|n,0\rangle,\ |n-1,1\rangle,\ldots,\ |0,n\rangle, \tag{A.15}$$

which shows that the measure of the energy alone does not allow us to pinpoint one proper state. The discrimination between all these states could be achieved by measuring the energy separately in the x and y direction, but there is another method that takes advantage of the angular momentum L_z. That operator is defined by

$$L_z = xp_y - yp_x, \tag{A.16}$$

or in other terms

$$L_z = i\hbar(a_x a_y^\dagger - a_x^\dagger a_y), \tag{A.17}$$

and it is clear that the $|n_x, n_y\rangle$ states are not eigenstates of L_z.

However, it is possible to show that

$$[H, L_z] = 0, \tag{A.18}$$

which indicates there must be a common eigenstate basis for the two operators. That

basis is made of the $|\psi_{k,M}\rangle$ eigenvectors which has the following properties:

$$H|\psi_{k,M}\rangle = \hbar\omega(2k+|M|+1)|\psi_{k,M}\rangle, \tag{A.19}$$

$$L_z|\psi_{k,M}\rangle = \hbar M|\psi_{k,M}\rangle. \tag{A.20}$$

We wish to express any $|\psi_{k,M}\rangle$ state in function of the $|n_x, n_y\rangle$ states. It is quite clear that $n = n_x + n_y = 2k + |M|$ and therefore for given k and M we have in general

$$|\psi_{k,M}\rangle = \sum_{i=0}^{n} c_i |n_x = n-i, n_y = i\rangle. \tag{A.21}$$

To find the analytical expression of the c_i coefficients, we need to define an intermediate basis as follow

$$a_r = \frac{1}{\sqrt{2}}\left(a_x - ia_y\right), \tag{A.22}$$

$$a_l = \frac{1}{\sqrt{2}}\left(a_x + ia_y\right), \tag{A.23}$$

where r and l stand for right and left, as those operators can be interpreted as annihilators of right and left "circular quanta". They are very similar to a_x and a_y, they follow the commutation rules

$$[a_r, a_r^\dagger] = [a_l, a_l^\dagger] = 1, \tag{A.24}$$

and all other combinations are zero. It is possible to express the regular ladder operators in function of the circular one and we find that

$$H = (N_r + N_l + 1)\hbar\omega, \tag{A.25}$$

$$L_z = \hbar(N_r - N_l), \tag{A.26}$$

with $N_r = a_r^\dagger a_r$ and $N_l = a_l^\dagger a_l$ the new number operators. We see that there is a $|\varphi_{n_r,n_l}\rangle$ basis in which both H and L_z are diagonal and which behaves exactly like the $|n_x, n_y\rangle$

basis. We also find

$$n = n_r + n_l = 2k + |M|, \tag{A.27}$$

$$M = n_r - n_l, \tag{A.28}$$

This result does allow to associate a definite $|\psi_{k,M}\rangle$ state to a single state $|\varphi_{n_r,n_l}\rangle$. There are two cases depending on the sign of M; if $M > 0$, it means $n_r > n_l$ and $|M| = n_r - n_l$ and $k = n_l$, if $M < 0$, then $|M| = n_l - n_r$ and $k = n_r$. Globally,

$$|\psi_{k,M}\rangle = |\varphi_{n_r=k+|M|,n_l=k}\rangle \text{ if } M > 0, \tag{A.29}$$

$$|\psi_{k,M}\rangle = |\varphi_{n_r=k,n_l=k+|M|}\rangle \text{ if } M < 0. \tag{A.30}$$

We see that a state with a positive helicity M has more "right" quanta than "left" quanta and inversely for $M < 0$. Now, to express a $|\varphi_{n_r,n_l}\rangle$ into a combination of $|n_x, n_y\rangle$ we have

$$|\varphi_{n_r,n_l}\rangle = \frac{1}{\sqrt{n_r! n_l!}} \left(a_r^\dagger\right)^{n_r} \left(a_l^\dagger\right)^{n_l} |\varphi_{0,0}\rangle, \tag{A.31}$$

$$= \frac{1}{\sqrt{2^n n_r! n_l!}} \left(a_x^\dagger + i a_y^\dagger\right)^{n_r} \left(a_x^\dagger - i a_y^\dagger\right)^{n_l} |0,0\rangle, \tag{A.32}$$

$$= \frac{1}{\sqrt{2^n n_r! n_l!}} \sum_{k=0}^{n_r} \sum_{l=0}^{n_l} \binom{n_r}{k} \binom{n_l}{l} \left(a_x^\dagger\right)^{n-k-l} \left(a_y^\dagger\right)^{j+k} (i)^{k-l} |0,0\rangle, \tag{A.33}$$

$$= \frac{1}{\sqrt{2^n n_r! n_l!}} \sum_{i=0}^{n} \sum_{j}^{\{-i,-i+2,\cdots,i\}} \binom{n_r}{\frac{i-j}{2}} \binom{n_l}{\frac{i+j}{2}} \left(a_x^\dagger\right)^{n-i} \left(a_y^\dagger\right)^{i} (i)^{j} |0,0\rangle, \tag{A.34}$$

$$= \frac{1}{\sqrt{2^n n_r! n_l!}} \sum_{i=0}^{n} \sum_{j=0}^{i} \binom{n_r}{j} \binom{n_l}{i-j} \left(a_x^\dagger\right)^{n-i} \left(a_y^\dagger\right)^{i} (i)^{2j-i} |0,0\rangle, \tag{A.35}$$

$$= \sum_{i=0}^{n} (-i)^i \sqrt{\frac{(n-i)!i!}{2^n n_r! n_l!}} \sum_{j=0}^{i} (-1)^j \binom{n_r}{j} \binom{n_l}{i-j} |n-i, i\rangle, \tag{A.36}$$

$$= \sum_{i=0}^{n} (-i)^i \sqrt{\frac{\binom{n}{n_r}}{2^n \binom{n}{i}}} \sum_{j=0}^{i} (-1)^j \binom{n_r}{j} \binom{n_l}{i-j} |n-i, i\rangle, \tag{A.37}$$

where on line (A.32) we simply used the definition of a_r and a_l and noted the ground state is the same in both basis, in (A.33) we used the binomial formula twice and in (A.34) we applied the change of variables $i = k + l$ and $j = k - l$. In order to span all values of (k, l) only once, we span all "antidiagonal" lines with $k + l = i$ $(i = 0, 1, \ldots, n)$ and along those lines we consider the elements $(k = \frac{i+j}{2}, l = \frac{i-j}{2})$ $(j = -i, -i + 2, \ldots, i - 2, i)$. The values of j should actually only go from $\max\{-i, i - 2n_l\}$ to $\min\{i, 2n_r - i\}$ in order not to go beyond $k = n_r$ and $l = n_l$ but we can simplify it since the binomial coefficients will yield zero if $k > n_r$ or $l > n_l$. In line (A.35) we applied yet another change of variable as $j' = \frac{i+j}{2}$ $(j = 0, 1, \ldots, i)$ and renamed j' as j, in (A.36) we applied the creation operators to the ground state and in (A.37) we multiplied the numerator and denominator in the root term by $n!$ and simplified the expression. The final sum on j may be expressed differently as we find that

$$\sum_{j=0}^{i}(-1)^j\binom{n_r}{j}\binom{n_l}{i-j} = \binom{n_l}{i}{}_2F_1(-i, -n_r; n_l - i + 1; -1), \tag{A.38}$$

with ${}_2F_1$ the hypergeometric function, but we choose to keep the sum as it is for its implementation simplicity.

Now, we need to express directly the $|\psi_{k,n}\rangle$ state in the $|n_x, n_y\rangle$ basis. Depending on the sign of M, we need to consider the state $|\varphi_{k+|M|,k}\rangle$ or $|\varphi_{k,k+|M|}\rangle$. The easiest way to see the effect of a swap of n_r and n_l is in line (A.33) where the only difference is i^{k-l} becoming $i^{l-k} = (-i)^{k-l}$. With that consideration, we finally have the c_i coefficients we wanted in (A.21) up to an overall phase:

$$c_i = (-\text{sign}(M)i)^i\sqrt{\frac{\binom{n}{k}}{2^n\binom{n}{i}}}\sum_{j=0}^{i}(-1)^j\binom{k+|M|}{j}\binom{k}{i-j}. \tag{A.39}$$

The last property we want to investigate is the relation

$$c_i = i^n(-1)^{n_l-i}c_{n-i}. \tag{A.40}$$

On the left hand side, we have

$$c_i = (-i)^i \sqrt{\frac{\binom{n}{n_r}}{2^n \binom{n}{i}}} \sum_{j=0}^{i} (-1)^j \binom{n_r}{j} \binom{n_l}{i-j}, \tag{A.41}$$

and on the right hand side

$$\begin{aligned} c_{n-i} &= (-i)^{n-i} \sqrt{\frac{\binom{n}{n_r}}{2^n \binom{n}{n-i}}} \sum_{j=0}^{n-i} (-1)^j \binom{n_r}{j} \binom{n_l}{n-i-j}, && \text{(A.42)} \\ &= (-i)^{n-i} \sqrt{\frac{\binom{n}{n_r}}{2^n \binom{n}{i}}} \sum_{j=n_l-i}^{n_r} (-1)^{n_r-j} \binom{n_r}{n_r-j} \binom{n_l}{n-i+j-n_r}, && \text{(A.43)} \\ &= (-i)^{n-i}(-1)^{n_r} \sqrt{\frac{\binom{n}{n_r}}{2^n \binom{n}{i}}} \sum_{j=n_l-i}^{n_r} (-1)^j \binom{n_r}{j} \binom{n_l}{i-j}, && \text{(A.44)} \end{aligned}$$

where in the second step we used the variable change $j' = n_r - j$ and in the last step simplified the expression. Aside from the phase, the only remaining difference is the borns of the sum but thanks to the binomial coefficients, that difference vanishes. Indeed, for both sums, the condition of having non zero terms is $\max\{0, i - n_l\} \leq j \leq \min\{i, n_r\}$, so that all terms considered outside those limits are zero. Of course, we have $|c_i| = |c_{n-i}|$.

A.2 Three Dimensional Harmonic Oscillator

In three dimensions, the Hamiltonian describing a particle of mass m subject to an isotropic harmonic potential is

$$H = \frac{p_x^2}{2m} + \frac{p_y^2}{2m} + \frac{p_z^2}{2m} + \frac{1}{2} m\omega^2 \left(x^2 + y^2 + z^2\right), \tag{A.45}$$

with x_i, p_i the position and momentum of the particle in the directions $i = x, y, z$ and ω a constant. Once again, since H is the sum of three oscillators Hamiltonians, the eigenvalues

of the hamiltonian will be written as

$$|n_x, n_y, n_z\rangle \equiv |n_x\rangle \otimes |n_y\rangle \otimes |n_z\rangle, \tag{A.46}$$

when the $|n_i\rangle$ are the eigenstates of the three one dimensional Hamiltonians. We may define the third annihilation operator:

$$a_z = \frac{1}{\sqrt{2}}\left(\sqrt{\frac{m\omega}{\hbar}}z + \frac{i}{\sqrt{m\hbar\omega}}p_z\right), \tag{A.47}$$

which behaves exactly as the others. We also define its number operator

$$N_z = a_z^\dagger a_z, \tag{A.48}$$

which allow us to write H as

$$H = \left(N_x + N_y + N_z + \frac{3}{2}\right)\hbar\omega. \tag{A.49}$$

The eigenstates are of the form

$$|n_x, n_y, n_z\rangle = \frac{1}{\sqrt{n_x! n_y! n_z!}}\left(a_x^\dagger\right)^{n_x}\left(a_y^\dagger\right)^{n_y}\left(a_z^\dagger\right)^{n_z}|0,0,0\rangle, \tag{A.50}$$

with $|0,0,0\rangle$ the ground state of the oscillator. This time for a definite energy $n = n_x + n_y + n_z$ there is a degree of degenerescence g_n of

$$g_n = \sum_{i=0}^{n}(i+1) = \frac{n(n+1)}{2} + (n+1) = \frac{1}{2}(n+1)(n+2). \tag{A.51}$$

Just as we introduced L_z in the two dimensional harmonic oscillator, we introduce the additional observable

$$\mathbf{L}^2 = \frac{1}{2}(L_+L_- + L_-L_+) + L_z^2, \tag{A.52}$$

with

$$L_+ = \hbar\sqrt{2}(a_z^\dagger a_l - a_r^\dagger a_z), \tag{A.53}$$

$$L_- = \hbar\sqrt{2}(a_l^\dagger a_z - a_z^\dagger a_r). \tag{A.54}$$

It can be checked that $[H, \mathbf{L}^2] = 0$ and $[L_z, \mathbf{L}^2] = 0$ which implies there must be a common set of eigenstates for H, L_z and $\mathbf{L}^2$. Those eigenstates are the $|\psi_{k,l,m}\rangle$ states and have the following properties

$$H|\psi_{k,l,m}\rangle = \hbar\omega(2k + l + \frac{3}{2})|\psi_{k,l,m}\rangle, \tag{A.55}$$

$$L_z|\psi_{k,l,m}\rangle = \hbar m|\psi_{k,l,m}\rangle, \tag{A.56}$$

$$\mathbf{L}^2|\psi_{k,l,m}\rangle = \hbar^2 l(l+1)|\psi_{k,l,m}\rangle, \tag{A.57}$$

$$L_\pm|\psi_{k,l,m}\rangle = \hbar\sqrt{l(l+1) - m(m\pm 1)}|\psi_{k,l,m\pm 1}\rangle. \tag{A.58}$$

$$\tag{A.59}$$

The last relation implies that m can take any integer value from $-l$ to l. So by repeatedly applying the L_- operator on a $|\psi_{k,l,l}\rangle$ state, we should be able to generate all states down to $|\psi_{k,l,-l}\rangle$. The first step is to find the expression of the $|\psi_{k,l,l}\rangle$ in the $|\varphi_{n_r,n_l,n_z}\rangle$ basis using the particular property $L_+|\psi_{k,l,l}\rangle = 0$. By identifying the quantum numbers we find

$$n = n_r + n_l + n_z = 2k + l, \tag{A.60}$$

$$m = n_r - n_l. \tag{A.61}$$

Since $n_r - n_l = m$ we can always write $n_r = K + m$, $n_r = K$ with K a positive integer and therefore we must have $n_z = n - m - 2K$, which cannot be negative hence we have

$K \leq \frac{n-m}{2}$. We are now able to write

$$|\psi_{k,l,l}\rangle = \sum_{K=0}^{k} c_K |\varphi_{n_r=K+l,n_l=K,n_z=2k-2K}\rangle, \tag{A.62}$$

since $\frac{n-l}{2} = k$ and with normalized coefficient c_K. The effect of L_+ on such a decomposition is

$$\begin{aligned} L_+|\psi_{k,l,l}\rangle &= \sum_{K=0}^{k} c_K \sqrt{2}\hbar \Big(\sqrt{K}\sqrt{2k-2K+1}|\varphi_{K+l,K-1,2k-2K+1}\rangle \\ &\quad - \sqrt{K+l+1}\sqrt{2k-2K}|\varphi_{K+l+1,K,2k-2K-1}\rangle \Big), \end{aligned} \tag{A.63}$$

which is zero if

$$c_K\sqrt{K+l+1}\sqrt{2k-2K} = c_{K+1}\sqrt{K+1}\sqrt{2k-2K-1}. \tag{A.64}$$

From that relation, we can express all c_K in function of c_0 and then normalize all coefficient. We have

$$c_K^2 = c_0^2 \prod_{j=0}^{K-1} \frac{(j+l+1)(2k-2j)}{(j+1)(2k-2j-1)}, \tag{A.65}$$

$$= c_0^2 \frac{(l+1)(l+2)\dots(l+K)(2k)(2k-2)\dots(2k-2K+2)}{(1)(2)\dots K(2k-1)(2k-3)\dots(2k-2K+1)}, \tag{A.66}$$

$$= c_0^2 \frac{(l+K)!}{l!K!} \frac{(2k)!!}{(2k-2K)!!} \frac{(2k-2K-1)!!}{(2k-1)!!}, \tag{A.67}$$

$$= c_0^2 \binom{l+K}{K} \frac{2^k k!}{2^{k-K}(k-K)!} \frac{(2k-2K)!}{2^{k-K}(k-K)!} \frac{2^k(k)!}{(2k)!}, \tag{A.68}$$

$$= c_0^2\, 2^{2K} \frac{\binom{l+K}{K}\binom{2k-2K}{k-K}}{\binom{2k}{k}}, \tag{A.69}$$

where $k!!$ is the double factorial of k which has the property

$$(2k)!! = (2k)(2k-2)\dots 2 = k!2^k, \tag{A.70}$$

$$(2k+1)!! = (2k+1)(2k-1)\dots 1 = \frac{(2k)!}{k!2^k}, \tag{A.71}$$

that we used in the process.

With that expression, we are now able to calculate the value of c_0 by normalizing the expression. We have

$$\sum_{K=0}^{k} c_K^2 = c_0^2 \sum_{K=0}^{k} 2^{2K} \frac{\binom{l+K}{K}\binom{2k-2K}{k-K}}{\binom{2k}{k}}, \tag{A.72}$$

$$= c_0^2 \frac{\binom{2(k+l+1)}{2k}}{\binom{k+l+1}{k}}, \tag{A.73}$$

Since that expression must be 1, we have he value of c_0. Finally, we get up to a global phase

$$|\psi_{k,l,l}\rangle = \sum_{K=0}^{k} 2^K \sqrt{\frac{\binom{l+K}{K}\binom{2k-2K}{k-K}\binom{k+l+1}{k}}{\binom{2k}{k}\binom{2(k+l+1)}{2k}}} |\varphi_{K+l,K,2k-2K}\rangle. \tag{A.74}$$

Bibliography

[1] F. Mintert, A. R. R. Carvalho, M. Kuś, and A. Buchleitner, Phys. Rep. **415**, 207–259 (2005).

[2] S. L. Braunstein and P. van Loock, Rev. Mod. Phys. **77**, 513 (2005).

[3] A. Pati, Phys. Lett. A **278**, 118 (2000).

[4] A. Peres, Phys. Rev. Lett. **77**, 1413–1415 (1996).

[5] J. Bell, Physics **1**, 195–200 (1964).

[6] W. Dür, Phys. Rev. Lett. **87**, 230402 (2001).

[7] O. Gühne, P. Hyllus, D. Bruß, A. Ekert, M. Lewenstein, C. Macchiavello, and A. Sanpera, Phys. Rev. A **66**, 062305 (2002).

[8] R. Simon, Phys. Rev. Lett. **84**, 2726–2729 (2000).

[9] L.-M. Duan, G. Giedke, J. I. Cirac, and P. Zoller, Phys. Rev. Lett. **84**, 2722–2725 (2000).

[10] H. F. Hofmann, Phys. Rev. A **68**, 034307 (2003).

[11] M. Hillery and M. S. Zubairy, Phys. Rev. Lett. **96**, 050503 (2006).

[12] A. A. Klyachko, B. Öztop, and A. S. Shumovsky, Phys. Rev. A **75**, 032315 (2007).

[13] G. A. Durkin and C. Simon, Phys. Rev. Lett. **95**, 180402 (2005).

[14] V. Giovannetti, S. Mancini, D. Vitali, and P. Tombesi, Phys. Rev. A **67**, 022320 (2003).

[15] E. Shchukin and W. Vogel, Phys. Rev. Lett. **95**, 230502 (2005).

[16] O. Gühne, Phys. Rev. Lett. **92**, 117903 (2004).

[17] G. S. Agarwal and A. Biswas, New J. Phys. **7**, 211 (2005).

[18] H. Nha and J. Kim, Phys. Rev. A **74**, 012317 (2006).

[19] H. Nha, Phys. Rev. A **76**, 014305 (2007).

[20] L. Song, X. Wang, D. Yan, and Z.-S. Pu, J. Phys. B **41**, 015505 (2008).

[21] E. Schrödinger, Sitzungsber. Preuss. Akad. Wiss., Phys. Math. Kl. **19**, 296 (1930).

[22] M. Horodecki, P. Horodecki, and R. Horodecki, Phys. Lett. A **223**, 1 (1996).

[23] A. Mair, A. Vaziri, G. Weihs, and A. Zeilinger, Nature **412**, 313–316 (2001).

[24] T. Tsegaye, J. Söderholm, M. Atatüre, A. Trifonov, G. Björk, A. V. Sergienko, B. E. A. Saleh, and M. C. Teich, Phys. Rev. Lett. **85**, 5013–5017 (2000).

[25] C. C. Gerry and R. Grobe, Phys. Rev. A **75**, 034303 (2007).

[26] W. Dür, G. Vidal, and J. I. Cirac, Phys. Rev. A **62**, 062314 (2000).

[27] A. Acín, A. Andrianov, L. Costa, E. Jané, J. I. Latorre, and R. Tarrach, Phys. Rev. Lett. **85**, 1560–1563 (2000).

[28] R. F. Werner, Phys. Rev. A **40**, 4277–4281 (1989).

[29] G. Tóth and O. Gühne, Phys. Rev. Lett. **94**, 060501 (2005).

[30] A. R. U. Devi, R. Prabhu, and A. K. Rajagopal, Phys. Rev. Lett. **98**, 060501 (2007).

[31] G. S. Agarwal and S. A. Ponomarenko, Phys. Rev. A **67**, 032103 (2003).

[32] M. S. Kim and G. S. Agarwal, Phys. Rev. A **57**, 3059–3064 (1998).

[33] G. V. Varada and G. S. Agarwal, Phys. Rev. A **45**, 6721–6729 (1992).

[34] M. Orrit, Science **298**, 369–370 (2002).

[35] C. Hettich, C. Schmitt, J. Zitzmann, S. Kuhn, I. Gerhardt, and V. Sandoghdar, Science **298**, 385–389 (2002).

[36] R. Loudon, *The Quantum Theory of Light*, Oxford University Press, London (2000).

[37] J. M. Fink, R. Bianchetti, M. Baur, M. Göppl, L. Steffen, S. Filipp, P. J. Leek, A. Blais, and A. Wallraff, Phys. Rev. Lett. **103**, 083601 (2009).

[38] G. S. Agarwal, *Quantum Statistical Theories of Spontaneous Emission and Their Relation to Other Approaches*, Springer, Berlin (1974).

[39] S. Filipp, P. Maurer, P. J. Leek, M. Baur, R. Bianchetti, J. M. Fink, M. Göppl, L. Steffen, J. M. Gambetta, A. Blais, and A. Wallraff, Phys. Rev. Lett. **102**, 200402 (2009).

[40] J. M. Fink, M. Goppl, M. Baur, R. Bianchetti, P. J. Leek, A. Blais, and A. Wallraff, Nature **454**, 315–318 (2008).

[41] M. Baur, S. Filipp, R. Bianchetti, J. M. Fink, M. Göppl, L. Steffen, P. J. Leek, A. Blais, and A. Wallraff, Phys. Rev. Lett. **102**, 243602 (2009).

[42] J. J. Sanchez-Mondragon, N. B. Narozhny, and J. H. Eberly, Phys. Rev. Lett. **51**, 550–553 (1983).

[43] G. S. Agarwal, Phys. Rev. Lett. **53**, 1732–1734 (1984).

[44] M. G. Raizen, R. J. Thompson, R. J. Brecha, H. J. Kimble, and H. J. Carmichael, Phys. Rev. Lett. **63**, 240–243 (1989).

[45] A. Boca, R. Miller, K. M. Birnbaum, A. D. Boozer, J. McKeever, and H. J. Kimble, Phys. Rev. Lett. **93**, 233603 (2004).

[46] P. Maunz, T. Puppe, I. Schuster, N. Syassen, P. W. H. Pinkse, and G. Rempe, Phys. Rev. Lett. **94**, 033002 (2005).

[47] R. J. Thompson, Q. A. Turchette, O. Carnal, and H. J. Kimble, Phys. Rev. A **57**, 3084–3104 (1998).

[48] E. Solano, G. S. Agarwal, and H. Walther, Phys. Rev. Lett. **90**, 027903 (2003).

[49] K. M. Birnbaum, A. Boca, R. Miller, A. D. Boozer, T. E. Northup, and H. J. Kimble, Nature **436**, 87–90 (2005).

Published articles

Tunable entanglement, antibunching, and saturation effects in dipole blockade

J. Gillet,[1] G. S. Agarwal,[2] and T. Bastin[1]

[1]*Institut de Physique Nucléaire, Atomique et de Spectroscopie, Université de Liège, B-4000 Liège, Belgium*

[2]*Department of Physics, Oklahoma State University, Stillwater, Oklahoma 74078-3072, United States of America*

(Received 12 July 2009; published 29 January 2010)

We report a model that makes it possible to analyze quantitatively the dipole blockade effect on the dynamical evolution of a two two-level atom system driven by an external laser field. The multiple excitations of the atomic sample are taken into account. We find very large concurrence in the dipole blockade regime. We further find that entanglement can be tuned by changing the intensity of the exciting laser. We also report a way to lift the dipole blockade paving the way to manipulate, in a controllable way, the blockade effects. We finally report how a continuous monitoring of the dipole blockade will be possible using photon-photon correlations of the scattered light in a regime where the spontaneous emission will dominate dissipation in the sample.

DOI: 10.1103/PhysRevA.81.013837 PACS number(s): 42.50.Ct, 03.67.Bg, 42.50.Nn

I. INTRODUCTION

Dipole-dipole interactions between atoms or molecules profoundly affect the light absorption that occurs in matter [1]. They have been known for several years to give rise to fascinating applications in quantum information science such as quantum logic operations in neutral atoms [2,3] or entanglement production in mesoscopic ensembles [4–6]. The level shifts associated with those interactions can strongly modify the laser excitation of adjacent atoms, up to a complete suppression of more than one excitation in nearby atoms. In this so-called *dipole blockade* effect, the first excited atom prevents any further excitation in a confined volume by shifting the resonance for its nonexcited neighbors, resulting in the production of singly excited collective states [4]. In past years, evidence for the dipole blockade effect was obtained with samples of Rydberg atoms because of their strong long-range interaction [7–10]. An analogous photon blockade effect in an optical cavity was also reported [11]. Recently, Rabi oscillations between the ground state of a pair of Rydberg atoms and the single-excited symmetric collective state were observed for atoms located more than a few micrometers apart [12,13]. In all those fascinating achievements, the residual effects resulting from possible multiple excitations of the atomic sample are usually not discussed, although they cannot be eliminated totally. This motivates a deeper quantitative analysis of the dipole blockade phenomenon to optimize its occurrence and understand its possible limitations [10,14]. In the present article, we report a model aimed at yielding quantitative results as a function of the most important experimental parameters including the dipole-dipole interaction strength. The system investigated is a two two-level atom system continuously driven by an external laser field. We report several characteristics of the dipole blockade including a tunable steady-state entanglement production and a saturation effect in strong driving condition. We also report how a continuous monitoring of the dipole blockade can be obtained with the help of the photon-photon correlation signal of the scattered light in a regime where the spontaneous emission will dominate the dissipation effects of the sample.

II. THE MODEL

We consider two atoms at fixed positions $\mathbf{x}_1$ and $\mathbf{x}_2$ with internal levels $|e\rangle$ and $|g\rangle$, dipolar transition frequency $\omega = 2\pi c/\lambda$, and single-atom spontaneous emission rate $2\gamma_s$. The system is conveniently described in the Dicke basis $|ee\rangle, |gg\rangle, |s\rangle \equiv (|eg\rangle + |ge\rangle)/\sqrt{2}$, and $|a\rangle \equiv (|eg\rangle - |ge\rangle)/\sqrt{2}$. We consider that the two atoms strongly interact when in state $|ee\rangle$ resulting in a shift $\hbar\delta$ of this doubly excited state. They are driven by a resonant external laser field with wave vector $\mathbf{k}_L$ and Rabi frequency 2Ω. In the rotating-wave approximation, the coherent evolution of the system is described by the interaction Hamiltonian

$$H = \hbar\delta|ee\rangle\langle ee| + \hbar\Omega(e^{i\mathbf{k}_L\cdot\mathbf{x}_1}S_1^+ + e^{i\mathbf{k}_L\cdot\mathbf{x}_2}S_2^+ + \text{h.c.}), \quad (1)$$

where $S_i^+ = (S_i^-)^\dagger$ $(i = 1, 2)$ is the atom raising operator $|e\rangle_i\langle g|$ and the term $\hbar\delta|ee\rangle\langle ee|$ accounts for the shift of the doubly excited state of the system induced by the dipole-dipole interaction. Throughout this article $\mathbf{k}_L$ is supposed to be perpendicular to the two-atom line and the reference frame is properly chosen so $\mathbf{k}_L \cdot \mathbf{x}_1 = \mathbf{k}_L \cdot \mathbf{x}_2 = 0$. When considering dissipation in the Markov and Born approximation, the time evolution of the system is governed by the master equation

$$\dot{\rho} = -\frac{i}{\hbar}[H, \rho] - \gamma \sum_{i=1}^{2}(S_i^+S_i^-\rho + \rho S_i^+S_i^- - 2S_i^-\rho S_i^+), \quad (2)$$

where $\gamma = \gamma_s + \gamma_d$, with $2\gamma_d$ the dissipation rate modeling nonradiative dissipative effects in the sample. We consider that the two atoms are separated by more than the transition wavelength λ so that we can neglect the imbalance among the decay rates of the Dicke states $|s\rangle$ and $|a\rangle$ [15]. This situation is encountered in most recent experiments, as in Ref. [12] where the atoms are located more than 20λ apart.

III. DIPOLE BLOCKADE PROPERTIES

In the presence of the dipole blockade mechanism, the doubly excited state $|ee\rangle$ is expected to be poorly populated though not totally depopulated. This is illustrated quantitatively in Fig. 1 where we compare the time evolution of the square of

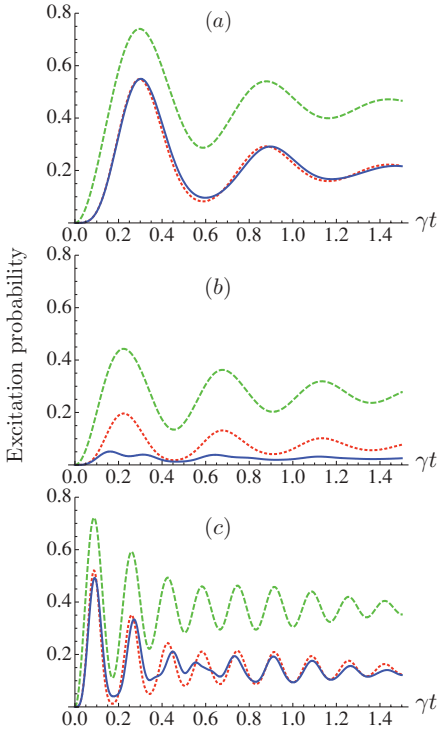

FIG. 1. (Color online) Time evolution of the excitation probability P_e (dashed green curve), its square (dotted red curve), and the probability P_{ee} of having both atoms excited (blue curve) [(a) $\Omega/\gamma = 5, \delta/\gamma = 5$; (b) $\Omega/\gamma = 5, \delta/\gamma = 30$; (c) $\Omega/\gamma = 15, \delta/\gamma = 30$]. The dipole blockade effect is well marked in case (b) where $P_{ee} \ll P_e^2$.

the probability $P_e = \langle e|\mathrm{Tr}_1\rho|e\rangle = \langle e|\mathrm{Tr}_2\rho|e\rangle$ of having one of the two atoms excited with the probability $P_{ee} = \langle ee|\rho|ee\rangle$ of finding both atoms excited, considering them initially in the ground state. When the dipole-dipole interaction is not strong enough [case (a) of Fig. 1] it has negligible effect and the atoms react as independent systems ($P_{ee} \simeq P_e^2$). For a greater dipole-dipole interaction [case (b)], the double excitation is blocked and the population of the $|ee\rangle$ state remains at insignificant levels though not zero. More importantly the double-excitation probability P_{ee} is much lower than P_e^2, giving a direct signature of the blockade mechanism. When the laser intensity is increased [case (c)], we observe that P_{ee} is again very similar to P_e^2. The population blockade is lifted and the atoms behave again as if they were independent without mutual influence. The dipole blockade effect can thus be circumvented by using strong laser fields. Case (b) exhibits a similar behavior of the system as that observed experimentally in Ref. [13].

The experimental results reported in Refs. [12,13] clearly imply the entanglement in the two-atom system. We can quantify such an entanglement. From the master equation we can obtain the complete time-dependent density matrix, which then can be used to compute the well-known measure of entanglement: the concurrence [16]. We show the results in Fig. 2. The concurrence is maximized when the dipole blockade mechanism is itself optimized. In case (a), the dipole-dipole interaction is too weak and the two-atom system behaves as a collection of independent atoms. No significant entanglement is produced. In case (b), the dipole blockade prevents the doubly excited state from being significantly populated and the two-atom system shares a collective single excitation. More population in the entangled $(|eg\rangle + |ge\rangle)/\sqrt{2}$ state is expected and significant amounts of entanglement are produced. In case (c), the dipole blockade is lifted and more population in the separable doubly excited state is expected. The concurrence is again less important than in case (b).

The two-atom state ρ subjected to the master equation [Eq. (2)] always stabilizes after a finite time around a steady state that we denote ρ^{SS}. The steady state is found by equating the right-hand term of Eq. (2) to zero. We get in the Dicke basis $\{|ee\rangle, |s\rangle, |a\rangle, |gg\rangle\}$

$$\rho^{\mathrm{SS}} = \frac{1}{16\Omega^4 + (4\Omega^2+\gamma^2)|\alpha|^2} \begin{pmatrix} 4\Omega^4 & 2\sqrt{2}\Omega^3\alpha & 0 & -2i\Omega^2\gamma\alpha \\ 2\sqrt{2}\Omega^3\alpha^* & 2\Omega^2(2\Omega^2+|\alpha|^2) & 0 & \sqrt{2}\Omega(2\Omega^2\alpha - i\gamma|\alpha|^2) \\ 0 & 0 & 4\Omega^4 & 0 \\ 2i\Omega^2\gamma\alpha^* & \sqrt{2}\Omega(2\Omega^2\alpha^* + i\gamma|\alpha|^2) & 0 & 4\Omega^4 + (2\Omega^2+\gamma^2)|\alpha|^2 \end{pmatrix}, \tag{3}$$

where $\alpha = -(\delta + 2i\gamma)$.

In the steady-state regime, the population of the doubly excited state $|ee\rangle$ decreases when δ increases. This is the usual dipole blockade effect where one excited atom prevents the excitation of a nearby atom. This effect is counterbalanced by an increase in the laser intensity. The dipole blockade effect is lifted with the use of a higher laser intensity. The ratio between the steady-state double-excitation probability P_{ee} and the square of the single-excitation probability P_e reads

$$\left.\frac{P_{ee}}{P_e^2}\right|_{\mathrm{ss}} = \frac{64\Omega^4 + 4(4\Omega^2+\gamma^2)|\alpha|^2}{(8\Omega^2+|\alpha|^2)^2}. \tag{4}$$

In the absence of the dipole-dipole interaction ($\delta = 0$) this ratio is trivially equal to one. This is obviously expected from the absence of correlation in the two-atom system in this case. When increasing $|\delta|$, the ratio monotonically decreases. This is a clear signature of the increasing correlation induced by the stronger and stronger dipole-dipole interaction shifting more and more the doubly excited state. We show more quantitatively the behavior of this ratio for different values of δ/γ, with respect to the field intensity in Fig. 3. It is quite clear that, for weak intensities of the field, the dipole blockade regime is dominant as there is less and less population in the $|ee\rangle$ state as δ/γ increases. However, increasing the

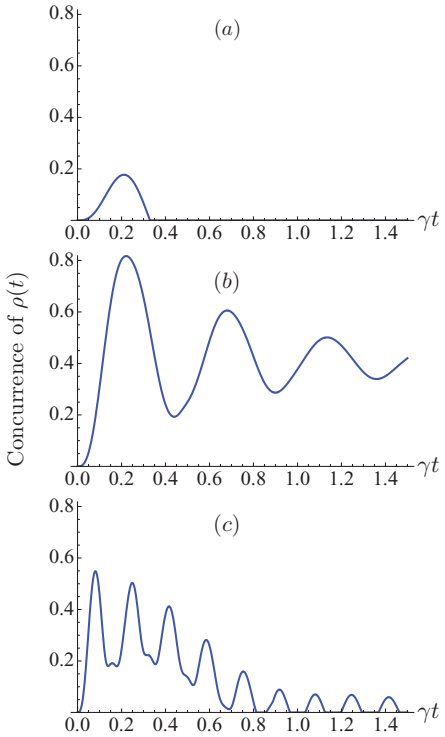

FIG. 2. (Color online) Time evolution of the concurrence C of the two-atom system [(a) $\Omega/\gamma = 5, \delta/\gamma = 5$; (b) $\Omega/\gamma = 5, \delta/\gamma = 30$; (c) $\Omega/\gamma = 15, \delta/\gamma = 30$].

field intensity has the effect of repopulating the $|ee\rangle$ state and therefore lifting the dipole blockade.

The concurrence of the steady state reads

$$C(\rho^{\mathrm{SS}}) = \mathrm{Max}\left\{0, \frac{\sqrt{2}\Omega^2(\lambda_+ - \lambda_-) - 8\Omega^4}{16\Omega^4 + (4\Omega^2 + \gamma^2)|\alpha|^2}\right\}, \tag{5}$$

with

$$\lambda_\pm = \sqrt{8\Omega^4 + \delta^2|\alpha|^2 \pm \delta|\alpha|\sqrt{16\Omega^4 + \delta^2|\alpha|^2}}. \tag{6}$$

In the absence of dipole-dipole interaction ($\delta = 0$), the steady state is not entangled. No entanglement is produced in this configuration since the two atoms behave as independent systems. This highlights the fundamental role of the dipole

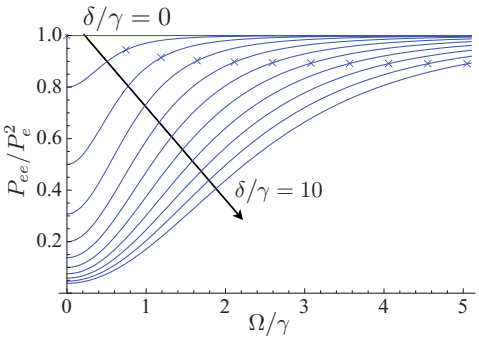

FIG. 3. (Color online) Plots of P_{ee}/P_e^2 with respect to Ω/γ for all integer values of δ/γ from 0 to 10. The crosses indicate for each curve the values of Ω/γ above which the steady state is separable.

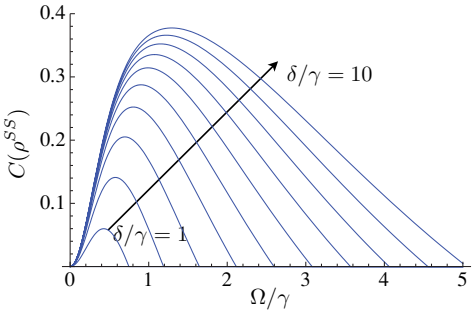

FIG. 4. (Color online) Plots of $C(\rho^{\mathrm{SS}})$ with respect to Ω/γ for integer values of δ/γ from 1 to 10.

blockade mechanism for long-term entanglement production of the two-atom system. For increasing values of δ, we show in Fig. 4 the concurrence of the steady state with respect to the field intensity. The amount of long-term entanglement in the system is clearly tunable with the laser intensity and can be reasonably high for well-adjusted values of δ and Ω. When the intensity of the field increases and lifts the dipole blockade, the amount of entanglement decreases accordingly. The steady state is entangled as long as

$$0 < 4\Omega^2 < \delta|\alpha|. \tag{7}$$

That upper limit on Ω is pointed on each plot of Fig. 3.

The photon-photon correlation signal gives information that is not contained in intensity measurements and is a good probe for the quantum nature of the investigated processes. In our setup, the photon-photon correlation function is given by [15,17]

$$g^{(2)}(\mathbf{r}_1, t; \mathbf{r}_2, t+\tau) = \frac{P(\mathbf{r}_2, t+\tau|\mathbf{r}_1, t)}{P(\mathbf{r}_2, t)}, \tag{8}$$

where $P(\mathbf{r}, t)$ is the probability of detecting a photon at position $\mathbf{r}$ and time t, and $P(\mathbf{r}_2, t+\tau|\mathbf{r}_1, t)$ is the conditional probability of finding a photon at $\mathbf{r}_2$ and $t+\tau$ assuming that a photon at $\mathbf{r}_1$ and t was recorded. The probabilities $P(\mathbf{r}_1, t)$ and $P(\mathbf{r}_2, t+\tau|\mathbf{r}_1, t)$ are given by $\langle D^\dagger(\mathbf{r}_1)D(\mathbf{r}_1)\rangle_{\rho(t)}$ and $\langle D^\dagger(\mathbf{r}_2)D(\mathbf{r}_2)\rangle_{\rho'(t+\tau;\mathbf{r}_1,t)}$, respectively, where $\rho(t)$ is the density operator of the two-atom system at time t, $\rho'(t+\tau;\mathbf{r}_1, t)$ is the density operator at time $t+\tau$ assuming a photon was detected at point $\mathbf{r}_1$ and time t, and $D(\mathbf{r})$ is the photon detector operator $S_1^- + e^{i\phi(\mathbf{r})}S_2^-$, where $\phi(\mathbf{r}) = k_L\hat{\mathbf{r}}\cdot(\mathbf{x}_1 - \mathbf{x}_2)$ and $\hat{\mathbf{r}} = \mathbf{r}/r$.

We show in Fig. 5 the photon-photon correlation function (8) with respect to τ in a time t when the system is in the steady state and where the two detectors are located such that $\phi(\mathbf{r}_1) = \phi(\mathbf{r}_2) = 2n\pi$ with n an integer. Although this is not yet the case in the first experimental observations of the dipole blockade manifestations [12,13], we consider here a regime where the spontaneous emission dominates all dissipative effects in the atomic sample ($\gamma \approx \gamma_s$). Similar experimental parameters to those used in Figs. 1 and 2 were considered. For low dipole-dipole interaction [case (a)], a usual antibunching behavior of the scattered photons is observed [17]. For higher dipole-dipole interaction [case (b)], the antibunching of the scattered photons is much more marked as the value of the correlation function for $\tau = 0$ is much smaller with a much higher slope with respect to τ. The dipole blockade enhances the antibunching behavior. For higher laser intensities

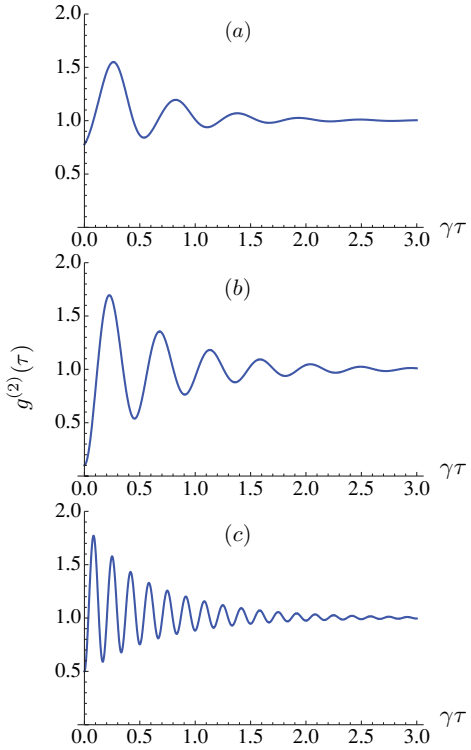

FIG. 5. (Color online) Second-order correlation function $g^{(2)}(\tau)$ [(a) $\Omega/\gamma = 5, \delta/\gamma = 5$; (b) $\Omega/\gamma = 5, \delta/\gamma = 30$; (c) $\Omega/\gamma = 15, \delta/\gamma = 30$].

[case (c)], $g^{(2)}(\tau = 0)$ increases again and the dipole blockade effect is less marked.

For $\tau = 0$ and considering time $t = 0$ when the system is in the steady state, we get

$$g^{(2)}(\mathbf{r}_1, 0; \mathbf{r}_2, 0) = \frac{4(16\Omega^4 + (4\Omega^2 + \gamma^2)|\alpha|^2)\cos^2[(\phi_1 - \phi_2)/2]}{[8\Omega^2 + |\alpha|^2(1 + \cos\phi_1)][8\Omega^2 + |\alpha|^2(1 + \cos\phi_2)]}, \quad (9)$$

with $\phi_i \equiv \phi(\mathbf{r}_i)$ $(i = 1, 2)$. Some particular detector positions are worth investigating. When $\phi_1 = \phi_2 = (2n + 1)\pi$ with n an integer, the photon-photon correlation function (9) exhibits a simple dependence to the dipole blockade parameter δ that appears only in the numerator through a quadratic dependence. The most interesting regime is reached when $\phi_1 = \phi_2 = (2n + 1)\pi/2$. In this case,

$$g^{(2)}(\mathbf{r}_1, 0; \mathbf{r}_2, 0) = \left.\frac{P_{ee}}{P_e^2}\right|_{\mathrm{SS}} \quad (10)$$

and the photon-photon correlation function identifies to the ratio (4) between the steady-state double-excitation probability and the square of the single-excitation probability. This ratio is a direct measure of the dipole blockade effect. The more it diverges from one, the more intense are the dipole-dipole interactions. For those particular detector positions, the coincident photon-photon correlation signal monitors quantitatively the dipole blockade in the two-atom sample. This monitoring works continuously as long as the system is permanently driven in its steady state and scatters the laser light.

IV. CONCLUSION

In conclusion, we provide a model able to analyze quantitatively the dipole blockade effect on the dynamical evolution of a two two-level atom system. We show that the dipole blockade is an efficient mechanism for production of significant long-term entanglement in the steady state of the system when it is continuously driven by a resonant laser field. This long-term entanglement, nonexistent in the absence of dipole blockade, is tunable with the laser intensity. We prove that the effect of the dipole blockade can be lifted in strong driving conditions. Finally, we show that, for particular detector positions, the photon-photon correlation function can continuously monitor the dipole-dipole interaction between the two atoms in a regime where the spontaneous emission will dominate all dissipative effects in the atomic sample. That will provide an efficient tool in the analysis of the occurrence of the dipole blockade.

ACKNOWLEDGMENTS

J.G. thanks the Belgian F.R.S.-FNRS for financial support.

[1] G. V. Varada and G. S. Agarwal, Phys. Rev. A **45**, 6721 (1992).
[2] D. Jaksch, J. I. Cirac, P. Zoller, S. L. Rolston, R. Côté, and M. D. Lukin, Phys. Rev. Lett. **85**, 2208 (2000).
[3] I. E. Protsenko, G. Reymond, N. Schlosser, and P. Grangier, Phys. Rev. A **65**, 052301 (2002).
[4] M. D. Lukin, M. Fleischhauer, R. Cote, L. M. Duan, D. Jaksch, J. I. Cirac, and P. Zoller, Phys. Rev. Lett. **87**, 037901 (2001).
[5] M. Orrit, Science **298**, 369 (2002); C. Hettich, C. Schmitt, J. Zitzmann, S. Kühn, I. Gerhardt, and V. Sandoghdar, *ibid.* **298**, 385 (2002).
[6] M. Saffman and T. G. Walker, Phys. Rev. A **66**, 065403 (2002); **72**, 042302 (2005); D. Møller, L. B. Madsen, and K. Mølmer, Phys. Rev. Lett. **100**, 170504 (2008); M. Saffman and K. Mølmer, *ibid.* **102**, 240502 (2009).
[7] D. Tong, S. M. Farooqi, J. Stanojevic, S. Krishnan, Y. P. Zhang, R. Côté, E. E. Eyler, and P. L. Gould, Phys. Rev. Lett. **93**, 063001 (2004).
[8] K. Singer, M. Reetz-Lamour, T. Amthor, L. G. Marcassa, and M. Weidemüller, Phys. Rev. Lett. **93**, 163001 (2004).
[9] T. Cubel Liebisch, A. Reinhard, P. R. Berman, and G. Raithel, Phys. Rev. Lett. **95**, 253002 (2005).
[10] T. Vogt, M. Viteau, J. Zhao, A. Chotia, D. Comparat, and P. Pillet, Phys. Rev. Lett. **97**, 083003 (2006); T. Vogt, M. Viteau, A. Chotia, J. Zhao, D. Comparat, and P. Pillet, *ibid.* **99**, 073002 (2007); R. Heidemann, U. Raitzsch, V. Bendkowsky, B. Butscher, R. Löw, L. Santos, and T. Pfau, *ibid.* **99**, 163601 (2007).

[11] K. M. Birnbaum, A. Boca, R. Miller, A. D. Boozer, T. E. Northup, and H. J. Kimble, Nature (London) **436**, 87 (2005).
[12] E. Urban *et al.*, Nat. Phys. **5**, 110 (2009).
[13] A. Gaetan *et al.*, Nat. Phys. **5**, 115 (2009).
[14] T. Pohl and P. R. Berman, Phys. Rev. Lett. **102**, 013004 (2009).
[15] J. von Zanthier, T. Bastin, and G. S. Agarwal, Phys. Rev. A **74**, 061802(R) (2006).
[16] W. K. Wootters, Phys. Rev. Lett. **80**, 2245 (1998).
[17] C. Skornia, J. von Zanthier, G. S. Agarwal, E. Werner, and H. Walther, Phys. Rev. A **64**, 063801 (2001).